



UIT

NORGES  
ARKTISKE  
UNIVERSITET

FACULTY OF SCIENCE AND TECHNOLOGY

Department of Geology

# Possible gas hydrates on the Bjarmeland Platform; seismic expression and stability modelling

---

**John Sverre Løvaas**

EOM-3901 Master thesis in Energy, Climate and Environment

*June 2016*











---

**UiT** / THE ARCTIC UNIVERSITY  
OF NORWAY

**Possible gas hydrates on the Bjarmeland Platform; seismic  
expression and stability modelling**

FACULTY OF SCIENCE AND TECHNOLOGY

Department of Geology

**John Sverre Løvaas**

EOM-3901 Master thesis in Energy, Climate and Environment

*June 2016*







## Abstract

Seismic evidence of shallow gas anomalies are prominent at Ververis Dome structure and Hoop Fault Complex in Bjarmeland Platform. Ubiquitous high amplitude anomalies at the same depth as these shallow gas anomalies infer a possible relation to gas hydrates. A wide range of fluid flow structures within the two study areas have previously been discovered and reported, and may possibly feed the base of the gas hydrate stability zone (BGHSZ) with upward migrating thermogenic gas.

This thesis focuses on seismic interpretation of gas hydrate-related bottom simulating reflectors (BSR) from high resolution 3D seismic data and high resolution 2D P-cable seismic data, as well as numerical modelling of gas hydrate stability conditions based on analyzed gas samples from geochemical data reports from well 7226/2-1 and 7324/8-1.

Numerical modelling of present day gas hydrate stability conditions indicate favorable conditions for gas hydrate stability both in Ververis and Hoop Fault Complex. Furthermore, the estimated depth of gas hydrate stability from numerical modelling coincides with the interpreted BSRs in both study areas. As such, confidence is built in the interpretation and mapping of gas hydrates in the study areas.

By using the results from ongoing work at Centre for arctic gas hydrate, environment and climate (CAGE) on numerical modelling of the ice sheet and isostatic conditions during the last glaciation, modelling of gas hydrate stability conditions indicate stable conditions for gas hydrates as deep as 618 m sub bottom depth in Ververis and 412 m sub bottom depth in Hoop Fault Complex during Last Glacial Maximum (LGM). The modelled gas hydrate stability zone in both study areas is thinning through deglaciation, possibly caused by unloading of vast ice sheets and the increasing bottom water temperatures.







## Acknowledgement

Da var tiden for innlevering av masteroppgave kommet. Jeg skal nå ut av studietilværelsen og inn arbeidslivet. Det føles merkelig, men også godt. Det har vært en fantastisk tid som student, noe jeg helt klart kommer til å savne. Men samtidig skal det også bli godt å tjene egne penger, og slippe å ringe hjem for å be om økonomisk hjelp flere ganger i måneden. Takk mamma og pappa for all (økonomisk) støtte gjennom min 5 år lange sivilingeniør utdanning!

Jeg har vært utrolig heldig å få skrive en masteroppgave med Statoil i Harstad, hvor jeg har fått fortsette å jobbe med samme temaet jeg også jobbet med i min sommerjobb hos dere! Tusen takk Oddbjørn Sivert Kløvjan for at du hjalp meg å initiere denne oppgaven med dere. Tusen takk Torbjørn Dahlgren for at du har bistått meg med data og kunne hjelpe meg å besvare alle mulige slags spørsmål jeg har hatt ifb min masteroppgave.

Til mine veiledere Karin Andreassen, Monica Winsborrow og Sunil Vadakkeyambatta: tusen takk for all hjelp dere har gitt meg med veiledning av min oppgave. Deres tips og råd har vært av største betydning, og oppgaven kunne ikke blitt den samme uten deres hjelp.

Sist, men ikke minst, til min studiegruppe: Nils Andreas, Lisa og Lena. Dere har vært mine allierte støttespillere og venner gjennom 5 år. Dere har vært min største motivasjon for å komme meg gjennom dette studiet. Alle de øyeblikkene med latter, tårer, glede og frustrasjon, det har alt vært verdt det. Dere har bidratt til å gjøre studietilværelsen min til en begivenhets- og minnerik tid. Tusen takk!

John Sverre Løvaas, Juni 2015





## Contents

1	Introduction.....	1
1.1	Objectives .....	1
1.2	Importance of gas hydrates.....	2
1.2.1	Possible impact on global climate change .....	2
1.2.2	Gas hydrates as a potential future energy resource.....	4
1.2.3	Gas hydrates as a geohazard.....	5
2	Fundamental theory.....	9
2.1	Gas hydrates .....	9
2.2	Identification of gas hydrates .....	10
2.3	Gas hydrate stability .....	12
2.4	Gas hydrate and fluid flow .....	14
2.5	Global Occurrences of Gas hydrates .....	17
2.6	Occurrences of Gas Hydrates in the SW Barents Sea.....	19
2.7	Contribution to this study.....	22
3	Geological setting and environment.....	23
3.1	Bjarmeland Platform .....	25
3.2	Hoop Fault Complex .....	27
3.3	Ocean temperatures and geothermal conditions .....	28
3.4	Glacial history of the SW Barents Sea .....	29
4	Data and Methods.....	33
4.1	Seismic data .....	33
4.1.1	Ververis 3D (ST07M16).....	33
4.1.2	Dataset at Hoop Fault Complex .....	34
4.1.3	P-cable dataset at Hoop Fault Complex.....	34
4.1.4	Petrel as interpretation tool.....	35
4.2	Gas composition .....	35
4.3	Gas Hydrate stability modelling .....	36
4.3.1	Model for present day conditions.....	38
4.3.2	Model for conditions during deglaciation (15 380 BP -16 830 BP).....	38
4.3.3	Model for conditions during Last Glacial Maximum (22 580 BP - 22 780 BP) ...	38
5	Results .....	39
5.1	Ververis 3D .....	39
5.1.1	Fluid flow systems .....	42

5.1.2	Distribution of BSR in the Ververis 3D .....	47
5.1.3	Gas Hydrate stability model at well 7226/2-1 .....	48
5.2	Hoop Fault Complex .....	51
5.2.1	Fluid flow systems .....	52
5.2.2	Distribution of BSR in the Hoop Fault Complex .....	56
5.2.3	Gas Hydrate stability model at well 7324/8-1 .....	57
6	Discussion .....	61
6.1	Study area .....	61
6.1.1	Seismic indications of gas hydrates.....	61
6.1.2	Gas migration and accumulation .....	62
6.1.3	Gas hydrate stability modelling.....	64
6.1.4	Numerical modelling and pitfalls .....	70
6.1.5	Impacts of LGM and deglaciation on present day gas hydrate accumulations .	71
7	Conclusion .....	77
8	References.....	79

# 1 Introduction

## 1.1 Objectives

Hoop area of the Bjarmeland Platform (Figure 1), is currently considered a ‘hot area for exploration’ in the SW Barents Sea. Possible gas hydrate accumulations in the area needs to be better understood to enhance the geological knowledge of the Bjarmeland Platform. The main objective of this thesis is to evaluate possible gas hydrate accumulations on the Bjarmeland Platform, SW Barents Sea, based on 2D and 3D seismic data (Figure 1) and well data.

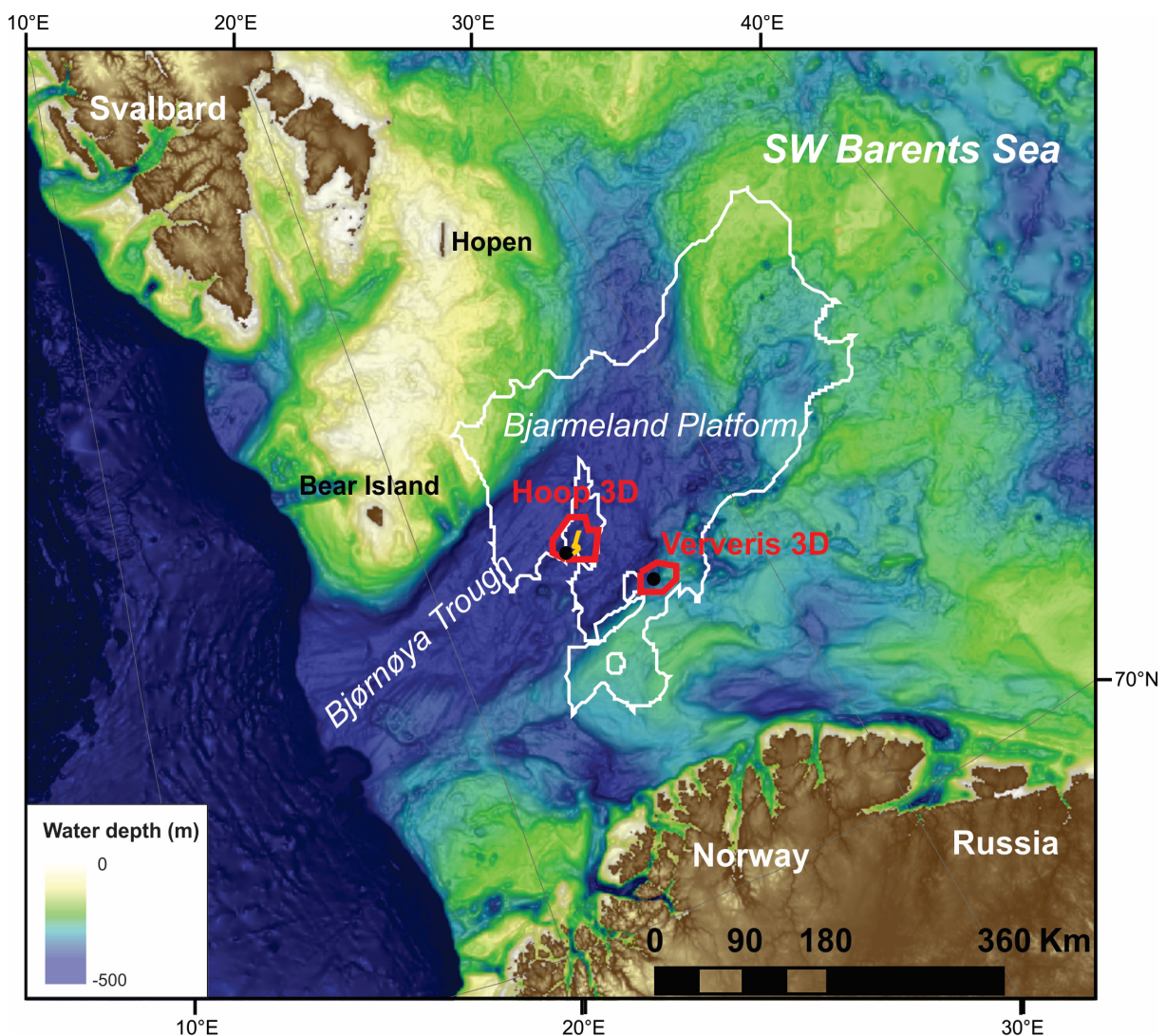


Figure 1. Overview map of the SW Barents Sea. The white polygon illustrates Bjarmeland Platform. The two red polygons indicate the two study areas in which this thesis is focusing at. The two black dots within the study areas indicate well 7324/8-1 (Hoop 3D) and 7226/2-1 (Ververis 3D). The yellow line within Hoop 3D is the P-cable 2D seismic data available for this thesis. Bathymetry dataset is ICAO version 3.0 (Jacobsen, et al., 2012).



Numerical modelling of the gas hydrate stability on Bjarmeland Platform will also be carried out, and will be compared with the interpreted BSR from the seismic data. Mapping of potential gas-related BSRs will be done based on 2D and 3D seismic data, whereas numerical modelling of the gas hydrate stability zone will be carried out for chosen locations based on results from the BSR mapping. Numerical modelling will be carried out based on well data and geochemical data reports provided by Statoil, where analysed gas samples from mud gas are available.

The gas hydrate stability modelling will be done for present conditions as well as for conditions during the Last Glacial Maximum and for conditions during deglaciation. Results from ongoing work at the Centre for arctic gas hydrate, environment and climate (CAGE) on numerical modelling of the ice sheet and isostatic conditions during the last glaciation will be used in the modelling of the gas hydrate stability during glacial conditions.

## 1.2 Importance of gas hydrates

In the recent past, significant attention has been related to gas hydrates due to their possible impact on the environment and to their potential as a future energy resource. In the last decade it has been an increasing interest for exploration in the Arctic region which also have put the attention on gas hydrates as a potential geohazard for drilling operations. Extensive research have been accomplished during the last decades with the aim for better understanding of the potential and impact of gas hydrates.

### 1.2.1 Possible impact on global climate change

Methane hydrate is a solid consisting of methane ( $\text{CH}_4$ ) and water, and is stable at low temperatures and high pressure. Methane is about 20 times more potent than  $\text{CO}_2$  as a greenhouse gas when integrated over 100 years, and its long-term stability in the form of gas hydrate deposits is a concern for global climate (Ruppel, 2011).

Gas hydrates occur in large quantities both in terrestrial and marine environments. In the marine environments, the occurrences are mainly in the sediments of marine continental

margins, and although only less than 5 % of the gas hydrates may experience dissociation in response to reasonable rates of global warming, its impact may be significant to the global climate (Ruppel, 2011). Gas hydrates mostly consist of methane (CH<sub>4</sub>) and water (H<sub>2</sub>O), but other molecules such as C<sub>2</sub>H<sub>6</sub>, C<sub>3</sub>H<sub>8</sub>, C<sub>4</sub>H<sub>10</sub>, CO<sub>2</sub> and H<sub>2</sub>S are also present (Judd & Hovland, 2007). The SW Barents Sea is considered a vast petroleum province in the Arctic region, and extensive occurrences of gas hydrates are inferred to exist in the region (Chand, et al., 2008; Vadakkepuliambatta, 2014). The impact from dissociation of these hydrates on the global climate are still unknown, and much further research is necessary to better understand both its potential impact on the climate, and its potential as a future resource.

Large amounts of methane are trapped in subsurface sediments in arctic regions within methane- and gas hydrate bearing sediments. As methane oxidizes to CO<sub>2</sub> in about a decade, which again will accumulate in the Earth's carbon cycle for millennia, Archer et al. (2009) emphasizes that methane hydrates may have the potential to cause a significant long-term impact on the global climate. Furthermore, it is concluded that mankind has the ultimately capacity to cause melting of significant fractions of methane hydrates in oceanic subsurface sediments. The climate impact of such a scenario would be on a time scale of millennia and longer (Archer, et al., 2009).

In contradiction, McGinnis et al. (2006) emphasizes that when gas hydrates dissociate in the seafloor, methane will rarely survive the trip from the hydrosphere to the atmosphere. For seafloor depths of more than 100 m, most of the methane will be lost due to oxidation of methane by aerobic microbes (McGinnis, et al., 2006). Ruppel (2011) claims that catastrophic and widespread dissociation of methane hydrates will not be triggered at the current rates of global warming (0.2°C per decade; IPCC 2007) even the next few hundred years. This could be explained by the fact that most of the gas hydrates occur at such great depths below the seabed and at such low saturations, that they barely will be affected by the global warming over the next 1000 years. When methane is dissociated from the gas hydrates, oxidative and physical processes may take place and greatly reduce the amount of methane reaching the atmosphere. However, Ruppel (2011) conclude that gas hydrate degradation may occur more rapidly on the Arctic continental shelves, where subsea permafrost thawing and methane hydrate dissociation have been triggered by warming and inundation since Late Pleistocene. Warming of these intermediate waters may cause more

rapidly dissociation of gas hydrates at the upper continental slopes. Dissociation of methane that reaches the seabed at the upper Arctic continental slopes, is much more likely to enter the atmosphere as methane (CH<sub>4</sub>), not CO<sub>2</sub>. (Ruppel, 2011).

There seems to be some disagreement amongst scientists concerning dissociation of gas hydrates related to global climate change, however it seems to be a broad agreement that immense amount of gas hydrates are stored at continental margins across the Earth's crust. It is important that gas hydrate distribution and their sensitivity to the global climate change are better understood, and hence, more research is required.

This thesis will model and interpret gas hydrates in Bjarmeland Platform (Figure 1), and numerical modelling from Last Glacial Maximum, deglaciation and present day conditions may help enlighten changes in the stability conditions and possible dissociation of gas hydrates.

### 1.2.2 Gas hydrates as a potential future energy resource

Gas hydrates are widely spread around the world, both in terrestrial and marine environments, particularly along continental margins worldwide (NETL, 2011). The large quantity of gas hydrates is suggested to be an important component of the global carbon cycle and a potential future energy resource. Milkov (2004) describes gas hydrates as a future energy resource because some individual gas hydrate accumulations may contain both significant volume and high concentrations, so that these accumulations may be profitably recovered in the future (Milkov, 2004). When pure methane hydrates are dissociated under normal surface temperature and pressure, 1 m<sup>3</sup> of solid methane hydrate may release up to about 164 m<sup>3</sup> of methane gas (Makagon, 1997; Kvenvolden, 2000; Grozic, 2010; NETL, 2011). This makes gas hydrates highly interesting in relation to energy supply, and it may be an important bridge fuel to a future where the demand for renewable energy resources is expected to increase significantly (NETL, 2011). Commercially production from gas hydrates is still heavily relied on future research, and detection of large enough concentrated quantities of gas hydrates requires advanced seismic techniques (Collett, 2002; Makogon, 2010).

In this thesis it will mainly be focused on the possible accumulations of gas hydrate in the

Bjarmeland Platform, and the potential link between the accumulations and the deeper petroleum related fluid flow system in the study area will be discussed. As such, the deeper fluid flow system may help provide information of focused flow from deeper petroleum reservoirs and sources, hence it may help localize where concentrated accumulations of gas hydrates may possibly exist in the study area.

### 1.2.3 Gas hydrates as a geohazard

Petroleum exploration and production in deep waters where gas hydrates may form, have increased significantly during the last decades. The operations of petroleum activities may thus alter ambient subsurface conditions and has caught significant attention lately. Gas hydrates have been regarded as a major concern in relation to petroleum activities due to instability caused by seabed vibrations, changes in geothermal gradient and temperature increases. Another concern related to gas hydrates is development of gas hydrates on the well head and other subsurface structures (Hovland & Gudmestad, 2001).

At the Louisiana continental slope in the Gulf of Mexico, data collection and analysis have demonstrated that gas hydrates in sediments are highly sensitive to even small changes in temperature. A relatively small temperature change of 1.0-1.5 °C in the water column, led to a distinct dissociation of gas hydrates and caused outgassing. Hence, all exploration and seabed construction development where formation and distribution of gas hydrates may exist, should include thoroughly research and evaluation regarded potentially geohazards (Hovland, 2005).

Maslin (2010) emphasizes that global warming could, via destabilization of gas hydrates, pose a potential threat to the stability of continental slope sediments. Destabilization of gas hydrates may cause significant removal of hydrostatic pressure, and could potentially lead to massive slope failure (Figure 2) (Maslin, et al., 2010). Kvenvolden (1999) exhibits that a lowering of sea level will reduce hydrostatic pressure and hence change the in situ pressure, which again could lead to instability of gas hydrates. To adjust to the new pressure, gas hydrates dissociate and creates a new fluidized layer at the bottom of the gas hydrate stability zone. This newly created fluidized layer is a weak layer of over-pressurized sediment, and may cause submarine slope failure. The same process may be caused by an



increase in bottom water temperature, when the temperature regime in the sediment changes (Kvenvolden, 1999).

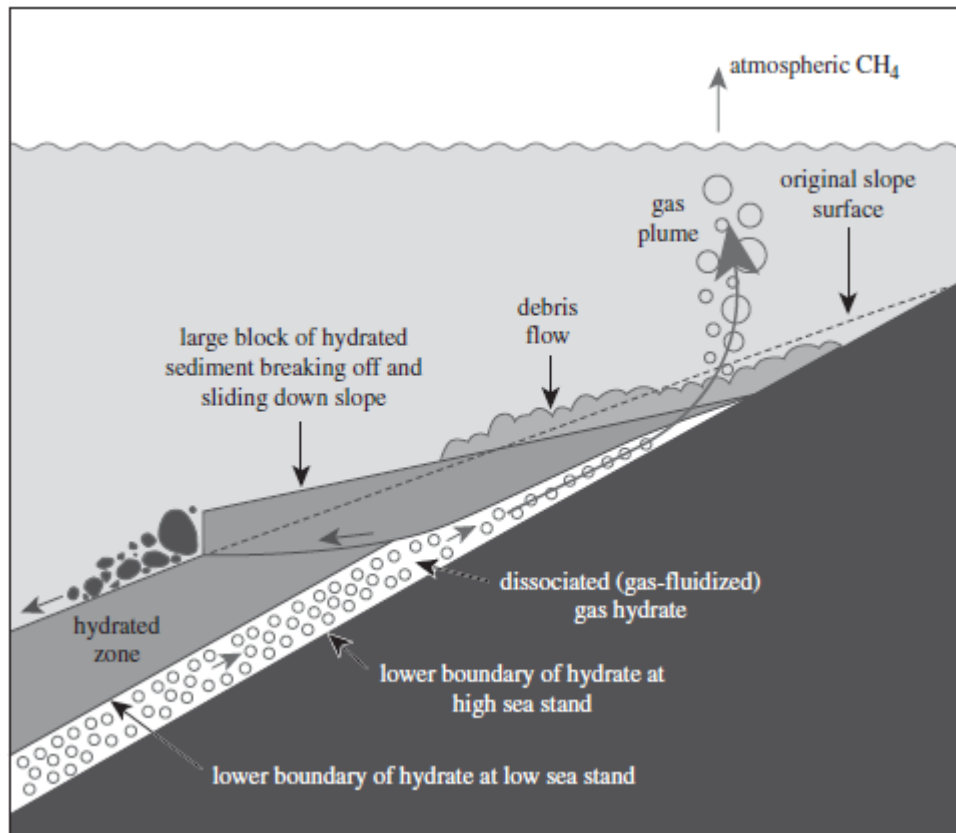


Figure 2. The model illustrates the effects of sea level changes on submarine gas hydrates, where large blocks of hydrated sediments break off and slide along a weak layer of over-pressurized sediments. From Maslin et al., (2010).

With the rise of sea level, hydrostatic pressure increases and causes gas hydrates to stabilize deeper in the subsurface. Lowering of sea level would cause the opposite effect, where gas hydrates may destabilize (Figure 2) due to the reduction in hydrostatic pressure. In this case, dissociation of gas hydrates at the bottom of the gas hydrate stability zone may cause loss of cementation and gas release, thus constitute a weak sediment layer. This weak layer of over-pressurized sediments, may in extreme scenarios lead to slope failure and could cause a gliding plane where massive wedges of hydrate cemented sediments slide downslope (Grozić, 2010). Storegga Slide at the mid-Norwegian margin has been suggested to be related to dissociation of gas hydrates, where the reduced hydrate stability conditions may have contributed to a sub-marine slope failure (Bryn, et al., 2005; Mienert, et al., 2005).

There are also hazards related to gas hydrates other than seabed stability. Drilling in gas hydrate bearing sediments may cause dissociation of hydrates. The dissociated free gas may

in some occasions form gas hydrates around the well head and the blow-out preventer (BOP), which in turn could lead mechanical systems to fail. Larger releases of gas could have fatal consequences for the stability of the rig, if the rig for example loose buoyancy. Such a scenario would seriously affect the safety of its crew and the rig itself. An even greater concern related to drilling in gas hydrate-bearing sediments is if the production of warm hydrocarbons causes heating and dissociation of gas hydrates in the surrounding sediments through the casing. This scenario could potentially lead to collapse of the casing due to excess local pressure, and a similar scenario has been reported at the Messakoya gas field in Siberia (Hovland & Gudmestad, 2001).

Dissociation of gas hydrates are also related to gas kicks during drilling operations when drilling through hydrate bearing sediments. In the Gulf of Mexico the subsurface sediments are well known for containing gas hydrates, and hydrates have been investigated as a potential contributor in the Deep Water Horizon accident in the Gulf of Mexico in 2010. Even though gas kicks are not common in the oil and gas industry today, it is likely to see more of such incidences in the future as the petroleum industry expands toward more extreme locations in their exploration for hydrocarbons (Helgeland, et al., 2012).

This thesis will elaborate on the relationship between fluid flow systems, seismic characterization of gas hydrates and numerical modelling of gas hydrate stability, which may provide better understanding of gas hydrate distribution in the study area. Hence, it may help avoid future drilling incidences due to petroleum exploration in the area.



## 2 Fundamental theory

### 2.1 Gas hydrates

Gas hydrates are ice-like crystalline compounds consisting of water and gas. Mostly gas hydrates consist of water (H<sub>2</sub>O) and methane (CH<sub>4</sub>), but other molecules such as C<sub>2</sub>H<sub>6</sub>, C<sub>3</sub>H<sub>8</sub>, C<sub>4</sub>H<sub>10</sub>, CO<sub>2</sub> and H<sub>2</sub>S are also present (Kvenvolden, 1998; Judd & Hovland, 2007). Gas hydrate forms when gas molecules are trapped within a clathrate structure of hydrogen-bonded water molecules, and the structures are formed in environments with adequate water and gas fluid flow, and under specific temperature and pressure conditions (Hovland, 2005).

Gas hydrates may occur in three forms; Structure I, II and H (Figure 3). Structure I consists of the smallest molecules and contains biogenic gases such as methane, carbon dioxide, ethane and hydrogen sulfide. This makes structural I hydrates the most common hydrates in the nature (i.e. biogenic methane). Structure II forms when higher order of hydrocarbons such as propane, iso-butane or other gas molecules larger than methane are present, which makes structure II hydrates more common in areas where exploration and production of hydrocarbons occur (Sloan, 1990; Sloan, 2003; Beauchamp, 2004). Structure H engages both smaller and larger molecules, and may thus occur in both natural environments and in environments where higher order of hydrocarbon gases are present (Beauchamp, 2004).



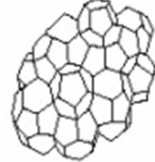
Hydrate structure	'Guest molecules'
 Structure I	Methane, ethane, carbon dioxide and so on
 Structure II	Propane, iso-butane and so on
 Structure H	Methane + neo-hexane, methane + cycloheptane, and so on

Figure 3. Gas hydrate structural types; structure I, II, and H. Guest molecules for each hydrate structure are indicated. Modified from Sloan, (2003)

According to Kvenvolden (1993), formation of gas hydrates requires low temperature and high pressure regimes. Another factor that also affects formation and stability zone of gas



hydrates is the ionic strength of water and gas composition (Kvenvolden, 1993). Different models have been suggested for the formation of gas hydrates, and Hyndman et al. (1992) proposed that formation of gas hydrates occurred due to removal of dissolved biogenic or thermogenic methane that originates from pore fluids which was upwelling and thus entering the gas hydrate stability zone (Hyndman & Davis, 1992). Another model was proposed by Minshull et al. (1994), where it was suggested that free gas was migrating upwards through permeable sediments due to buoyancy, capillary forces and overpressuring mechanisms (Minshull & Singh, 1994).

## 2.2 Identification of gas hydrates

The base of the hydrate stability zone may be recognized in seismic data via bottom-simulating reflectors (BSR). BSR typically appear as strong reflections caused by high acoustic contrasts between the relatively high-velocity of gas hydrates and the low-velocity sediments underneath (Judd & Hovland, 2007). The BSR corresponds to the base of the gas hydrate stability zone (BGHSZ), and it is believed to mark the transition between gas hydrate bearing sediments above and free gas bearing sediments below (Holbrook, et al., 1996; Bünz & Mienert, 2004). The appearance of BSR in seismic data would be expected to parallel or sub-parallel the seafloor in environments where gas composition, water composition, sediment composition and regional heat flow are relatively homogenous and stable. The BSR differs from sedimentary bedding plane reflections as it may cross cut them in seismic section where bedding planes are dipping relative to the seafloor (Shipley, et al., 1979). BSR has reversed polarity relative to the seafloor, which indicates a decrease in acoustic impedance because of decreasing compressional wave velocity when going from gas hydrates into free gas sediments (Andreassen, et al., 1996). Because the BSR typically is caused by free gas below the hydrates, it is believed that gas hydrates can exist without a seismic BSR where free gas is not present (Holbrook, 2000; Bünz & Mienert, 2004; Mienert, et al., 2005). When free gas is not present, only very high concentrations of gas hydrates may cause significant seismic amplitude anomalies and thus a bottom simulating reflection (Hornbach, et al., 2003). The seismic characteristics of a BSR broadly mimics the dipping seabed and shows a polarity reversal relative to the seafloor seismic reflection (Figure 4).

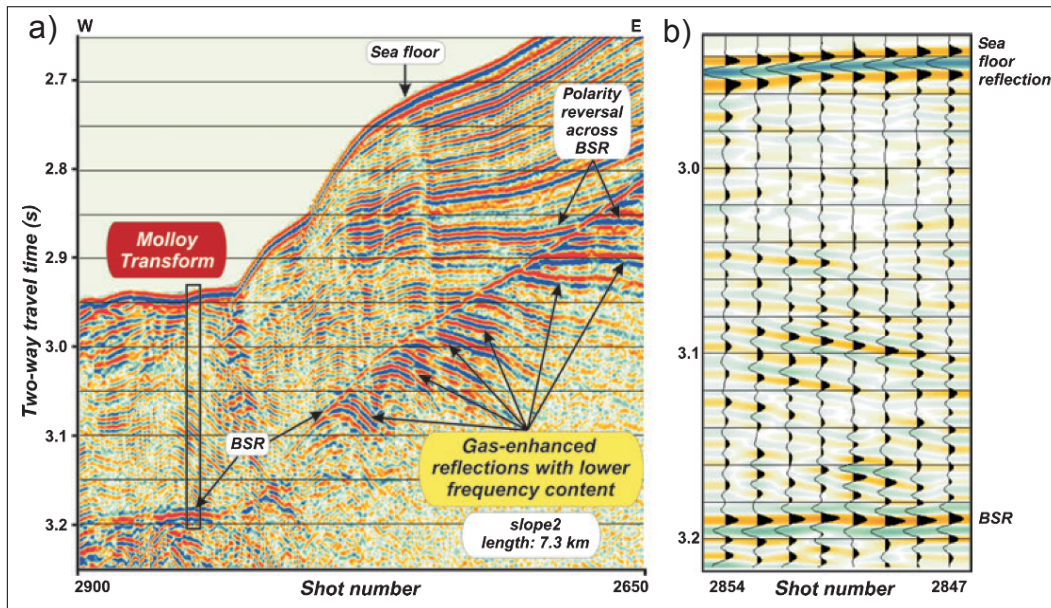


Figure 4. a) Seismic BSR from west of Svalbard close to Molloy Transform Fault. The BSR is shows reversed polarity compared to the seabed, and crosscut bedding planes. There is also a polarity reversal across the BSR. b) Wiggle display of the sea floor reflection and the BSR. The image indicates a polarity reversal of the BSR relative to the sea floor reflection. Modified from Vanneste, et al., (2005)

When using seismic methods to identify gas hydrates, an assumption is that the P-wave velocity of sediment containing gas hydrates increases, compared to similar sediments where hydrates are not present. Furthermore, the P-wave velocity decreases below the BSR as a result of either absence of hydrates or presence of free gas. Change in S-wave velocity is only expected if gas hydrates are cementing the sediments and thus altering the shear moduli of the sediments (Chand & Minshull, 2003). As a supplementary indication of presence of gas hydrates, amplitude- or seismic blanking has been frequently used. The dimming or reduction of seismic amplitudes are related to decreasing acoustic impedance contrast due to cementation of hydrate bearing sediments (Shipley, et al., 1979; Holbrook, et al., 1996). Holbrook et al. (2002) emphasizes that amplitude blanking alone should be considered a tenuous indicator of gas hydrates.

Although BSR is the most important seismic indication of presence of gas hydrates, other indirect indicators may also support interpretation of gas hydrates. Theoretical modelling and borehole logging may provide evidence of gas hydrates, and sonic logging have shown that both P-wave velocity and S-wave velocity increases when high concentrations of hydrates are present (Chand, et al., 2003). Within gas hydrate cemented sediments, P-wave velocity have been measured to between 1700-2400 m/s, whereas in free gas sediment the

P-wave velocity may decrease significantly to below 1500 m/s (Murphy, 1984; Lee, et al., 1993).

Gas hydrate-related BSR may occur worldwide, however pressure-temperature conditions, and gas composition and volume, restricts occurrences of gas hydrates into two regions: Polar Regions and oceanic continental margins (Kvenvolden, 2000).

### 2.3 Gas hydrate stability

For gas hydrates to form and remain stable, its environment requires very specific conditions; the primary factors for its stability is pressure, temperature and sufficient quantities of water and methane flux. However, other factors may also impact the stability of gas hydrates. Salinity may restrict formation of gas hydrates, and high salinity content may thus change the gas hydrate stability zone (GHSZ) upwards in sediments. It also exist factors that may change the GHSZ downward in the sediments and thus make it possible for gas hydrates to form at higher temperatures; higher orders of hydrocarbons. Presence of higher order of hydrocarbons like  $C_2H_6$ ,  $C_3H_8$ ,  $C_4H_{10}$ ,  $CO_2$  and  $H_2S$ , may increase the stability of gas hydrates and thicken the GHSZ (Kvenvolden, 1998; Judd & Hovland, 2007; NETL, 2011). Sloan (1990) suggests a variety of factors that may affect the stability of gas hydrates: geothermal gradient, bottom water temperature, thickness of water column, gas composition, pore water salinity, and concentration of other dissolved chemicals (Sloan, 1990). Later studies also suggests heat flow through chimneys and faults, and salt tectonics as major controlling factors for gas hydrate stability (Chand, et al., 2008; Vadakkepuliambatta, et al., 2014; Vadakkepuliambatta, et al., 2016 (submitted)).

Due to positive thermal gradient in the Earth, gas hydrates can only exist in stable form within the first few hundred meters of the sediment in deep ocean sediments (Phrampus & Hornbach, 2012). Kvenvolden (2000) emphasizes that presence of gas hydrates are restricted to Polar Regions and oceanic continental margins, due to the specific pressure-temperature requirements and the necessary gas composition and volume.

In Arctic shelf areas, the past ice loads and glacial induced geothermal gradient have had a major effect on the gas hydrate stability zone (Fichler, et al., 2005), and also in the SW Barents Sea glacial episodes have had a major implication on the gas hydrate stability, due to

both ice thickness and cooler bottom water temperature (Chand, et al., 2012; Ostanin, et al., 2013). The retreatment of ice sheets in the Barents Sea after the late Weichselian glacial maximum (LGM), may have caused a reduction of 1400-2200 m for the gas hydrate stability zone (GHSZ) (Chand, et al., 2008). Much of this thinning of the GHSZ is thought to be caused by reduction in pressure due to glacial unloading, but a significant increase in the bottom water temperature up to 7 °C may have had a significant contribution to the decrease in the GHSZ (Dore & Jensen, 1996; Chand, et al., 2008). Chand et al. (2008) suggests that isostatic uplift and erosion in the Barents Sea may have caused expansion of gas reservoirs resulting in fracturing of cap rock and migration of dissolved methane gas from formation water, which again have caused formation of methane hydrates. Furthermore, migration of higher order of hydrocarbons from deeper reservoirs into the GHSZ, could possibly have increased the stability of gas hydrates and shifted the BGHSZ downward in the sediments (Chand, et al., 2008). Pure methane hydrates are considered to be stable only in a smaller part of the SW Barents Sea, mostly in the Bjørnøya Trough where they are suggested to be stable down to 150 m below the seafloor (Figure 5)(Chand, et al., 2008; Vadakkepuliambatta, et al., 2014). However, local variation in the geothermal gradient may push the methane hydrate stability zone down to around 250 m below the seafloor in a few areas in Bjørnøya Trough (Vadakkepuliambatta, et al., 2014).

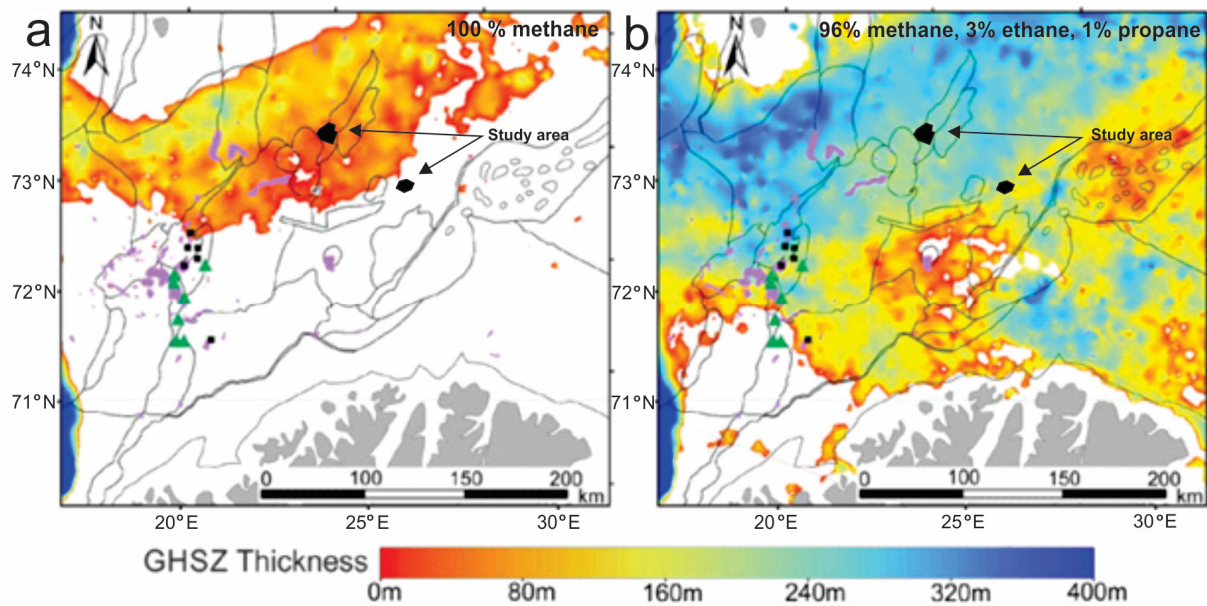


Figure 5. Two models of gas hydrate stability thickness in the SW Barents Sea: a) Gas composition of 100% methane. b) Gas composition of 96% methane, 3% ethane and 1% propane. For both a) and b): Large gas chimneys illustrated in pink areas (Vadakkepuliyambatta, et al., 2013), black squares indicates locations of known gas hydrate accumulations (Andreassen, et al., 1990) (Løvø, et al., 1990) (Laberg & Andreassen, 1996) (Chand, et al., 2012) (Ostanin, et al., 2013), location of gas flares indicated in green triangles (Chand, et al., 2012) and major structural elements illustrated in black lines (NPD). Study areas are marked in black polygons. Modified from Vadakkepuliyambatta, et al., (2014).

## 2.4 Gas hydrate and fluid flow

Gas hydrate bearing sediments are often associated with fluid migration. Seismic blanking or amplitude blanking, wipe-outs, pockmarks, acoustic masking and acoustic turbidity may be regarded as indirect indicators of fluid flow. Evidence of these features within or below the GHSZ in seismic sections, may thus be regarded as indirect indicators for formation of gas hydrates (Chand & Minshull, 2003). Vertical zones of reduced amplitudes in seismic sections are often recognized as gas chimneys, and they are thought to represent conduits for fluid flow from deeper sediments into shallower sediments (Løseth, et al., 2009). Migration of gas through vertical chimney structures have been reported numerous times to be related to formation of gas hydrates in areas where favorable pressure-temperature conditions for gas hydrate formation are present, and examples are Vestnesa Ridge (Bünz, et al., 2012), South Hydrate Ridge (Bangs, et al., 2011), Cascadia Margin (Suess, et al., 1999), Loppa High (Rajan, et al., 2013) and Hammerfest Basin (Ostanin, et al., 2013). Occurrence of faults in regions where gas hydrates exist, have been inferred to act as migration pathways for hydrocarbons from deeper sources and reservoirs, and hence also suggested as a controlling factor for

distribution of gas chimneys, mud volcanoes and pockmarks (Chand & Minshull, 2003; Berndt, et al., 2003; Judd & Hovland, 2007). Both faults and fractures are considered to be good conduits for fluids across low permeable sedimentary layers, and they are usually associated with high amplitude acoustic anomalies along their fault plane or adjacent sedimentary strata (Løseth, et al., 2009). Polygonal faults can be formed in fine grained sediments caused by contraction of sediment and fluid expulsion, and are also believed to act as migration pathways for deeper seated fluids (Cartwright, 1994; Berndt, et al., 2003; Bünz, et al., 2003). Vadakkepuliambatta et al. (2014) suggests that distribution of gas hydrates in the SW Barents Sea are controlled by leakage from large gas chimneys, faults and other structural elements which may act as conduits for deeper thermogenic gases (Vadakkepuliambatta, et al., 2014). Fluid migration through carrier beds is another good fluid flow conduit which may be related to lateral formation and distribution of gas hydrates (Judd & Hovland, 2007; Freire, et al., 2011; Rajan, et al., 2013). Other major conduits for fluid flow related to gas hydrates are salt tectonics and mud diapirs (Chand & Minshull, 2003; Chand, et al., 2008; Vadakkepuliambatta, et al., 2014; Vadakkepuliambatta, et al., 2016). Chand & Minshull (2003) illustrates how gas hydrates may be related to mud volcanoes (Figure 6), salt diapirs or faults. In regions where fault conduits reaches the seabed, active gas venting and pockmarks may be present (Chand & Minshull, 2003).



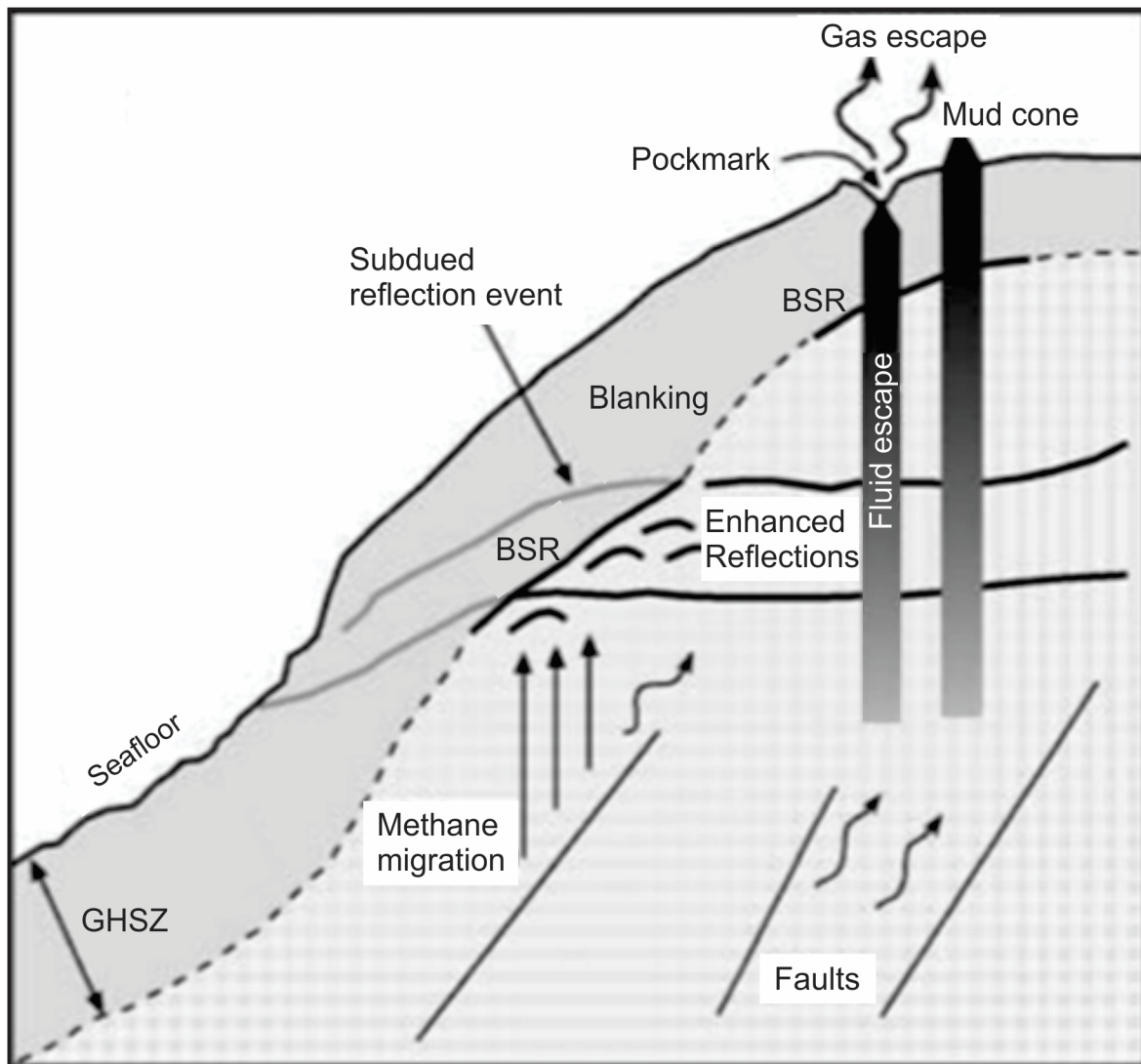


Figure 6. Illustration of gas hydrate related features along passive continental margins. Included in the illustration are major features such as subdued reflection event between the BGHSZ and the seabed, acoustic turbidity, blanking, enhanced reflection below the BSR, leakage along faults, and fluid flow features such as pockmarks, mud volcanoes and wipe-outs. Modified from Chand & Minshull, (2003).

When fluid containing methane migrates into the GHSZ, a drop in solubility towards the seabed may cause methane to precipitate from its fluid solution and crystallize into gas hydrate. The formation rate of hydrates depends strongly on the decrease in solubility and the upward flow rate of the methane (Chand & Minshull, 2003). Normally, gas hydrates would not extend up to the seabed due to lower concentrations of gas relative to the solubility in the shallowest sediments (Suess, et al., 1999). Faults may act as conduits for highly focused flow of gas, water and heat, which may disturb the gas hydrate stability and either increase or decrease the thickness of gas hydrates (Wood, et al., 2002; Haacke, et al., 2007). Judd and Hovland (2007) suggest that decomposition of gas hydrates can result in

leakage of fluid upward to the seabed through plumbing systems such as chimneys, faults or fractures. Decomposition of gas hydrates may be possible in areas where periods of regression has occurred. During periods of glaciation when the sea level falls, buried gas hydrates would gradually become depressurized which would lead to destabilization and melting (Judd & Hovland, 2007). When gas hydrates destabilizes, it may cause rapid eruption of methane and other gases to the seabed which can create pockmarks on the seabed (Mienert & Posewang, 1999; Judd & Hovland, 2007). Pockmarks may vary in size, from a few meters to hundreds of meter in diameter. Their depth may vary from 1 meter to about 45 meters in some cases (Hovland, et al., 2002). Pockmarks are suggested to relate to eruption of gas and/or pore water, often followed by a period (from 1 year to thousands of years) of escaping fluid from the lithosphere to the hydrosphere. In the Barents Sea pockmarks have been reported earlier by Solheim and Elverhøi (1985), where smaller pockmarks (diameter 10-20 m) were detected in the northwestern Barents Sea, about 50 km southeast of Hopen Island (Solheim & Elverhøi, 1985). Chand et al (2008) have reported pockmarks within Nordkapp Basin and suggested a relationship to faults and gas hydrate system of post-glacial times (Chand, et al., 2008).

## 2.5 Global Occurrences of Gas hydrates

Methane- and gas hydrates are observed and known to occur in both terrestrial and marine environments (Figure 7). In arctic regions, terrestrial occurrences of methane hydrate may be hosted within and beneath the permafrost. Occurrences of methane- and gas hydrates in marine sediments are not limited just to Polar Regions, but may also occur along ocean continental margins (Kvenvolden, 2000; NETL, 2011). These are regions where temperature and pressure conditions may be so that gas hydrates can form if high enough flux of water and methane are present (NETL, 2011).

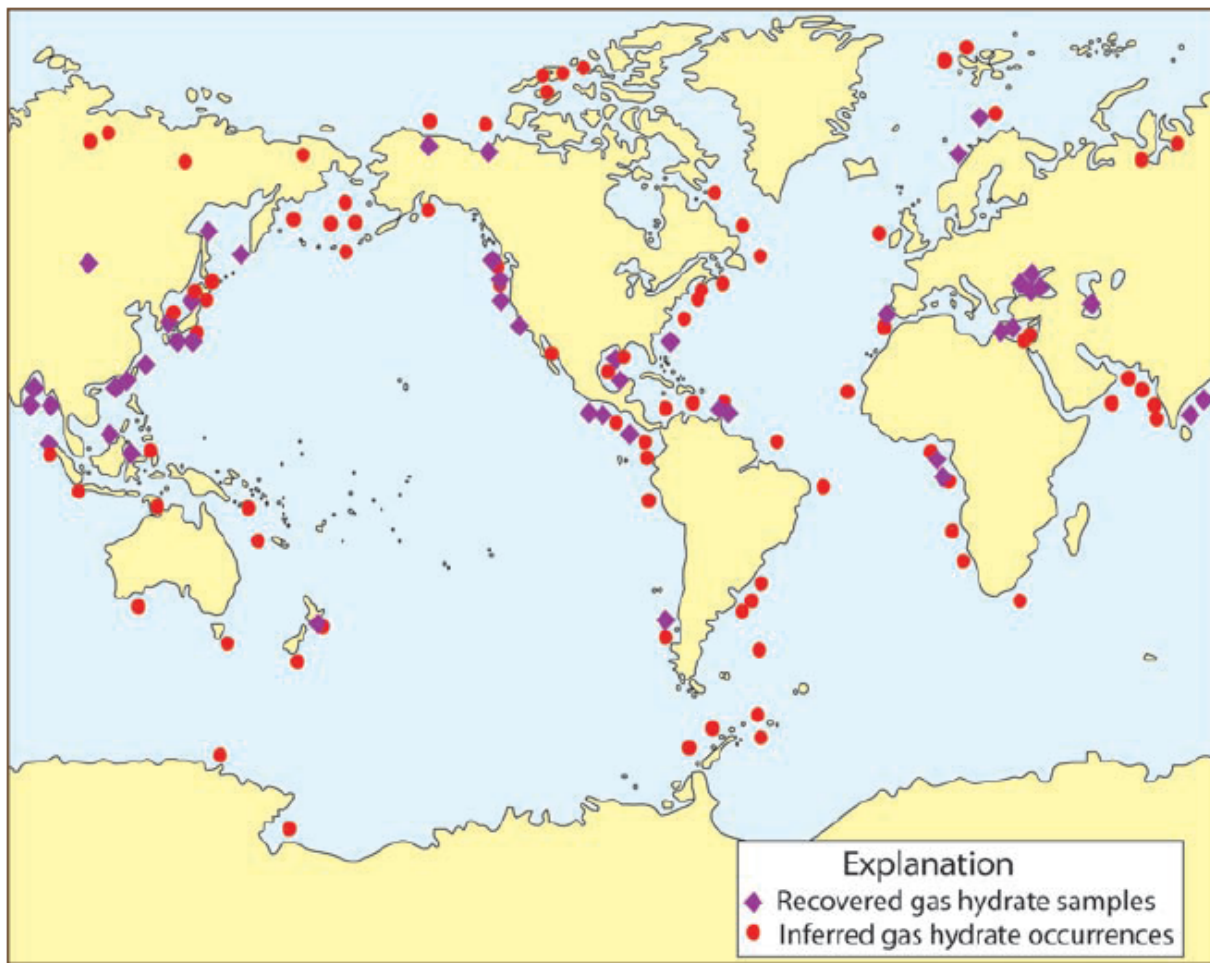


Figure 7. Location of inferred and sampled occurrences of gas hydrates worldwide. From NETL, (2011).

The methane captured in gas hydrates may have been formed either through biogenic or thermogenic processes. Biogenic produced methane are considered to be the dominant source of methane trapped in accumulations of gas hydrates in shallow marine sediments. Thermogenic methane is produced from buried organic material that have been heated under high pressure for a prolonged period of time. Due to the high pressure and temperature, oil and gas molecules such as methane, ethane, propane, butane etc., are expelled from organic-rich source beds. These expelled hydrocarbons will migrate upwards due to their relative buoyancy, and where sufficient quantities reaches the gas hydrate stability zone, gas hydrates may form if water are present.

Gas hydrates are not expected to occur in very deep oceans. This is related to the absence of high biologic productivity and the lack of rapid sedimentation rates that is required to bury the organic matter into depth. However, these conditions do exist along continental margins, and vast amount of gas hydrates are thus expected to occur along the margins

(NETL, 2011). Ruppel & Noserale (2012) estimates that 99% of all gas hydrates are located in oceanic sediments, whereas only 1% are located in permafrost regions. More specifically, around 95 % of the Earth's gas hydrates are inferred to occur within deep-water sediments, which means water depths of around 1000 m or deeper. 3.5% of the Earth's gas hydrates are inferred to occur within sediments in upper continental slopes, and less than 1% are suggested to occur within shallow water continental shelves as in the Arctic region (Ruppel & Noserale, 2012).

## 2.6 Occurrences of Gas Hydrates in the SW Barents Sea

In the recent past, significant attention has been related to gas hydrates in the SW Barents Sea. This is mainly related to their possible impact on the environment and to their potential as a future resource. The SW Barents Sea is considered a vast petroleum province in the Arctic region. Repeated periods of glaciation and erosional processes during Cenozoic has been suggested to have led to failure of petroleum traps and thus leakage of hydrocarbons from deeper reservoirs into shallower sediments. In the shallower sediments, migration of hydrocarbons have formed shallow gas accumulations, and gas hydrates where the conditions for formation of hydrates are present (Vadakkepuliyambatta, 2014). The stability of gas hydrates in the SW Barents Sea are highly variable, and factors such as presence of higher order hydrocarbons, heat flow and salt tectonics may play a significant role for the stability conditions (Chand, et al., 2008)

*Vadakkepuliyambatta (2014)* have modelled the gas hydrate stability field in the SW Barents Sea (Figure 5). The model has taken into account the lateral variations of the geothermal gradient, bottom water temperature, and gas composition. As control points for gas compositions and geothermal gradient, and to improve the gas hydrate stability zone depths, the model has been using information from 73 exploration wells in the area. The stability model indicates that gas hydrates in the SW Barents Sea can be stable, although highly variable in thickness (Vadakkepuliyambatta, 2014). In some parts of the SW Barents Sea, the gas hydrate stability zone may extend up to 400 m below the seafloor (i.e. Bjørnøya Trough). Assuming a gas composition of 96% methane, 3% ethane and 1 % propane, the lateral extent of gas hydrate stability seems to be present in most parts of the SW Barents

Sea (Figure 5b). There are also smaller locations of gas hydrate instability, such as in Tromsø Basin and smaller isolated areas near Samson Dome. Variation in the geothermal gradient and bottom water temperatures are inferred by Vadakkepuliyaambatta (2014) to have caused such local variations. In Tromsø Basin, the bottom water temperature has been measured to about 6°C, which makes the basin unstable even for gas compositions where higher order of hydrocarbons are present (Vadakkepuliyaambatta, 2014). In Nordkapp Basin, numerous salt diapirs in the shallower sediments are inferred to have increased the water salinity and thus the geothermal gradient. The geothermal gradient in the Nordkapp Basin varies from 22.8°C/km to 69.3°C/km, and have led to gas hydrate instability in parts of the basin (Vadakkepuliyaambatta, 2014) (Chand, et al., 2008).

In Finnmark Platform, small areas in the eastern and western part of the basin are suggested to not be within the gas hydrate stability zone. The major factors that could cause this variation in gas hydrate stability within the basin, are suggested to be related to high bottom water temperature and variation in the geothermal gradient (Vadakkepuliyaambatta, 2014).

The gas hydrate stability model (Figure 5) illustrates a GHSZ in the SW Barents Sea that is highly variable, and its thickness varies from a few tens of meter to up to 400 meter. The model also indicate that pure methane hydrates are unstable in most part of the SW Barents Sea, thus higher order of hydrocarbons are necessary for gas hydrate stability in most of the SW Barents Sea. Furthermore, variations in the thickness of GHSZ may be related to changes in water depth, bottom water temperatures, gas composition and geothermal gradient. The geothermal gradient is suggested to play an important role for GHSZ thickness in locations where there are intrusions of salt diapirs (Vadakkepuliyaambatta, et al., 2014). Chand et al. (2008) suggests the gas hydrate stability in the SW Barents Sea to be controlled by higher order of hydrocarbons, heat flow and salt tectonics. Variation in the bottom water temperature are suggested to not be a significant variable for the gas hydrate stability (Chand, et al., 2008).

Seismic evidence of gas hydrates are also interpreted in many basins of the SW Barents Sea, although most of these interpreted BSRs are small and isolated. Interpretations of BSR related to gas hydrates are located in Bjørnøya Fault Complex, Polheim Sub Platform, Loppa High, Samson Dome, Hammerfest Basin and Bjørnøya Basin (Andreassen, et al., 1990; Løvø, et al., 1990; Laberg & Andreassen, 1996; Chand, et al., 2012; Ostanin, et al., 2013). The BSR



interpreted from the seismic datasets, may be regarded as indirect evidence of gas hydrates, especially where it coincides with the base of the modelled gas hydrate stability zone. However, lack of BSR from seismic data does not rule out the possibility of gas hydrates in the shallower sediments that may extend outside of indirect evidence such as BSR (Vadakkepuliyambatta, 2014).

Vadakkepuliyambatta (2014) have modelled and interpreted gas hydrate-related BSRs within Samson Dome, Bjørnøya Fault Complex and Hammerfest Basin (Figure 8).

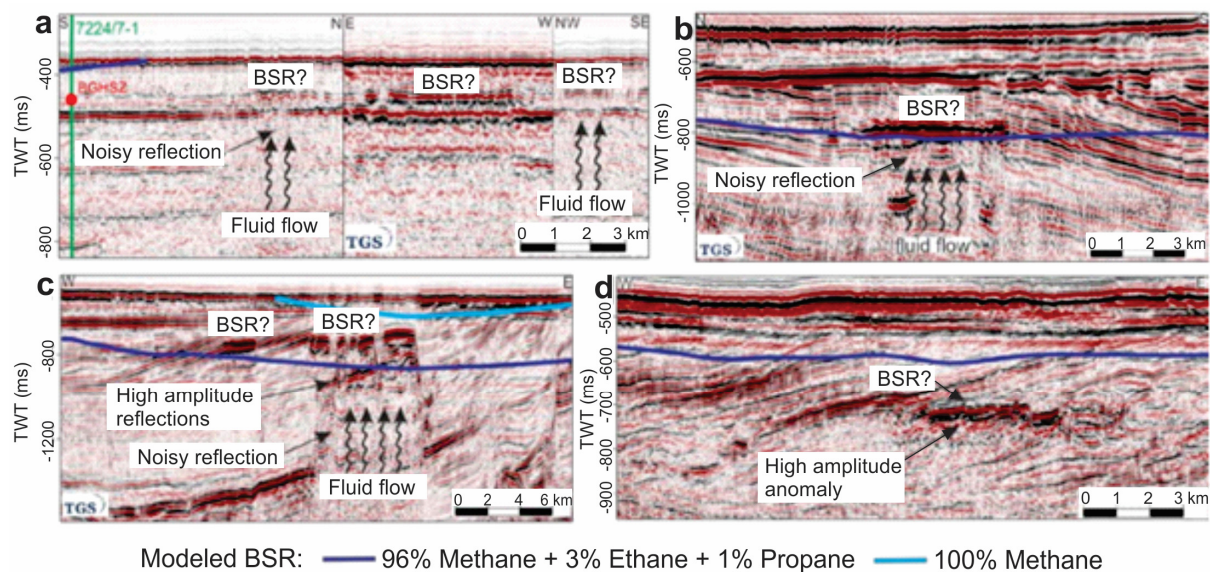


Figure 8. Interpreted gas hydrate related BSRs in the SW Barents Sea. a) Seismic section from Samson Dome showing a possible BSR. Chaotic reflections in the seismic indicates fluid migration from deeper formations. b) Interpreted BSR from Bjørnøya Fault Complex. c) Discontinuous BSR from Bjørnøya Fault Complex. d) Seismic section from Hammerfest Basin showing a BSR related to gas hydrates. From Vadakkepuliyambatta, et al., (2014).

The interpreted BSR from Samson Dome (Figure 8a) is slightly deeper than the modelled gas hydrate stability zone using a gas composition where higher orders of hydrocarbons are present. The interpreted BSR from Bjørnøya Fault Complex (Figure 8b) matches the modelled BSR for a gas composition of 96% methane, 3% ethane and 1% propane. Figure 8c is also from Bjørnøya Fault Complex, and the interpreted BSR lies just above the modelled gas hydrate stability zone for a gas composition of 96% methane, 3% ethane and 1% propane, and below a gas composition of 100% methane. The seismic section from Hammerfest Basin (Figure 8d) indicates that the interpreted BSR is located below the modelled gas hydrate stability zone. It has been suggested that this is due to even higher

concentrations of higher order of hydrocarbons than the gas composition the model have suggested. Despite this anomaly, most of the observed BSRs falls within the gas hydrate stability zone, using a gas composition of 96% methane, 3% ethane and 1% propane. Large portions of the observed BSRs are also located in relation to large chimneys, faults and other structural elements, where migration from deeper reservoirs is natural, indicating that the distribution of gas hydrates in Hammerfest Basin is vastly controlled by gas sources and gas composition (Vadakkepuliyaambatta, 2014).

## 2.7 Contribution to this study

Seismic evidence of gas hydrates has been interpreted in many areas in the SW Barents Sea, examples are Bjørnøya Fault Complex, Polheim Sub Platform, Loppa High, Samson Dome, Hammerfest Basin and Bjørnøya Basin. Most of these interpreted gas hydrates are related to fluid flow conduits, such as chimneys, pipes, faults, polygonal faults, fractures, pockmarks, active gas venting, etc. Numerical modelling of gas hydrate stability in the SW Barents Sea has also been carried out, and both Chand et al. (2008) and Vadakkepuliyaambatta et al. (2014) suggest gas hydrate stability in most parts of the SW Barents Sea.

Vadakkepuliyaambatta et al. (2014) suggest a gas hydrate stability around Ververis Dome structure of approximately 25 m.

With the access to a detailed geochemistry data report (Mørkved, et al., 2008) from well 7226/2-1 in the study area Ververis 3D and the geochemistry data report (Harding, et al., 2014) from well 7324/8-1 in the study area Hoop 3D, this thesis aims to provide an improved gas hydrate stability model at the well locations in both study areas. Additionally this thesis aims to model gas hydrate stability during both Last Glacial Maximum and deglaciation, and thus help enlighten the relationship between fluid flow conduits and the shallow gas anomalies possible related to gas hydrates in the study areas.

### 3 Geological setting and environment

The Barents Sea is part of the Arctic Ocean, located north of Norway and Russia (Figure 9).

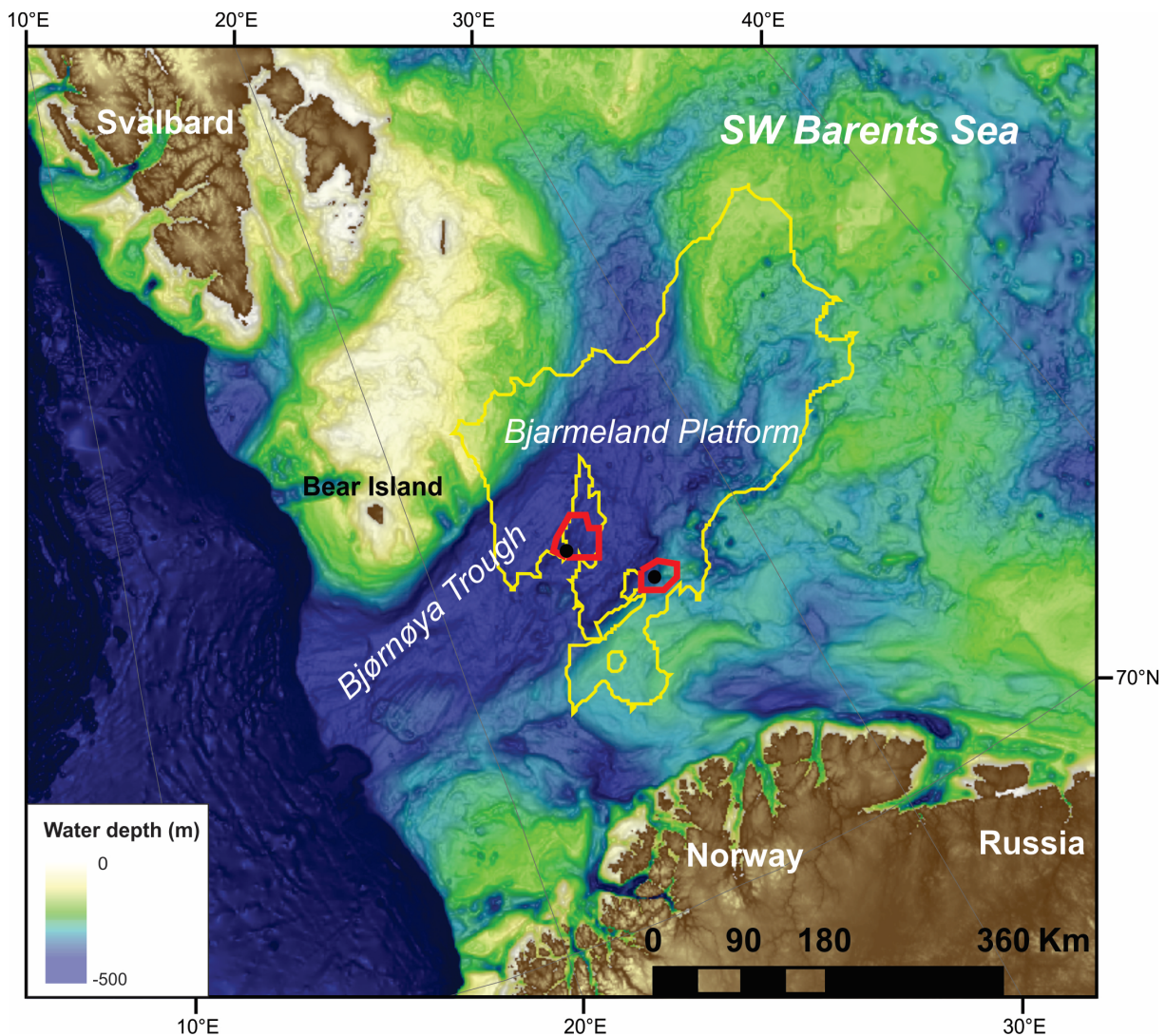


Figure 9. Map of the SW Barents Sea. The study areas are illustrated in red polygons, and the black dots inside each polygon illustrate the well positions of well 7226/2-1 and 7324/8-1. The larger yellow polygon illustrate Bjarmeland Platform. Bathymetry dataset is ICAO version 3.0 (Jacobsen, et al., 2012).

The main feature of the continental shelf in the SW Barents Sea is Bjørnøya Trough, which is a 150-200 km wide trough running about 750 km in northeast-southwest direction, and have a water depth between 300-500 m (Pau, et al., 2014). One important factor related to the Barents Sea region is the major tectonism and uplift during Paleocene, and the following erosion during Paleocene and Neogene. The tectonism during Paleocene has been suggested to be partly related to the opening of Atlantic and Arctic oceans from plate tectonic movements. Much of the erosion took place in the Quaternary when glacial conditions increased the rates of erosion (Halland, et al., 2013). Seismic surveying and coring have



shown that the Barents Sea are covered by thin, continuous Quaternary sediments on the seabed consisting of marine sediments underlain by till sheets. In the central Barents Sea, the Quaternary sediment thickness is typically less than a few tens of meters. The Barents Sea has been glaciated multiple times over the Cenozoic, and the erosive power of these ice sheets is evidenced by large prograding fans (Svendsen, et al., 2003). These prograding fans are often interpreted at the mouth of glacially eroded troughs, along the western margin of the Barents Sea. The mouth fan of Bjørnøya Trough is dominated by glacially derived debris flow deposits, generated by the transport of ice sheet during Weichselian (Laberg & Vorren, 1995).

### 3.1 Bjarmeland Platform

The shelf of the southern Barents Sea is divided into several structural elements, and the main ones are Hammerfest Basin, Nordkapp Basin, Finnmark Platform, Loppa High and Bjarmeland Platform (Figure 10).

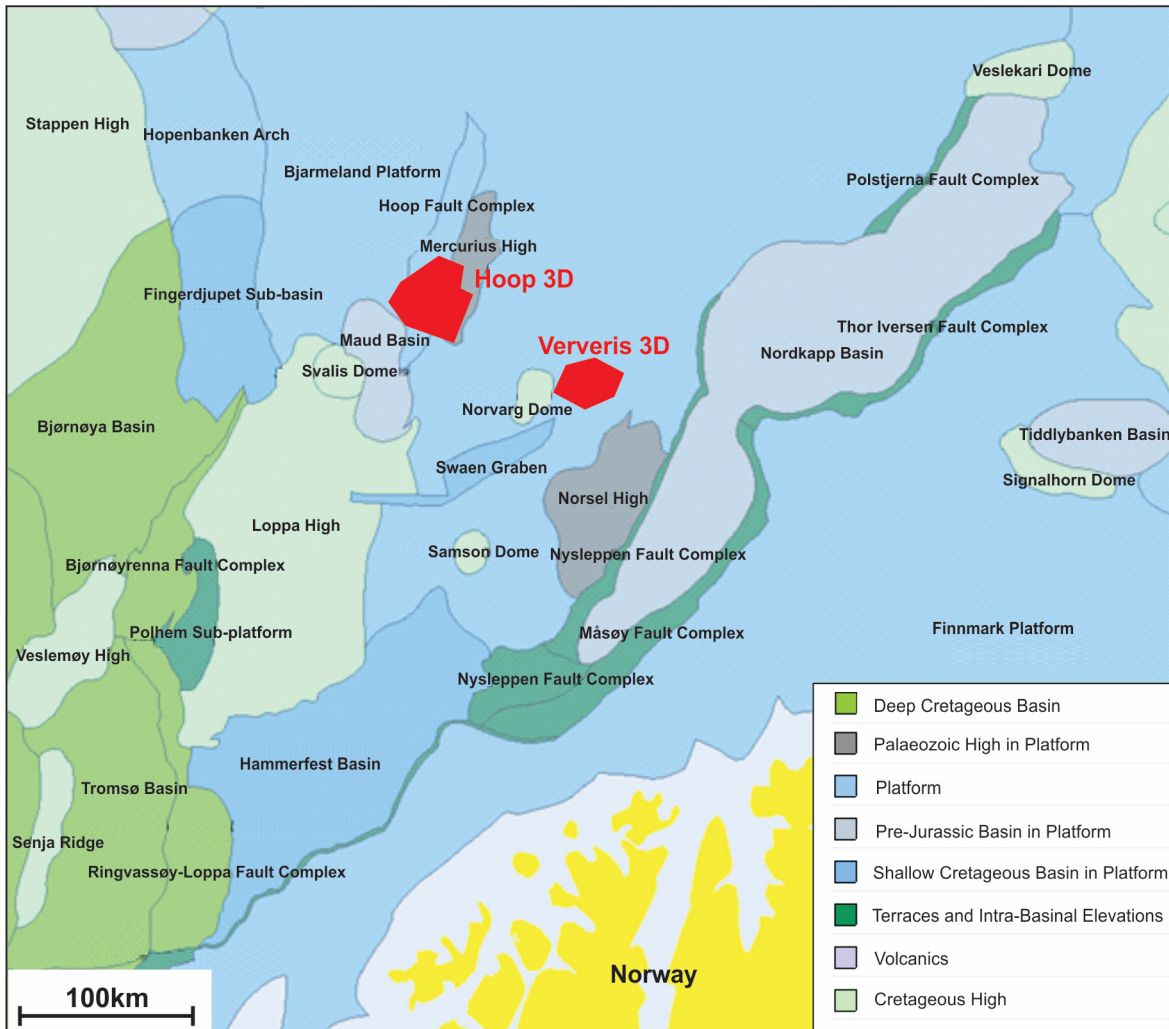


Figure 10. Structural elements of the SW Barents Sea. The two study areas are marked in red polygons. Modified from NPD FactMaps 2016.

Bjarmeland Platform is located east of Loppa High and north of the Nordkapp Basin (Figure 10), and the platform was formed in the Late Carboniferous and Permian. Within Bjarmeland Platform, successively older rocks overlies unconsolidated Pleistocene sediments towards north due to tilting of Paleozoic and Mesozoic sequences towards the south of the platform (Halland, et al., 2013). Included in the platform area are Samson Dome, Nordvarg Dome, Ververis Dome, Norsel High, Mercurius High, the Svalis Dome, the Swaen Graben, the Maud

Basin, and parts of the Hoop Fault Complex (Figure 10). The platform dips slightly towards south as a result of Tertiary uplift (Gabrielsen, et al., 1990). The Bjarmeland Platform is characterized by a progradational thick unit of Triassic clinoforms (Figure 11), extending from northern parts of Hoop area. The clinoforms in Bjarmeland Platform are of Olenekian age, whereas the clinoforms in Hoop Fault Complex are of Anisian and Ladinian age (Lundschien, et al., 2015).

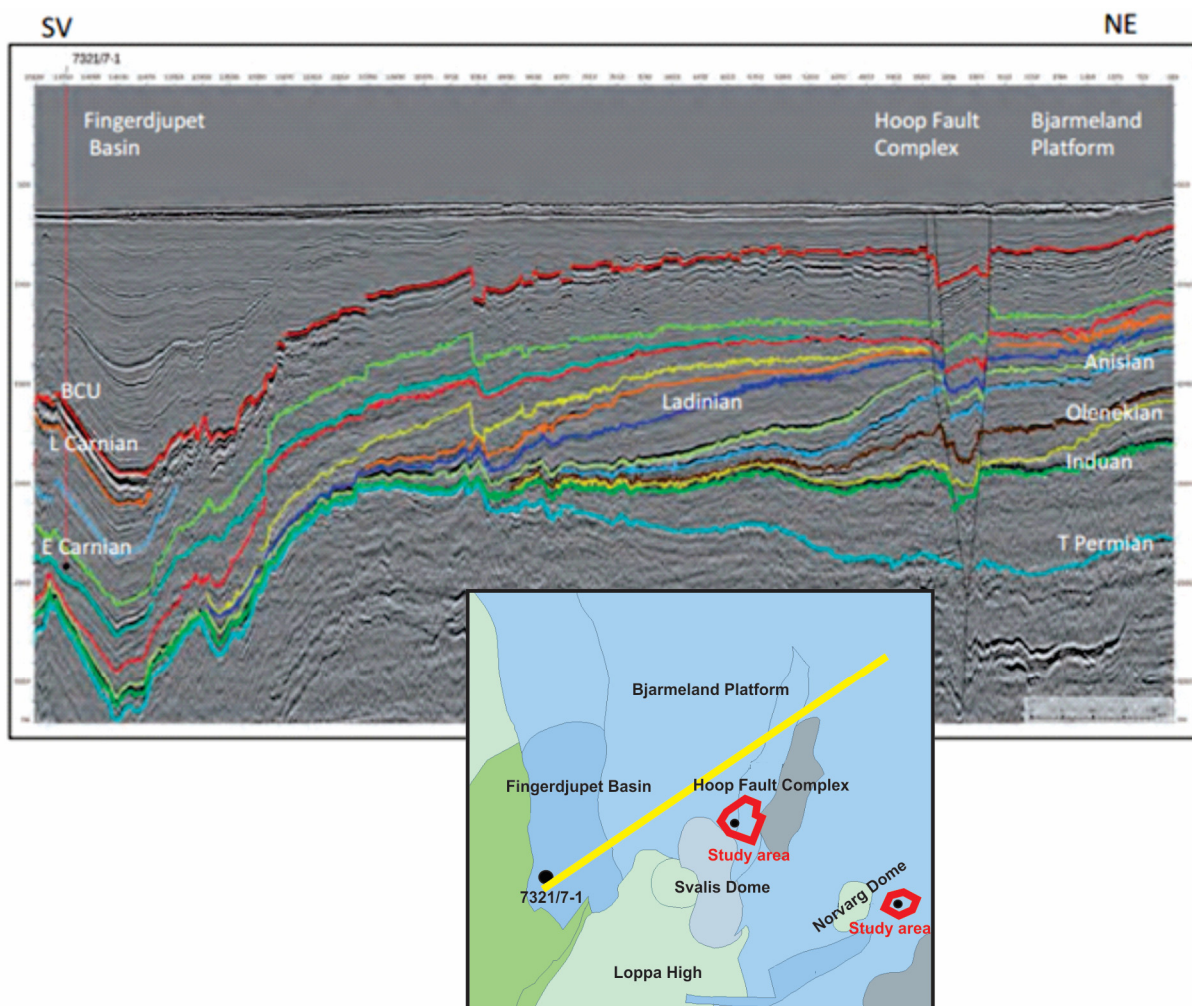


Figure 11. Clinoform sequences prograding in the Bjarmeland Platform, Hoop Fault Complex and Fingerdjupet Sub Basin area. Study area illustrated in inset map. Modified from Lundschien, et al., (2015).

The Bjarmeland Platform may be characterized by a thicker Triassic succession which condenses towards Fingerdjupet Sub Basin (Figure 11). The drilled thickness of the Triassic succession is 2862 m on the Nordvarg Dome (well 7225/3-1) (Halland, et al., 2013). From seismic interpretation (Figure 11), it is suggested that the Hoop Fault Complex is of post

Jurassic age in the northern part, where there are no significant Triassic synsedimentary faults disrupting the clinoform sequences (Lundschieen, et al., 2015).

### 3.2 Hoop Fault Complex

The Hoop Fault Complex (Figure 12) is crosscutting Loppa High and Bjarmeland Platform, and it is one of several trending lineaments from northeast to southwest in the SW Barents Sea. Towards north, the complex consists of considerable amounts of faults cutting the Bjarmeland Platform, whereas the southern part of the complex is related to a narrow graben on Loppa High. The central part of Hoop Fault Complex relates to the development of Maud basin and Svalis Dome. The complex have been suggested to be an old zone of weakness where activities in the central part have been controlled by sedimentation patterns from Late Carboniferous and Permian. The later reactivations are suggested to origin from Middle Triassic, Late Jurassic-Early Cretaceous and perhaps Tertiary age. The characteristics of Hoop Fault Complex (Figure 12) are normal faulting, and the center part has been related to subsidence of Maud Basin. In relation to salt movements in the Maud Basin, tectonic movement have caused later listric faulting in the complex where the development of some salt-related anticlinal structures have appeared (Gabrielsen, et al., 1990). The characteristic of Hoop Graben is related to a deep fault-cut succession of Carboniferous overlain by Triassic, Jurassic and Cretaceous successions that have been offset by series of faults trending from north-northeast to south-southwest. The Upper Triassic section have later been affected by another fault-system trending from east to west, which add to the complex structural system in the Hoop Fault Complex (Kjølhamar, et al., 2015).

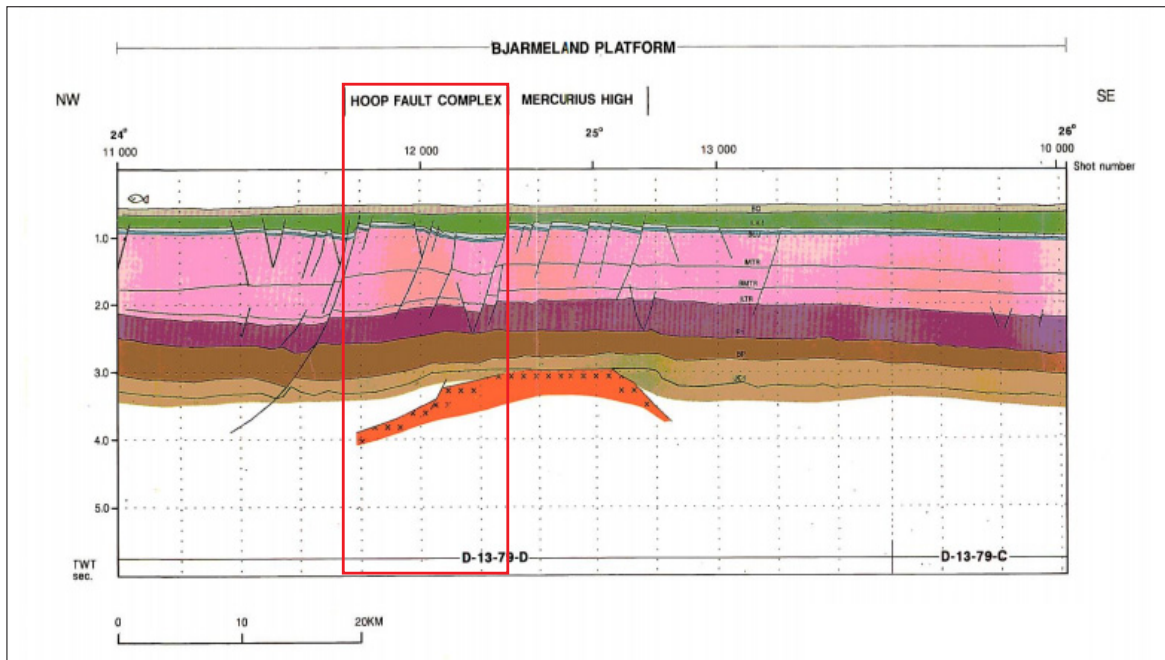


Figure 12. Profile across Bjarmeland Platform, where Hoop Fault Complex are illustrated in the red box. Colors on the sediment packages from top to bottom: Quaternary (grey), Cretaceous (green), Jurassic (light and dark blue), Triassic (pink), Upper Permian (brown), Lower Permian (light brown) and Basement (orange). Modified from Gabrielsen, et al., (1990).

### 3.3 Ocean temperatures and geothermal conditions

The cold Arctic water and the relatively warmer Atlantic water meet in the SW Barents Sea, which results in a warmer water in the southern part and cooler water in the northern part. The bottom water temperature varies significantly in the SW Barents Sea (Figure 13), and using bottom water temperatures from CTD measurements (NODC, 2009) gives a variety from -1.5 °C to 10 °C. The geothermal gradient in the SW Barents Sea is highly variable and ranges from 22.8 °C/km to 69.3 °C/km, with an average geothermal gradient of 36 °C/km (Vadakkepuliyambatta, et al., 2014). Chand et al. (2008) proposes three factors that may have significant implication on the geothermal gradient; proximity of mud diapirs and salt domes, basin inversion resulting in shallow basement rock, and focused fluid flow due to presence of faults (Chand, et al., 2008). Most of the higher geothermal gradients are inferred to be located in the Nordkapp Basin, where there are several occurrences of intrusive salt domes (Figure 13).



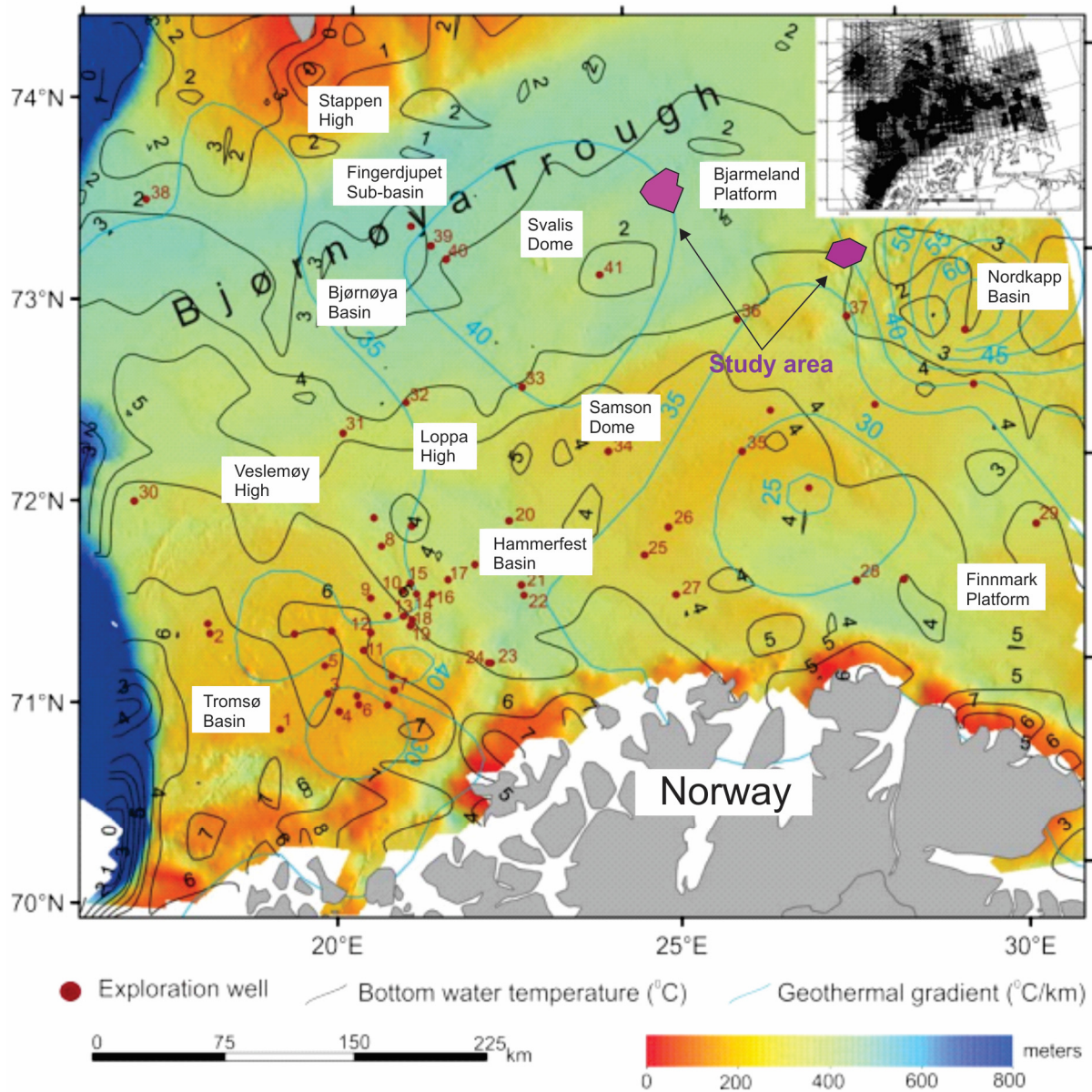


Figure 13. Bathymetry of the SW Barents Sea. Bottom water temperatures indicated along black lines (NODC, 2009). Geothermal gradients are indicated along blue lines (NPD; Bugge, et al., 2002). Purple polygons illustrates study areas. Modified from Vadakkepuliambatta, et al., (2014).

### 3.4 Glacial history of the SW Barents Sea

The glacial history of the Barents Sea involves build-up and decay of ice sheets on the continental shelves during the Quaternary, where the Barents Sea continental shelf has been waxed and waned numerous of times (Jakobsson, et al., 2014; Patton, et al., 2015). This have led to glacial erosion on the continental shelf, and deposition and subsidence at continental margins which have been recorded in thicker sediment packages in the south-western most

outer continental shelf (Faleide, et al., 1996; Solheim, et al., 1996; Vorren & Laberg, 1997; Butt, et al., 2000). At the SW Barents Sea margin the glacial sediments are up to 3-4 km thick, whereas they thin out to few hundred meters in the central Barents Sea (Vorren, et al., 1984; Elverhøi, et al., 1989). The glacial sediments and the older sedimentary bedrock are separated by the erosional Upper Regional Unconformity (URU) (Vorren, et al., 1986). Several studies have indicated that a major ice sheet was initiated and built up over the north-western Barents Sea shelf during Late Weichselian (25-10 ka) (Figure 14) (Lubinski, et al., 1996; Polyak, et al., 1997; Landvik, et al., 1998; Kleiber, et al., 2000). Eventually this major ice sheet expanded to the northern and western margins, and according to Landvik et al. (1998) the front of the ice reached the western shelf edge between 19 and 15 ka (Landvik, et al., 1998). The maximum ice thickness in the Barents Sea was between 1500-1800 m during the Late Weichselian glacial maximum (Svendsen, et al., 2004).

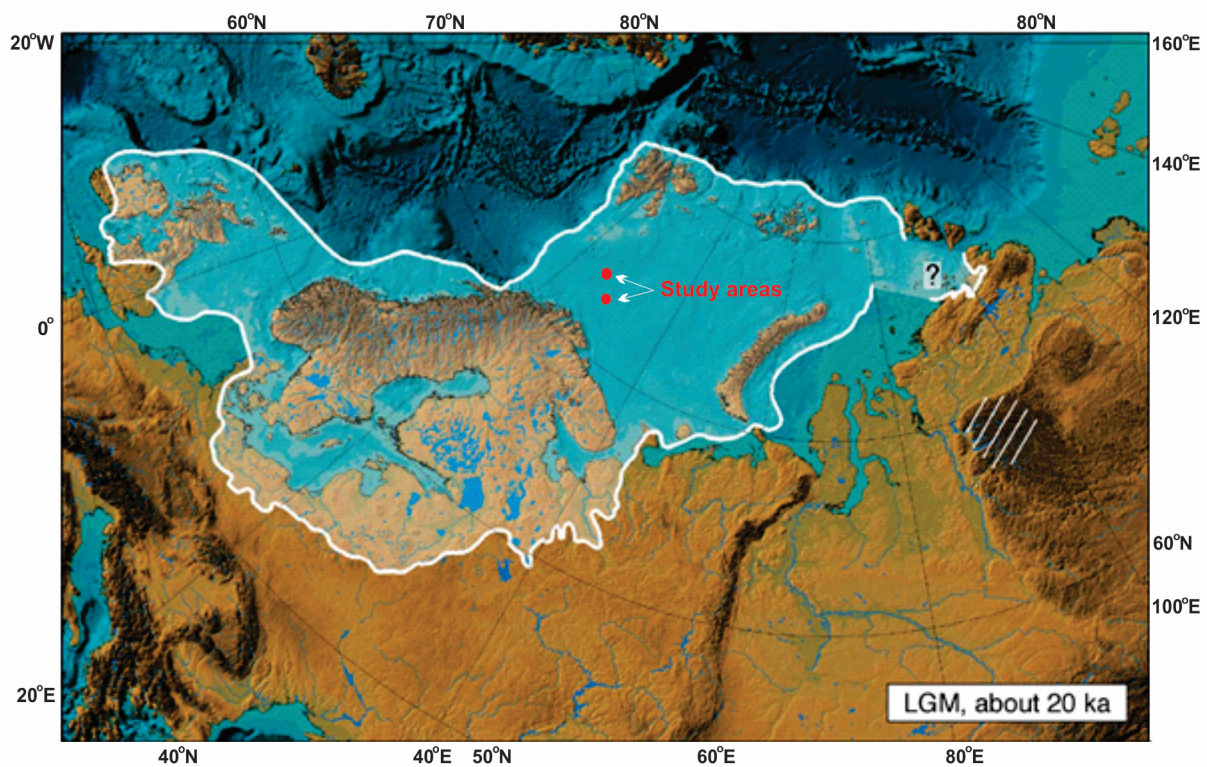


Figure 14. The figure shows a reconstruction of the Eurasian ice sheets at the Late Weichselian glacial maximum (LGM). Glacier distribution in this figure only focuses on the distribution of Eurasian ice sheets, hence ice distribution over Iceland, Greenland Alps and other mountains areas are not shown here. Study areas illustrated in red dots. Modified from Svendsen, et al., (2004).

During the LGM, the drainage of ice was dominated by Bjørnøya Trough Ice Stream, which was fed by ice streams from other source areas in the central Barents Sea such as



Sentralbanken Trough, Storbanken and Storbanken Trough (Bjarnadóttir, et al., 2014). Deglaciation was first initiated along the western continental margin at around 19 calibrated years before present (cal ka BP), and coincides with rising global eustatic sea level. The Bjørnøya Trough Ice Stream (Figure 15) is suggested to have retreated rapidly with periods of stagnation, which is evidenced by grounding zone wedges (Winsborrow, et al., 2010).

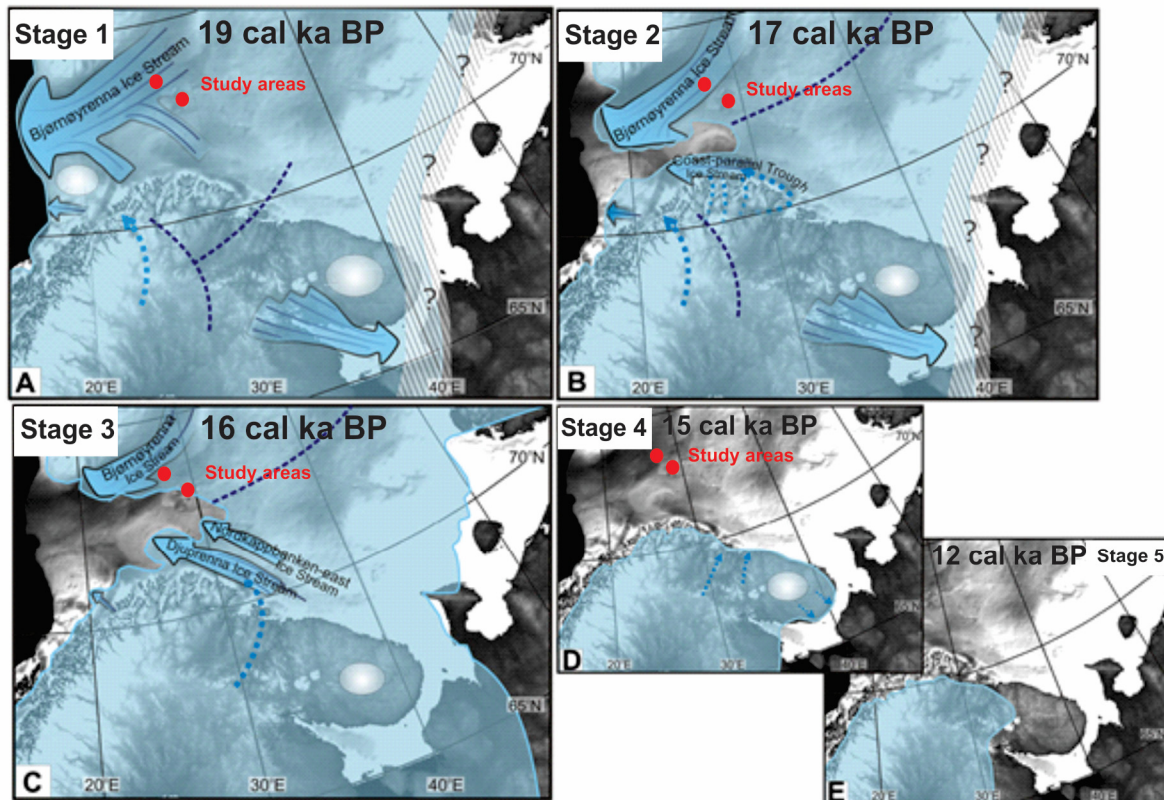


Figure 15. The figure shows a five stage reconstruction of the Late Weichselian glacial maximum and its subsequent deglaciation. The construction is made by (Winsborrow, et al., 2010). In the figure; ice streams (blue arrows) warm-based ice (dashed blue arrows), cold-based ice (white discs), possible ice divides (dashed dark blue lines). Modified from Winsborrow, et al., (2010).

The whole Barents Sea continental shelf was covered by ice at the Late Weichselian maximum (Figure 15; stage 1). Bjørnøya Trough dominated drainage of ice sheets, and it was fed by vast sources to the north and north-east. When deglaciation was initiated at around 19 cal ka BP, it happened rapidly with a withdrawal of ice sheets from the western Atlantic margin into the Bjørnøya Trough and eastward (Figure 15; stage 2). The period of withdrawal was around 2000 years, and during this retreat several episodes of rapid readvance occurred, separated by short periods of ice margin stability (Figure 15; stage 3). The ice margin had retreated onshore by 15 cal ka BP (Figure 15; stage 4), and by this stage the pace



of deglaciation had slowed significantly. The onshore ice sheet retreatment occurred at a slow pace, and by 12 cal ka BP the ice sheet still covered most of the northern Scandinavia (Figure 15; stage 5). Bjørnøya Trough was almost ice free by 16 cal ka BP (Winsborrow, et al., 2010), and most of the SW Barents Sea was ice free by 15 cal ka BP (Vorren & Laberg, 1996; Landvik, et al., 1998). Winsborrow et al (2010) emphasize that deglaciation of the Barents Sea, coincides with, and was most likely triggered by the rising global eustatic sea level. It is suggested that the rapid removal of ice sheets in the western Barents Sea was permitted by large iceberg calving, whereas the rate of retreat slowed significantly when the ice retreated onshore (Winsborrow, et al., 2010).

## 4 Data and Methods

### 4.1 Seismic data

The seismic datasets used in this thesis are located in Bjarmeland Platform, Hoop Fault Complex and partly Mercurius High (Figure 16).

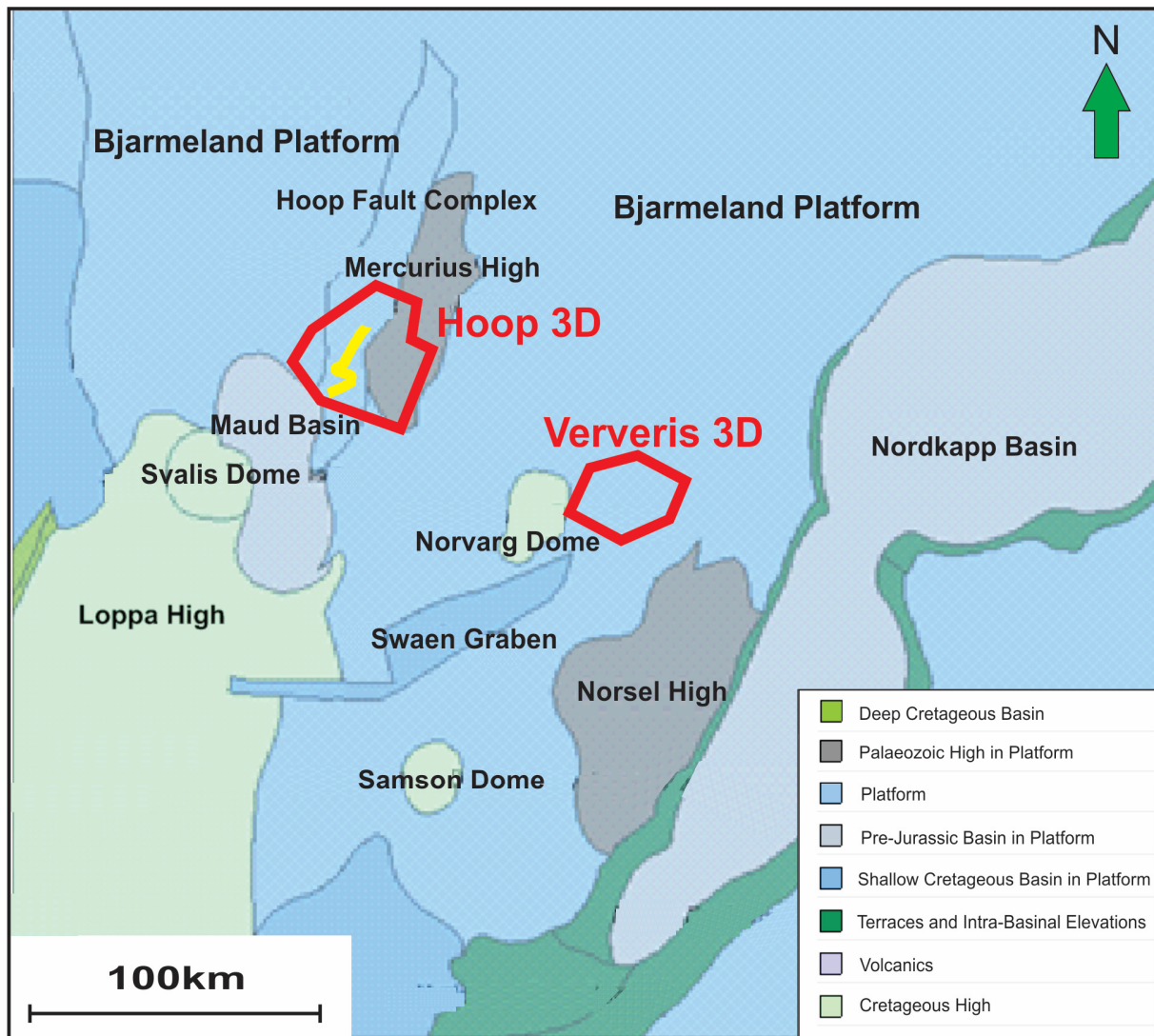


Figure 16. Map illustrating the location of the seismic datasets. The red polygons illustrate the 3D datasets and the yellow line illustrate the location of the 2D P-cable seismic section. Modified from NPD FactMaps 2016.

#### 4.1.1 Ververis 3D (ST07M16)

The 3D seismic dataset Ververis 3D (Figure 16) was acquired in two phases, the first from 30<sup>th</sup> September 2006 – 20<sup>th</sup> October 2006, and the second from 20<sup>th</sup> May 2007 – 20<sup>th</sup> June 2007. The survey was acquired by the vessel MV Geowave Command on behalf of Statoil ASA, at the location of the Ververis dome structure located in PL395 on Bjarmeland Platform

in the SW Barents Sea. The geometry of the acquisition comprises dual sources which were fired in flip-flop fashion with 8 cables, thus generating a swath of 16 subsurface lines. The airgun was a BOLT LLX, and the shot interval was 12.5 m, with a receiver group interval of 12.5 m. The sample rate at acquisition was 2 ms, and the sampling interval in the processed dataset is 4 ms, insinuating a frequency content up to 250 Hz.

#### 4.1.2 Dataset at Hoop Fault Complex

The 3D dataset Hoop 3D (Figure 16) is a reprocessing of the five vintage surveys: HFC09, HFCE11, HFCW11, HFCN11 and HFCNW13. The reprocessing occurred between January 2015 and August 2015, and the dataset covers 7701 km<sup>2</sup> in the Hoop Fault Complex (Figure 16). This reprocessing aimed to provide a seamless volume processed through the Clari-Fi™ sequence and thus enhance the bandwidth, and utilizing modern demultiple techniques at the same time. The result is a broadband seismic dataset which provides greater richness of both high frequencies which aid temporal resolution, and more robust low frequencies which provides better imaging of deeper structures. The five reprocessed datasets was all gathered from an airgun with shot interval 37.5 m, and a receiver group interval of 12.5 m. Sampling rate for all datasets at acquisition was 2 ms, whereas the sampling rate at the reprocessed datasets are both 2 ms and 4 ms.

#### 4.1.3 P-cable dataset at Hoop Fault Complex

The 2D P-cable dataset was acquired from June 2014 – December 2014. The 2D survey was acquired by the vessel WGP Bergen Surveyor on behalf of Statoil ASA, and the survey stretches 733 km around Bjarmeland Platform and Hoop Fault Complex. The dataset was acquired from an airgun with a shot point interval of 12.5 m and a sampling rate of 0.5 ms. The gun depth was 2.5 m, and a water bottom mute (PRCMIG) was used during acquisition. During processing, the dataset was resampled from 0.5-1 m and processed through the Clari-Fi™ sequence to enhance the bandwidth (TGS, 2014). Only the part of the P-cable seismic dataset within Hoop Fault Complex is available for the purpose of this thesis (Figure 16).

#### 4.1.4 Petrel as interpretation tool

Schlumbergers Petrel 2014 software is used in this thesis for visualization and interpretation of the seismic datasets. The P-cable dataset is solely a 2D seismic dataset where the seismic sections are illustrated in to-way-travel time (TWT), whereas for the 3D seismic datasets from Hoop and Ververis the seismic sections are interpreted and illustrated both in to-way-travel time (TWT) and true vertical depth (TVD). Two attribute analysis tools are used in this thesis to help interpret and illustrate distribution of gas hydrates and their possible relation to the deeper fluid flow system of the SW Barents Sea:

*Variance*: Extract value from a seismic variance cube may help provide information of fault patterns in the sediments. This attribute analyses and illustrates the local variance in the seismic signal, and is thus useful when investigating discontinuities in seismic reflectors related to stratigraphic terminations and fault structures.

*Minimum Amplitude* attribute generates reflectivity within a time/depth window in seismic datasets, and is used as a hydrocarbon indicator as hydrocarbons often cause negative amplitudes in seismic data. In this thesis it may help generate distribution maps of BSRs as the base of gas hydrates often overlies free gas sediments.

## 4.2 Gas composition

Analyses from shallow gas samples in the SW Barents Sea are very few or non-existent, hence gas samples from wells may provide a good approximation of the gas which forms gas hydrates. Depending on temperature and pressure changes, the gas composition may vary as it migrates upward in the sediments (Vadakkepuliambatta, et al., 2014). However, changes in quantity of methane is considered relatively small, and should not have a significant impact on the estimated depth of the BSR (few tens of meters) (Ostanin, et al., 2013; Vadakkepuliambatta, et al., 2014). When doing the gas hydrate stability modelling for the study area within Ververis Dome structure, it has been chosen a gas composition of 100% methane and a detailed gas composition from well 7226/2-1. For the gas hydrate stability modelling within Hoop Fault Complex, a relatively shallow gas composition (198 m depth) from well 7324/8-1 is used to generate the model. This would provide a good approximation of the estimated BSR where higher order of hydrocarbons are present. It has

also been carried out a gas hydrate stability model for a gas composition of 100% methane, to establish if pure methane hydrates may be stable in the area.

### 4.3 Gas Hydrate stability modelling

The gas hydrate stability models were generated using the CSMHYD software from Sloan (1998). This software calculates the pressure-temperature conditions for the phase transition between free gas and gas hydrates (Sloan, 1998). CSMHYD calculates the pressure conditions at the transition phase at which hydrates may be stable at a given temperature, hence the input parameters are gas composition and bottom water temperature. The program can also include a variable salinity component, and in the study area a salinity of 35‰ has been chosen. This matches the salinity of previous gas hydrate stability models made for the SW Barents Sea, i.e. Chand et al. (2008) and Vadakkepuliambatta et al. (2014). The geothermal gradient for well 7226/2-1 has previously been suggested to be at around 0.036 °C/m by Vadakkepuliambatta, et al., (2014). The geothermal gradient in well 7324/8-1 is estimated to be around 0.04 °C/m (Rokstad, et al., 2014). However, shallow bottom hole temperatures from the well, in combination with estimated bottom water temperature from World Ocean Database (NODC, 2009) is used to generate a more accurate geothermal gradient for the shallowest sediments. Such a shallow geothermal gradient approximation will also be carried out and discussed for well 7226/2-1, although the bottom hole temperatures here are logged deeper in the sediments.

Included in the generated models (Figure 17) are phase boundaries for 100% methane (blue curve) and phase boundaries which contain gas composition (red curve) from the nearby well from where the model is generated. The seafloor is also included (black line), and from the seafloor and downwards in the sediments are the geothermal gradient (yellow line). At the crossing point of the geothermal gradient and the phase boundaries are the modelled BSR, which are illustrated in each model (dashed blue and dashed red lines).

## GHS model: Illustration

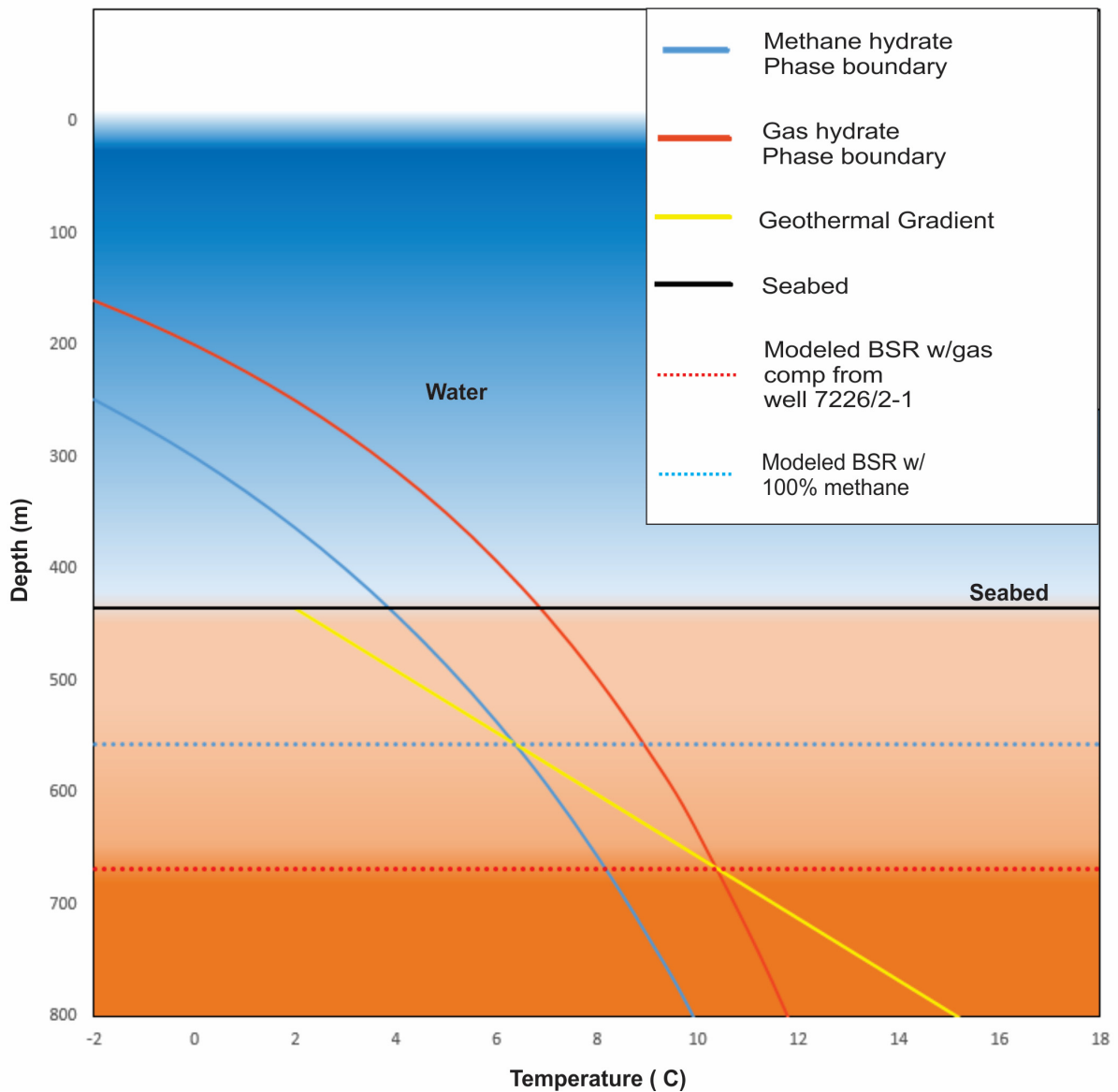


Figure 17. Illustration figure of a gas hydrate stability model. Included in the model are: methane hydrate phase boundary (blue curve), gas hydrate phase boundary (red curve), seafloor (black line), geothermal gradient (yellow line), modelled BSR for 100% methane (blue dashed line) and modelled BSR for gas composition from well 7226/2-1 (red dashed line). The gas composition in this illustration (well 7226/2-1) is 98% C1, 1.2% C2, 0.31% C3, 0.04% iC4, 0.03% nC4, 0.02% C6 and 0.38% CO<sub>2</sub>. Conditions during times of deglaciation at location of well 7226/2-1 is used in this illustration model.

For each modelled location in this thesis, three different models have been made: a model for present day conditions, a model for assumed conditions at around Last Glacial Maximum (22 580 BP - 22 780 BP) and a model for assumed conditions during deglaciation (15 380 BP - 16 830 BP). Conditions such as ice sheet thickness and bottom ice temperatures at Last Glacial Maximum, and eustatic sea level at the start of deglaciation time is estimated by researcher Henry Patton from CAGE and the methods is described in Patton et al. (2016) (In

Prep) and Auriac et al. (2016) (In Press). The gas composition used in the gas hydrate stability modelling is the same for present day conditions, conditions during deglaciation and conditions during Last Glacial Maximum. For these three conditions it has also been carried out a model for gas composition of 100% methane. The geothermal gradient for these three conditions has also been kept the same, as it would be highly complicated to elaborate the possible changes in geothermal gradient through such a prolonged time event.

#### 4.3.1 Model for present day conditions

The gas composition in the exploration well 7226/2-1 is generated at a depth of 534 m below the seafloor. The gas composition from well 7324/8-1 is generated at a depth of around 198 m below the seafloor. Bottom water temperatures are estimated from CTD measurements (NODC, 2009). The density of the sea water is set to 1027 kg/m<sup>3</sup> in the models.

#### 4.3.2 Model for conditions during deglaciation (15 380 BP -16 830 BP)

The relatively water depths at the time of deglaciation is calculated by a model described in Hubbard (2004), and would be thicker in all modelled locations compared to present day conditions. The bottom water temperature in the study areas have been assumed to be 2°C.

#### 4.3.3 Model for conditions during Last Glacial Maximum (22 580 BP - 22 780 BP)

During Last Glacial Maximum it has been calculated an ice sheet of around 1870 meters in the Bjarmeland Platform at location of well 7226/2-1, and 1723 m at the location of well 7324/8-1. For the model this means that seawater is exchanged with a thick layer of ice, thus the density changes from 1027 kg/m<sup>3</sup> in seawater to a density of 920 kg/m<sup>3</sup> in ice. The ice thickness will have a major implication on the gas hydrate stability, as the pressure conditions increases significantly.



## 5 Results

2D and 3D seismic datasets from locations around Ververis Dome structure and Hoop Fault Complex on the Bjarmeland Platform, have been used to identify the lateral and vertical distribution of possible BSRs in the area. BSR-like features have been inferred to provide indirect evidence of gas hydrates in the study area. Attribute maps and seismic sections given in this chapter aims to provide information of the possible correlation between gas hydrates and the deeper fluid flow system in the study areas.

Additionally, it has been carried out numerical models for the stability field for gas hydrates in chosen locations in the study area. The gas hydrate stability modelling is carried out for present day conditions as well as for conditions during the last Glacial Maximum and for early deglaciation. The aim of the numerical modelling is to support the indirect evidence of gas hydrates from the seismic datasets, as well as to model out gas hydrate stability conditions during deglaciation and Last Glacial Maximum.

### 5.1 Ververis 3D

Ververis is a faulted dome structure located in PL395 on Bjarmeland Platform in the SW Barents Sea. The Ververis 3D survey area is approximately 540 km<sup>2</sup>. Within the seismic dataset located around Ververis, well 7226/2-1 was drilled in 2008. The well showed gas in the Kobbe Formation, and was plugged and abandoned in July 2008 as a gas discovery. The gas composition from this well has been central for the numerical modelling of the BSR. The bathymetry of the seafloor in the seismic survey (Figure 18) shows a seafloor that varies in depth from approximately 400 m in the north-west to approximately 200 m in the south-east.

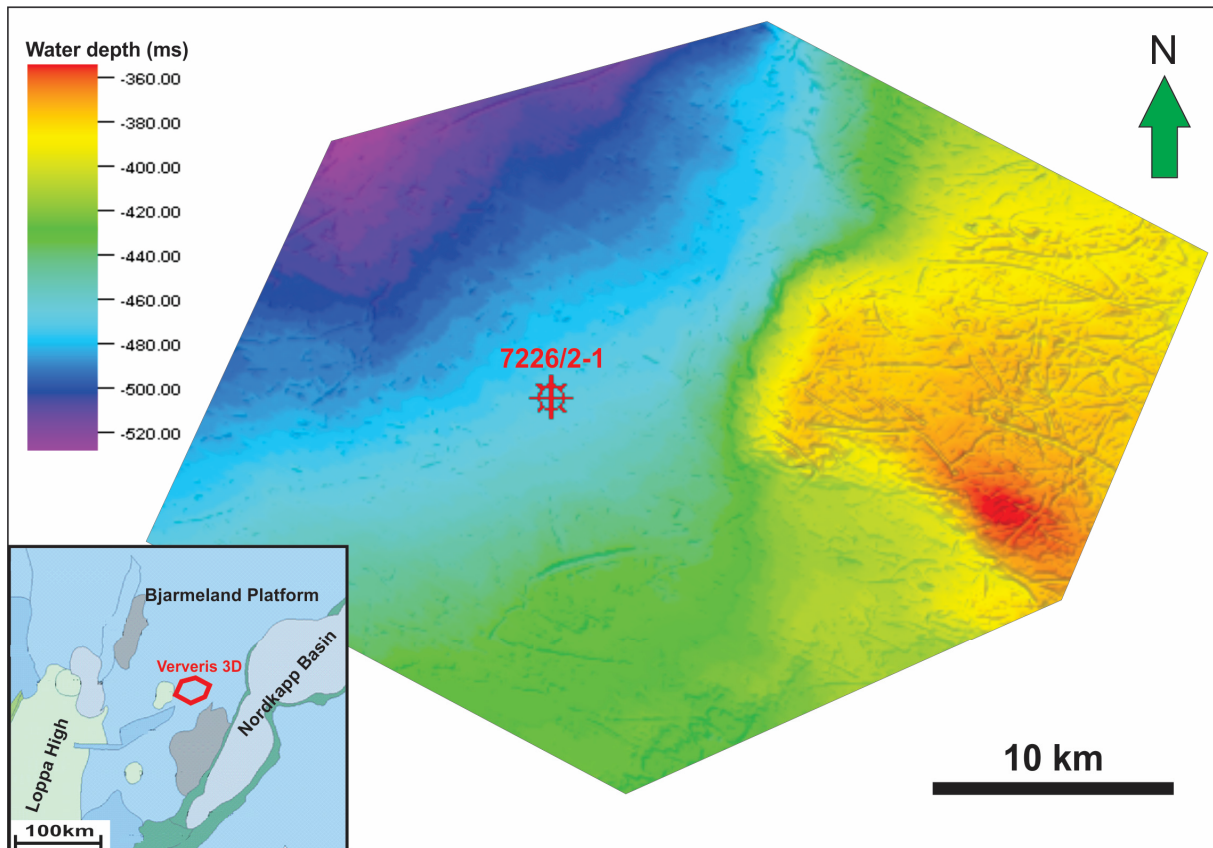


Figure 18. Bathymetric map of the seabed around Ververis Dome structure. Location of well 7226/2-1 is illustrated in the Figure. The inset map illustrates the location of the study area in the SW Barents Sea.

The location of well 7226/2-1 is located at 347 m water depth (Downs & Knox, 2007). The seafloor is reported to consist of 1-2 m soft clay sediments overlying firm silty clay (Kleiven & Ersdal, 2008). Throughout the survey there are numerous iceberg ploughmarks and many of the ploughmarks are partly infilled (Figure 19).

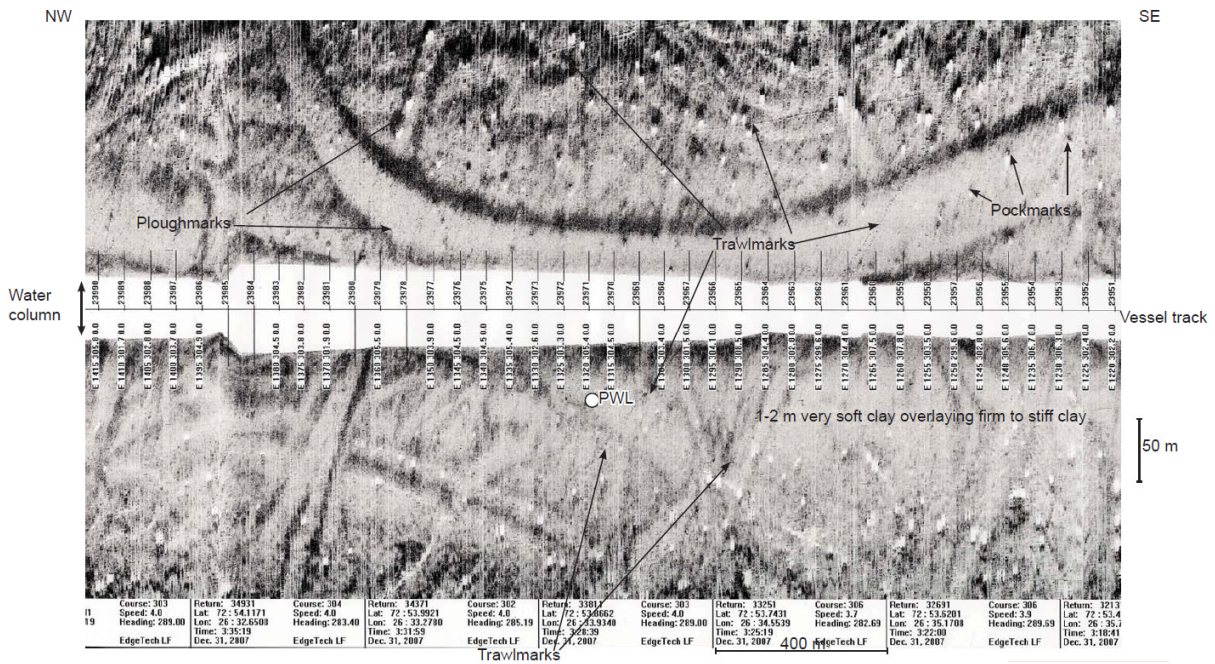


Figure 19. Vessel track of seafloor from side scan sonar-line ST0792-04010 in the study area. Site surveying shows presence of ploughmarks, trawls and pockmarks on the seafloor within the study area. From Kleiven & Ersdal, (2008).

The side scan sonar line (Figure 19) illustrates trawl marks, ploughmarks and pockmarks on the seafloor within the study area. The trawl marks are typically caused by fishing trawls and differs in all directions, and are typically much thinner than ploughmarks. The ploughmarks are generally 50-100 m wide and 1-3 m deep, and they are reported to vary in length from hundreds to kilometers with no preferred orientation. The interpreted pockmarks observed (Figure 19) have previously been described as numerous small depressions on the seafloor in the survey area, generally in the range of 1-3 m deep and up to 20 m in diameter (Kleiven & Ersdal, 2008).



### 5.1.1 Fluid flow systems

Previous site survey report from the study have suggested faulted and deep-rooted faults (Figure 20) below Pleistocene deposits (Kleiven & Ersdal, 2008).

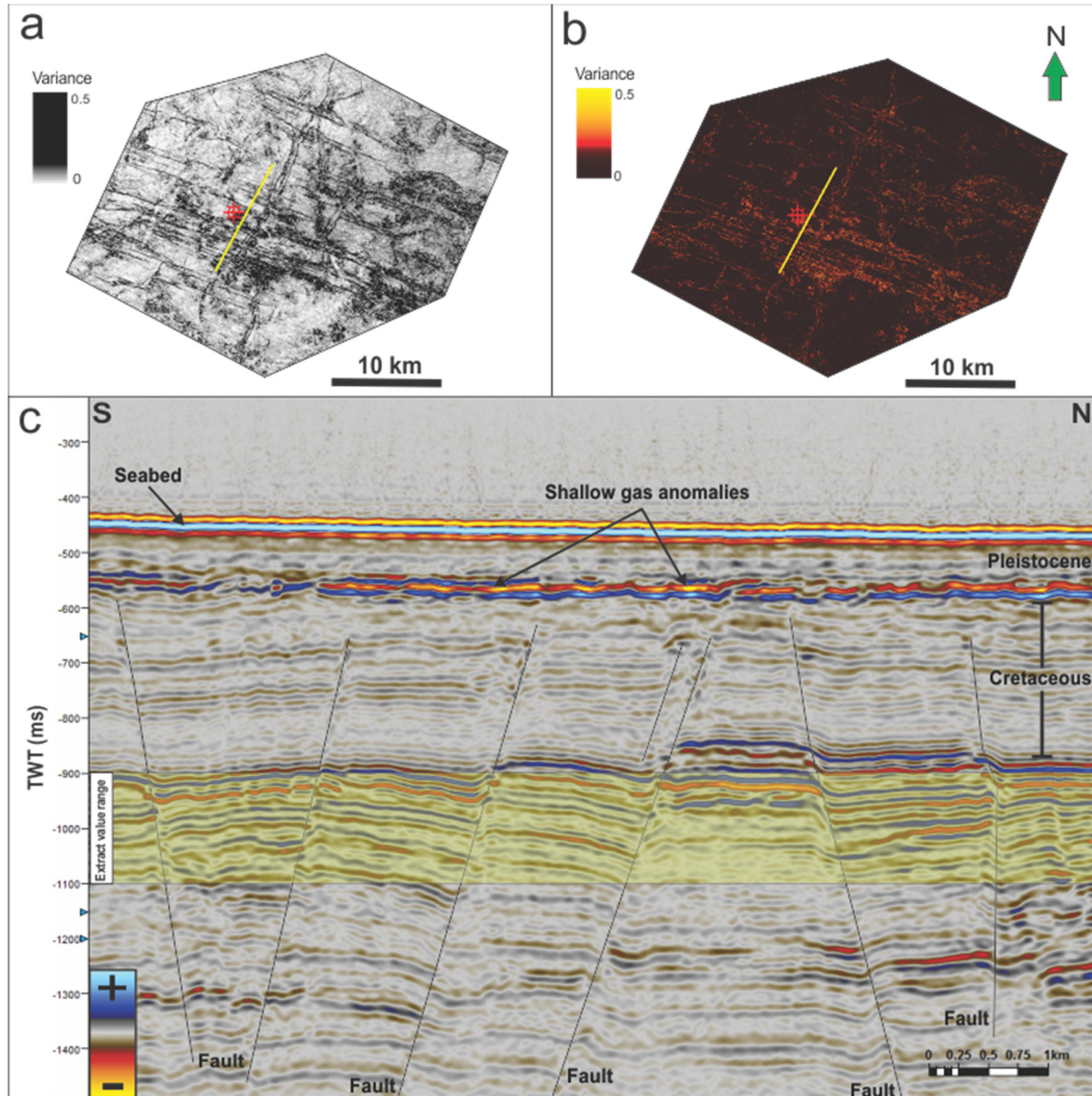


Figure 20. a-b) The variance attributes are generated from the unit package illustrated in yellow transparency in c. The yellow line in a) and b) indicates the seismic section illustrated in c. c) Seismic section illustrating a system of faults, and overlying shallow gas anomalies. Both horst and graben structures may be observed in c.

The variance maps (Figure 20a, Figure 20b) illustrate the lateral pattern and distribution of the fault system in the area, and it may be suggested that there is a system of faults extending from northwest to southeast. It is also possible to observe several faults extending diagonally across this NW-SE system of faults in the survey. Seismic section (Figure 20c)

through the area suggest deep-rooted faults extending through Cretaceous sediments and almost up to the interpreted shallow gas anomalies below the Pleistocene sediment package. Although most faults seem to be dipping towards north in the seismic section, some of the faults dip towards south and form a Graben structure in the southern part of the seismic section. Slightly towards the northern part in the seismic section, a faulted Horst structure has been formed followed by a possible Graben structure towards north. Above these faulted structures exist a strong, but discontinuous reflector which has been interpreted to be shallow gas anomalies. These shallow gas anomalies are paralleling or sub-parallel the seabed at around 100-105 ms, and may be suggested to relate to gas hydrates and may thus be inferred to be bottom simulating reflectors (BSR). However, this is also the depth at which the URU is expected to be located, hence more evidence should be considered before interpreting it as BSR.

Kleiven & Ersdal (2008) have described and interpreted the shallow sediments at the location of well 7226/2-1 (Figure 21) to be of firm to stiff silty clay, with an overlying thin (1-2 m) layer of very soft clay. The clay becomes stiffer with depth, and coarser material up to boulder size may be present in the sediment package. At the base of this sediment package there is a tentative discontinuous reflector with normal polarity at the well location, which has been interpreted to be an erosion surface near the base of the Pliocene/Pleistocene sequence. Below this erosion surface it has been observed a thicker sequence of weak, discontinuous and sub-parallel reflectors which have been interpreted to consist of claystone, siltstone and calcareous grading marl with occasionally lenses of sandstone. Below this package of weak discontinuous reflectors it has been observed a package of much stronger sub-parallel reflectors with normal polarity. This package has been interpreted to consist of claystone. Both the package of claystone, siltstone and calcareous grading marl, and the package of claystone has been disturbed by heavy faulting (Kleiven & Ersdal, 2008).

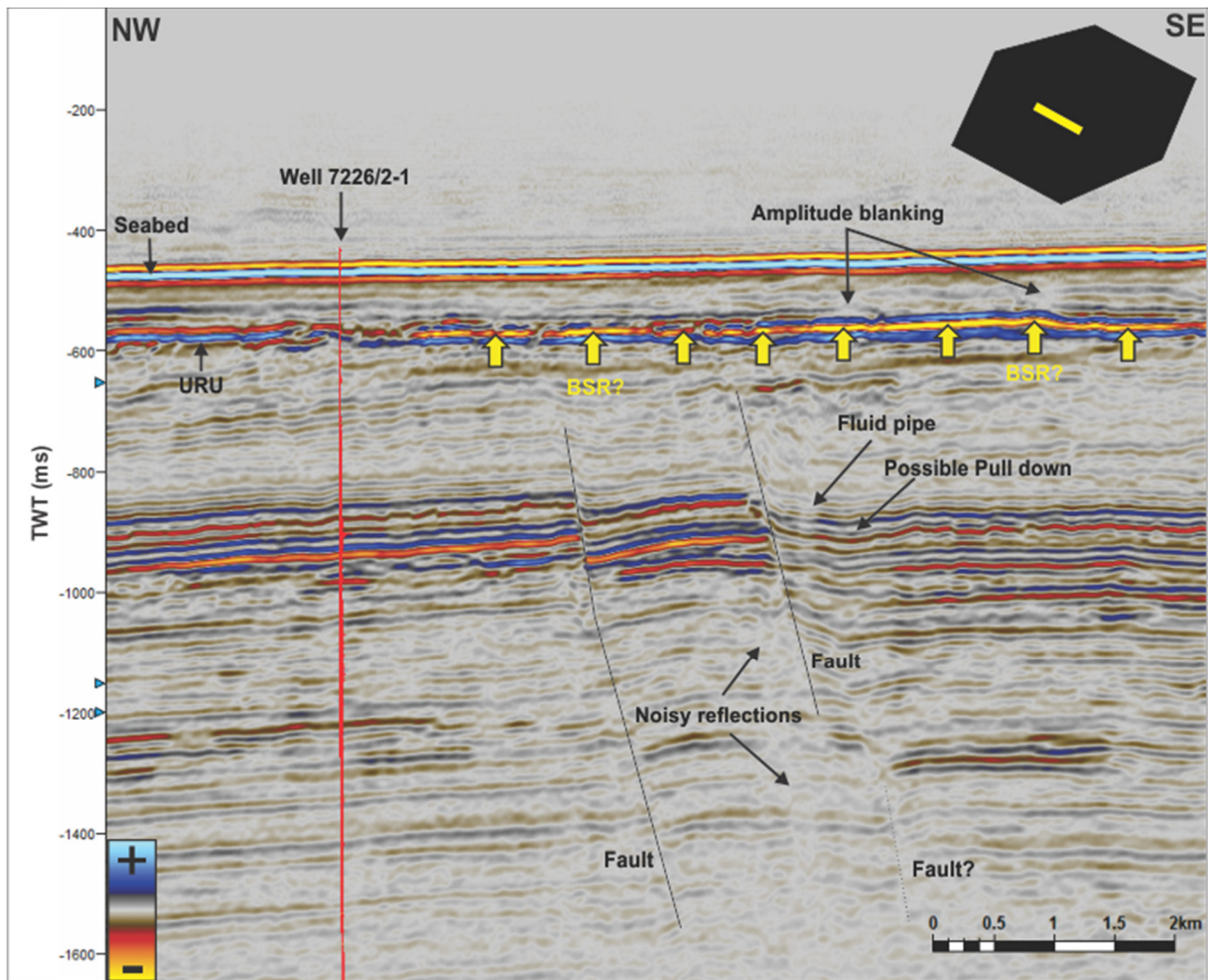


Figure 21. Seismic section crossing well 7226/2-1. The yellow line in the black polygon in the corner indicated where the seismic section is generated from. The vertical red line in the seismic section indicates well 7226/2-1. Interpretations in the sections are indicated with black arrows: Seabed, URU, fluid pipes, faults, noisy reflections, and possible pull down. The yellow arrows indicates interpreted BSRs.

Around 100-120 ms below the seafloor at well 7226/2-1 (Figure 21), a high amplitude reflection appears in the seismic section. This reflection seems to have a normal polarity just at the location of the well and in the northwest direction of it. This suggests that the reflector may be related to the separation of the Pliocene/Pleistocene sediments from the underlying Cretaceous, hence it has been interpreted as the URU. Just below the URU it is observed a package of weaker sediments which are dipping relative to the URU, and may be suggested to be truncated by the URU. Following the interpreted URU at the south-eastern side of the well position, it seems clear that the seismic reflection changes to reversed polarity and extends 6-7 km towards southeast in the study area. Such a reversed polarity is often related to gas anomalies, and it may indicate trapped gas below the Pliocene/Pleistocene package or at the top of the truncated sediments below the URU. The



shallow gas anomaly may also be related to gas hydrates, hence it may be interpreted as BSR. Below this possible BSR appear a few pipe like structures with distorted and dimmed seismic response interpreted as possible fluid pipes, and 2-3 faults, indicating possible fluid migration pathways. There is a possible pulldown on the south-eastern side of the rightmost fault in the seismic section (Figure 21), although this may also be inferred as a subduction related to the fault. Deeper in the seismic section it is observed noisy or patchy reflections, which may suggest possible upward migrating fluids.

At around 5-6 km north-northeast of the location of well 7226/2-1, there is strong evidence of fluid flow (Figure 22), and several fluid flow related features are observed:

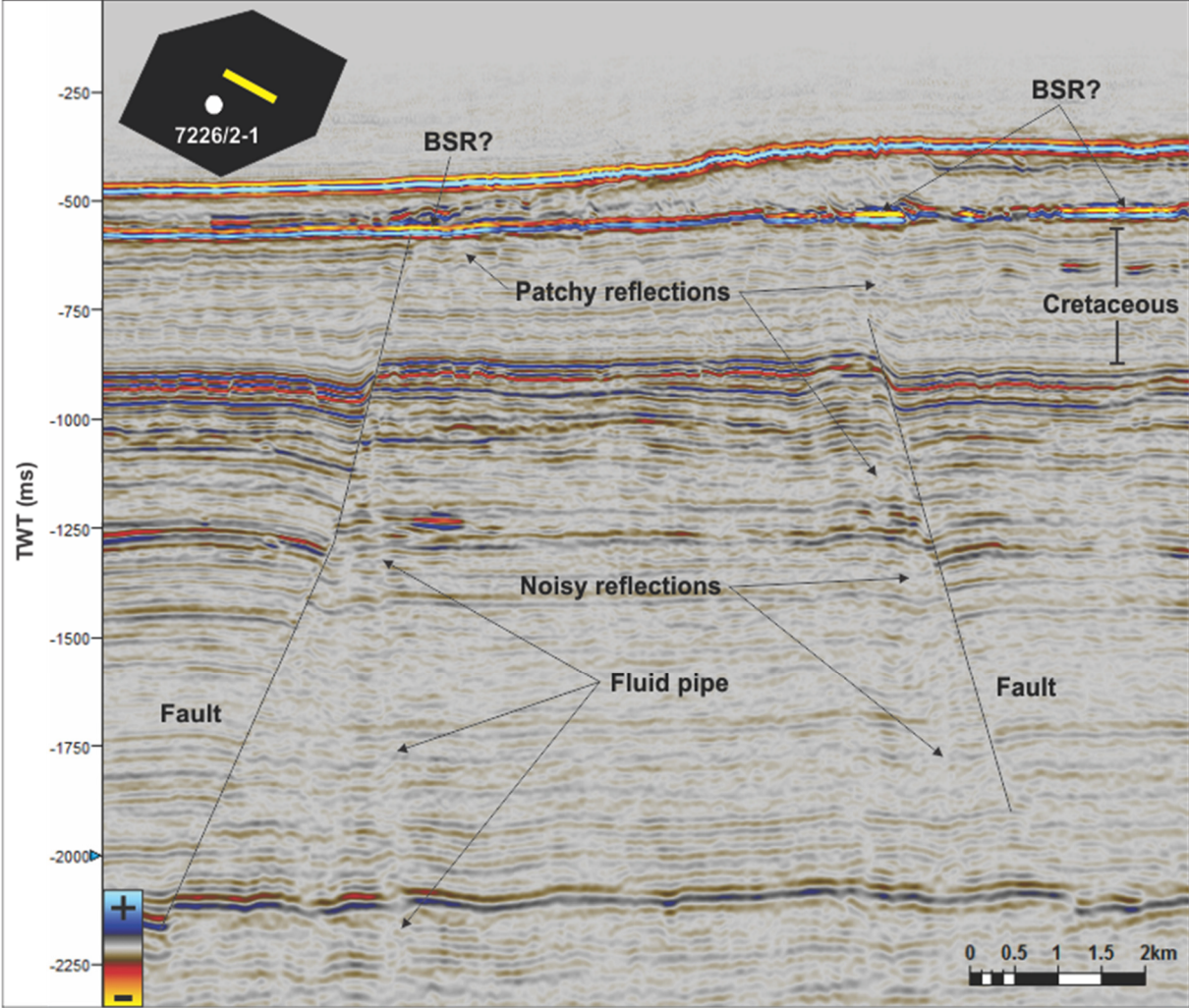


Figure 22. Seismic section north-east of well 7226/2-1. Indicated in the section are fluid flow features such as faults and fluid pipes. Other seismic indications of fluid flow indicated are noisy and patchy reflections. BSR-like features are also indicated. The yellow line in the black survey polygon indicated the location of the seismic section.



Pipe like structures with distorted and dimmed seismic response, interpreted as possible fluid pipes appear in the deeper part of the seismic section (Figure 22) and seems to extend up until it reaches the faults just below the Cretaceous sediments. Above the two interpreted faults in the seismic section it exist high amplitude reflectors with reversed polarity compared to the seafloor reflector. The high amplitude reflector towards northwest extends 3-4 km in the seismic section (Figure 22), whereas the anomaly above the fault in the south eastern part of the seismic section is less than 1 km wide. Both these reflections brightens up just above the two faults in the seismic section. This may be suggested to relate to fluid migration from the underlying fluid pipes and faults, hence it is interpreted as shallow gas anomalies. Far southeast of the same seismic section it appears another high amplitude anomaly with reversed polarity compared to the seafloor reflector, and this anomaly is around 1.5 km wide. This anomaly may also be related to shallow gas anomalies. All these shallow seismic gas anomalies are located at what is inferred to be the base of the Pliocene/Pleistocene sediments, and it correlates with most of the shallow gas anomalies observed in the study area (i.e. Figure 20 and Figure 21). The depth-correlation with other observations of shallow seismic gas anomalies in the area, the strong relations to the underlying fluid flow system, and the shallow depth at which these seismic anomalies are observed, may suggest that they are related to gas hydrates.

### 5.1.2 Distribution of BSR in the Ververis 3D

The distribution of inferred gas hydrate related BSRs is widespread in the Ververis 3D study area (Figure 23).

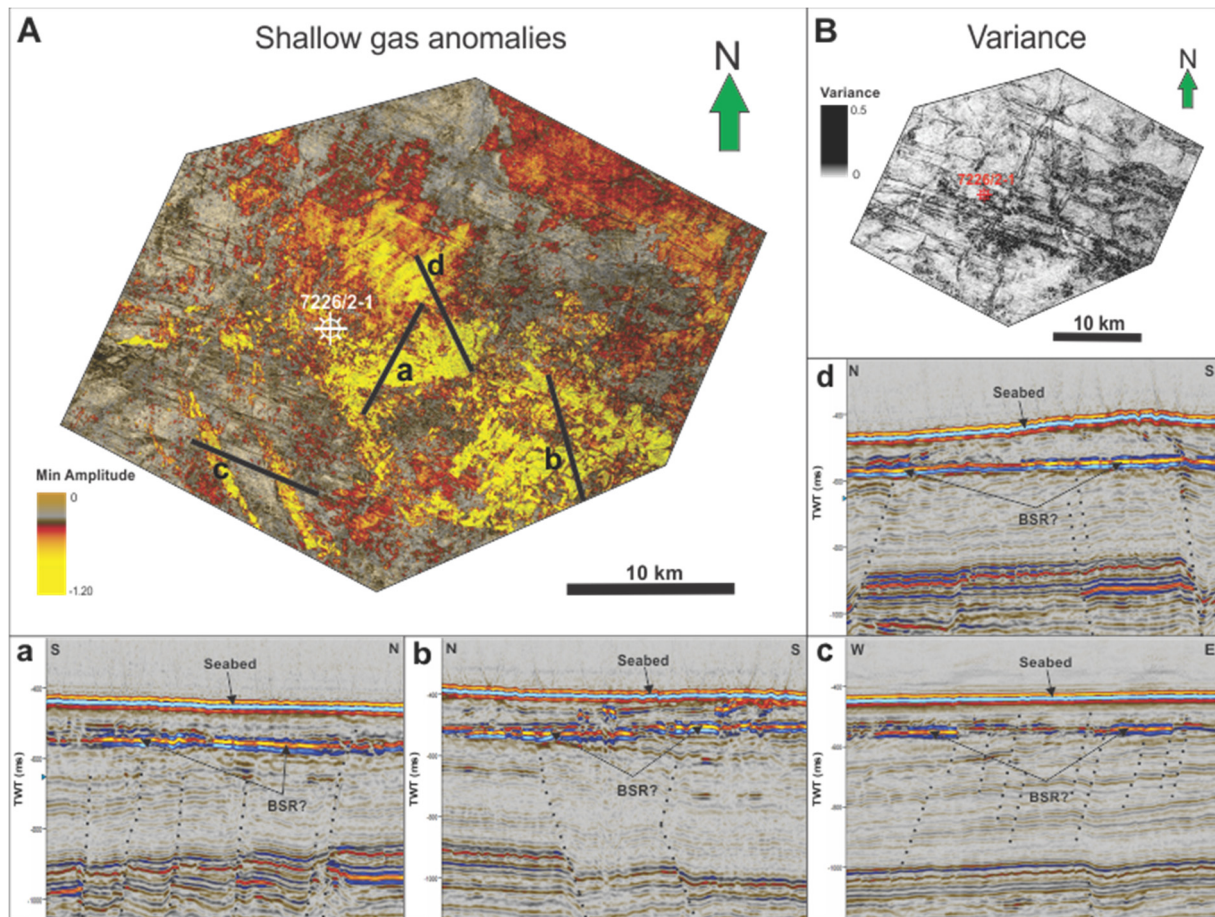


Figure 23. A) Minimum amplitude map of the shallow gas anomalies at the base of Pleistocene sediment package. The yellow colored areas shows the distribution of shallow gas anomalies in the study area. In the gray areas it is absence of shallow gas anomalies. Black lines indicate seismic sections in a,b,c and d. B) Variance map from 900-1100 ms, with the purpose of illustrating fault systems in relation to the distributions of the overlying shallow gas anomalies. Seismic sections a,b,c and d illustrates shallow gas anomalies or gas hydrate related BSRs. Black dashed lines in the seismic sections indicates possible faults.

A minimum amplitude map (Figure 23A) is a useful surface attribute to illustrate possible distribution of shallow gas anomalies or BSRs related to gas hydrates. Within the study area these shallow gas anomalies are widespread, but it is a relatively high density of shallow gas anomalies around and to the east-southeast of well 7226/2-1. This observation of the distribution of shallow gas anomalies correlates nicely with the underlying fault system (Figure 23B), where there are numerous faults located around and southeast of well 7226/2-

1. The seismic sections (Figure 23) illustrates examples of shallow gas anomalies inferred to be gas hydrate related BSRs. The interpreted faults in the same sections may be suggested as possible fluid migration pathways for the shallow gas anomalies.

5.1.3 Gas Hydrate stability model at well 7226/2-1

The numerical model for gas hydrate stability (GHS) at the location of well 7226/2-1, uses the exact gas composition given in the geochemistry data report (Mørkved, et al., 2008; Table 1) for the well. The gas composition is sampled at 534 meters sub-bottom depth. Although gas composition may change as it migrate upwards due to changes in temperature and pressure (Vadakepuliambatta, et al., 2014), the changes are considered relatively small and should only have a smaller impact on the depth (few tens of meter) of the estimated BSR (Ostanin, et al., 2013). The gas composition used for the modelling is described in Table 1:

<b>Gas type</b>	<b>C1%</b>	<b>C2%</b>	<b>C3%</b>	<b>iC4%</b>	<b>nC4%</b>	<b>iC5%</b>	<b>nC5%</b>	<b>C6%</b>	<b>CO<sub>2</sub></b>
<b>Value (%)</b>	98	1.2	0.31	0.04	0.03	0.01	0	0.02	0.38

*Table 1. The table shows the content of gas composition used for the GHS model at the location of well 7226/2-1.*

The gas composition (Table 1) is used in the model for both present day conditions, conditions during deglaciation and for conditions during Last Glacial Maximum at the location of well 7226/2-1. For each model, it has also been generated a numerical model for a gas composition of 100% methane. Table 2 provides information about other important parameters used in the GHS model at the location of well 7226/2-1:

	Present day	Early Deglaciation	Last Glacial Maxim
<b>BWT/Bottom ice Temp.</b>	3.7°C	2.0°C	-3.2°C
<b>Geothermal Gradient</b>	0.036 °C/m	0.036 °C/m	0.036 °C/m
<b>Water/Ice column</b>	347 m (water)	435 m (water)	1 870 m (Ice)

Table 2. The table provide information about the bottom water temperature (BWT), geothermal gradient water/ice column used in the GHS model at the location of well 7226/2-1.

Well 7226/2-1 did not provide bottom water temperature, thus bottom water temperature has been estimated from CTD measurements (NODC, 2009) in the study area. The geothermal is suggested to be at around 0.036 °C/m (Vadakkepuliambatta, et al., 2014). Based on the values in Table 1 and Table 2, the models (Figure 24) indicates the numerical depths of both gas hydrates and pure methane hydrates at present day conditions, during early deglaciation, and during Last Glacial Maximum:

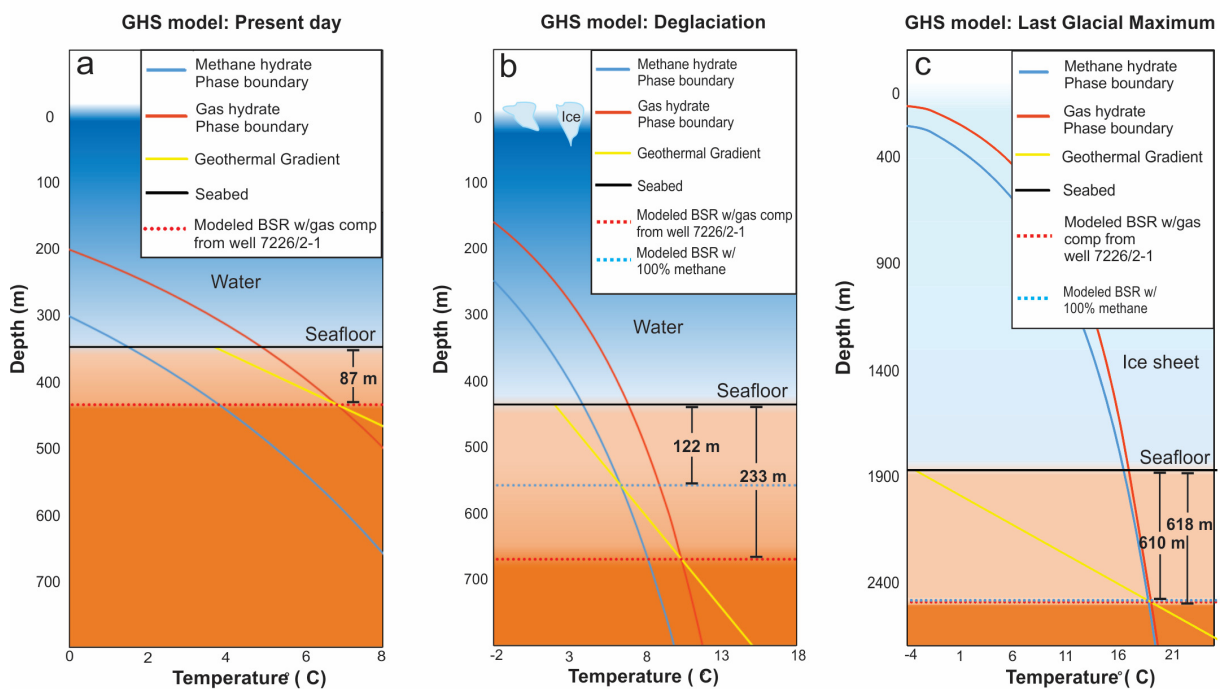


Figure 24. Gas hydrate stability model for location around well 7226/2-1. a) GHS model for present day condition: water column of 347 m, modelled gas hydrate stability down to 87 m below seafloor. b) GHS model for time of deglaciation (15 380 BP): water column of 435 m, modelled methane hydrate stability down to 122 m below seafloor, modelled gas hydrate stability down to 233 m below seafloor. c) GHS model for time of LGM (22 780 BP): ice sheet column of 1870 m, modelled methane hydrate stability down to 610 m sub bottom depth, modelled gas hydrate stability down to 618 m sub bottom depth.

The gas hydrate stability (GHS) model for present day conditions (Figure 24a) shows that pure methane hydrates are unstable in the study area at the location of well 7226/2-1. However, the model indicate gas hydrate stability conditions down to 87 m below the seafloor when using the sampled gas composition from the well. This suggests that gas hydrate stability conditions are present in the area at present day conditions. For gas hydrate stability conditions during early deglaciation (around 15 380 BP) (Figure 24b), the numerical modelling suggests presence of stable conditions for both pure methane hydrates and gas hydrates. The stability conditions for methane hydrates is calculated to be stable down to 122 m below the seafloor, whereas the stability conditions for gas hydrates is estimated to be stable down to 233 m below the seafloor. For gas hydrate stability conditions during Last Glacial Maximum (around 22 780 BP) (Figure 24c), numerical modelling suggests presence of stable conditions for both pure methane hydrates and gas hydrates. Methane hydrates is estimated to be stable down to 610 m below the seafloor, whereas gas hydrates is estimated to be stable down to 618 m below the seafloor.



## 5.2 Hoop Fault Complex

The Hoop Fault Complex is located between Loppa High and Bjarmeland Platform, and is a trending lineaments stretching from northeast to southwest in the SW Barents Sea. This thesis will focus on the part of Hoop Fault Complex which is centered around the well Wisting Central in PL 537 and PL 614 (Figure 25). The well 7324/8-1 (Wisting Central) was drilled in 2013 and was an oil discovery. The well was drilled down flanks on the structure, hence it may be a gas cap on the upper part (Rokstad, et al., 2014). The reservoir was located only 238 m below the seabed, which makes the gas composition from this well particularly interesting for numerical modelling of the BSR.

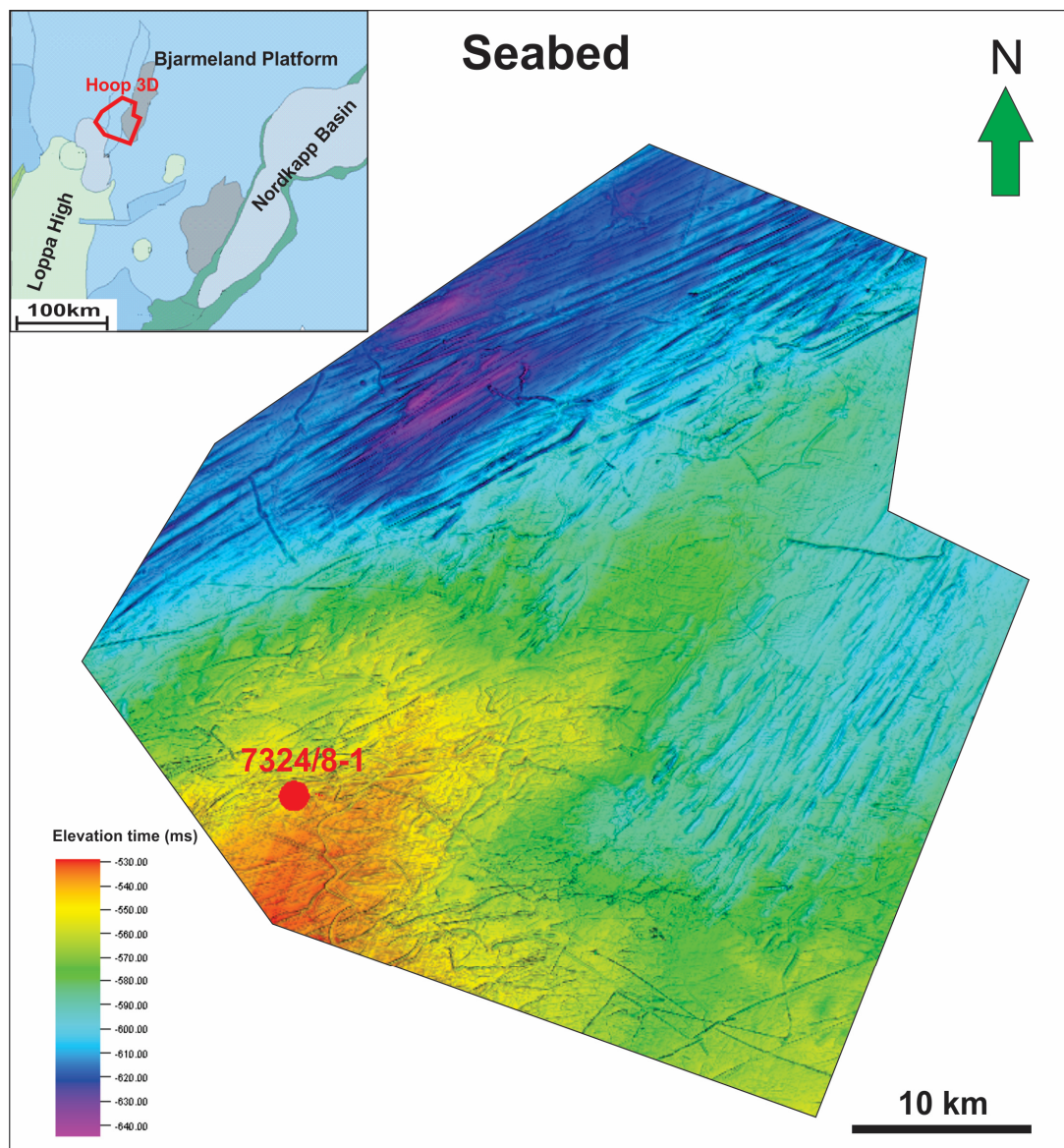


Figure 25. Bathymetric map of the seabed around Wisting Central. Location of well 7324/8-1 (Wisting Central) is illustrated in the figure. The inset map illustrates the location of Hoop 3D within the SW Barents Sea.

The bathymetry of the seafloor in the seismic survey (Figure 25) illustrates a seafloor that varies in depth from approximately 390 m to 480 m. The water depth at the location of well 7324/8-1 is 398 m. Within the survey it may be observed some major glacial lineation (MGL) extending from northeast to southwest. Throughout the survey numerous ploughmarks may also be observed, and they show no preferred orientation in the study area. The ploughmarks are typically a few tens of meter wide, few meters deep, and may extend up to several km in length. The quaternary package is reported to consist of comprising sand and clay, which gradually transforms into sandstone and claystone with depth. The quaternary is also described as partly silty (Rokstad, et al., 2014).

### 5.2.1 Fluid flow systems

Hoop Fault Complex are characterized by normal faulting (Figure 26). There are also reported listric faulting due to the development of anticlinal salt-related structures in the Maud Basin next to Hoop Fault Complex (Gabrielsen, et al., 1990).



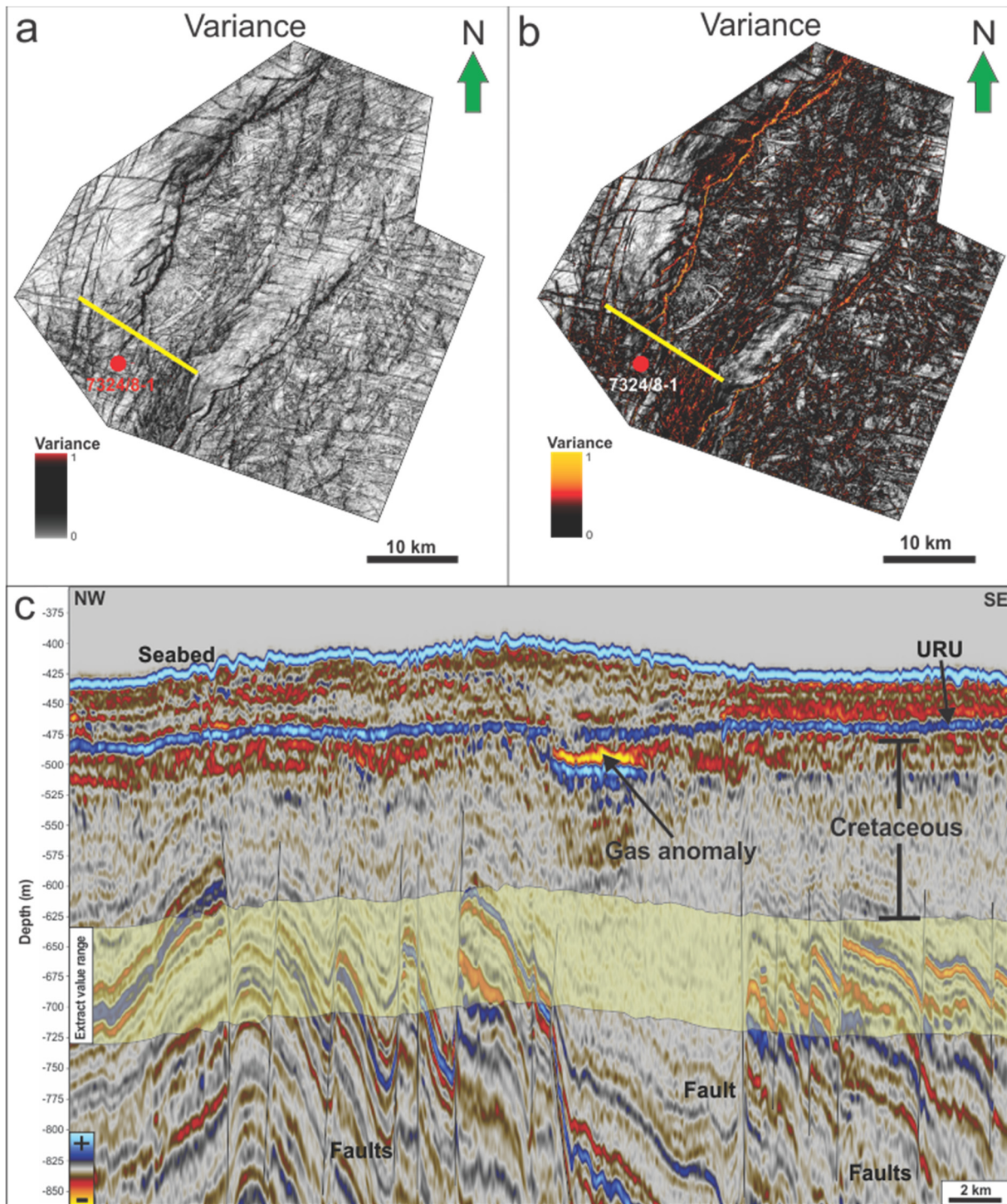


Figure 26. a-b) The variance attributes are generated from the unit package illustrated in yellow transparency in c. The yellow line in a) and b) indicates the seismic section illustrated in c. c) Depth converted seismic section illustrating a system of faults, and overlying shallow gas anomalies.

The variance maps (Figure 26a, Figure 26b) illustrate the lateral pattern and distribution of the fault system in the study area. It may be suggested that the fault system extends from northeast to southwest, and the seismic section (Figure 26c) suggests normal faulting in the area. The faults are deep-rooted and extends into lower and middle parts of the Cretaceous



unit package. Above this system of faults, it may be observed a high amplitude reflector stretching 3-4 km from southeast to northwest in the seismic section (Figure 26c) at the northeastern side of the location of well 7324/8-1. Such a high amplitude reflector is also observed just 5-6 km to the east of well 7324/8-1 (Figure 27), and is located at around 25-30 m below the URU. These high amplitude reflectors may be interpreted as shallow gas anomalies.

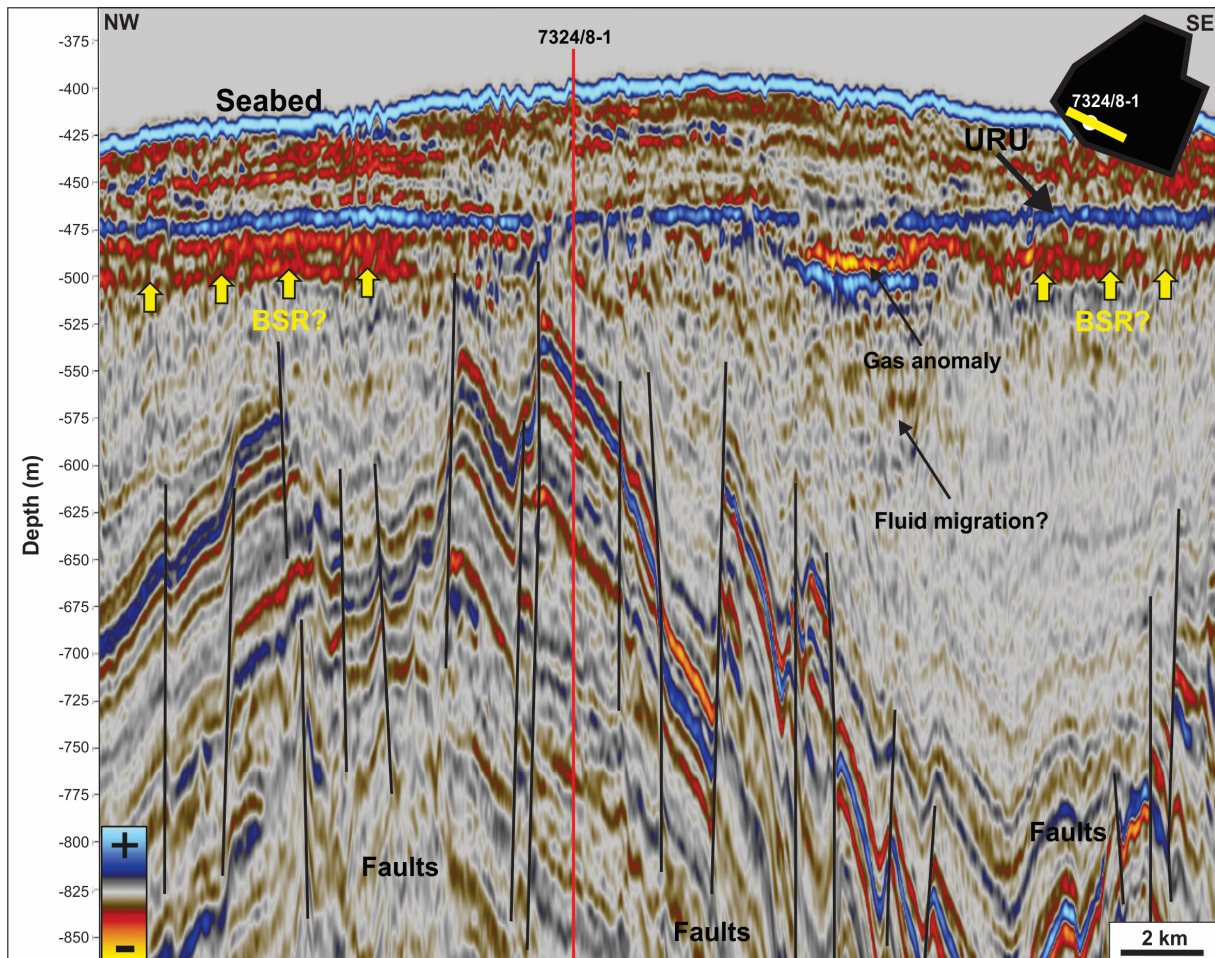


Figure 27. Depth converted seismic section located across well 7324/8-1. Possible BSRs are indicated by yellow arrows and faults are illustrated by black lines.

At the same depth as this shallow gas anomaly in the seismic section (Figure 27), there is an extensive high amplitude reflector with reversed polarity compared to the seafloor. This may lead to infer gas filled sediments at this depth which may possibly be related to gas hydrates. The underlying fault system may act as a migration pathway for fluids, thus feeding the overlying sediments with upward migrating thermogenic gas. Hence, this high amplitude reflector below the URU may be inferred as a BSR.

In the study area it has also been acquired 2D P-cable seismic data (Figure 28). This seismic



dataset is acquired and processed to extract high resolution seismic sections within Bjarmeland Platform and Hoop Fault Complex.

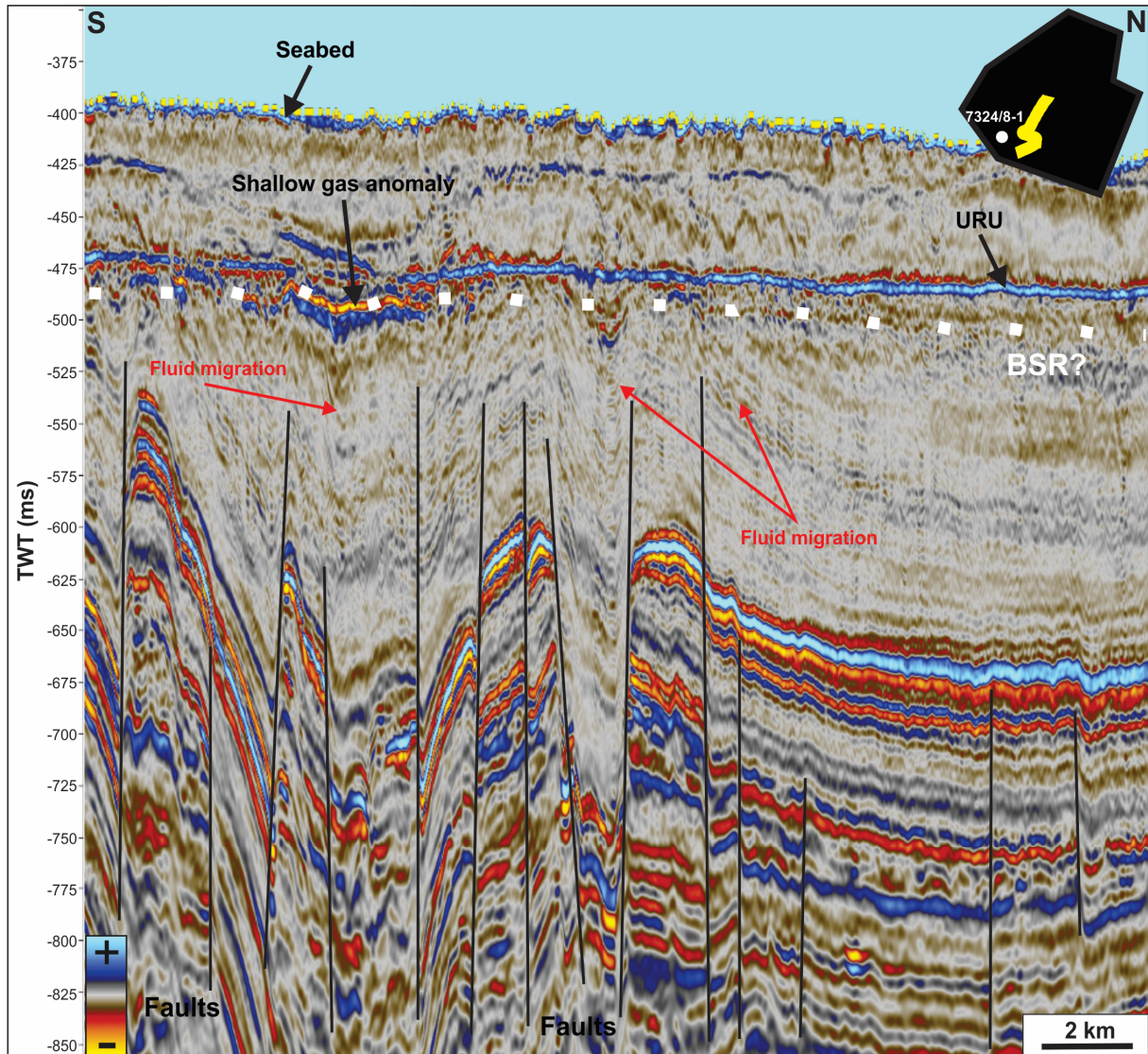


Figure 28. 2D P-cable seismic section from the eastern side of well 7324/8-1. Illustrations are: fault (black lines), possible BSRs (white dotted line) and fluid migration (red arrows).

The P-cable dataset provides high quality seismic evidence (Figure 28) of fluid flow in the study area. The seismic section suggests a large quantity of faults below the shallow gas anomaly just east of well 7324/8-1, where the fault extends almost up to the interpreted gas anomaly itself. This would provide excellent fluid migration pathways through the underlying sediments. From this dataset it may also be observed upward dipping reflectors in the Cretaceous unit at the northern side of the shallow gas anomaly, suggesting possible migration through carrier beds within the Cretaceous unit. Below the URU and at the same depth as the shallow gas anomaly, it may be observed a seismic reflector with reversed polarity



compared to the seabed. This reflector subparallel the seafloor reflector and coincides with the high amplitude reflectors observed below the URU at the depth converted seismic dataset (i.e. Figure 26, Figure 27). Hence, it may be inferred as possible BSRs related to gas hydrates.

### 5.2.2 Distribution of BSR in the Hoop Fault Complex

The distribution of inferred gas hydrate related BSRs is widespread in the Hoop 3D study area (Figure 29).

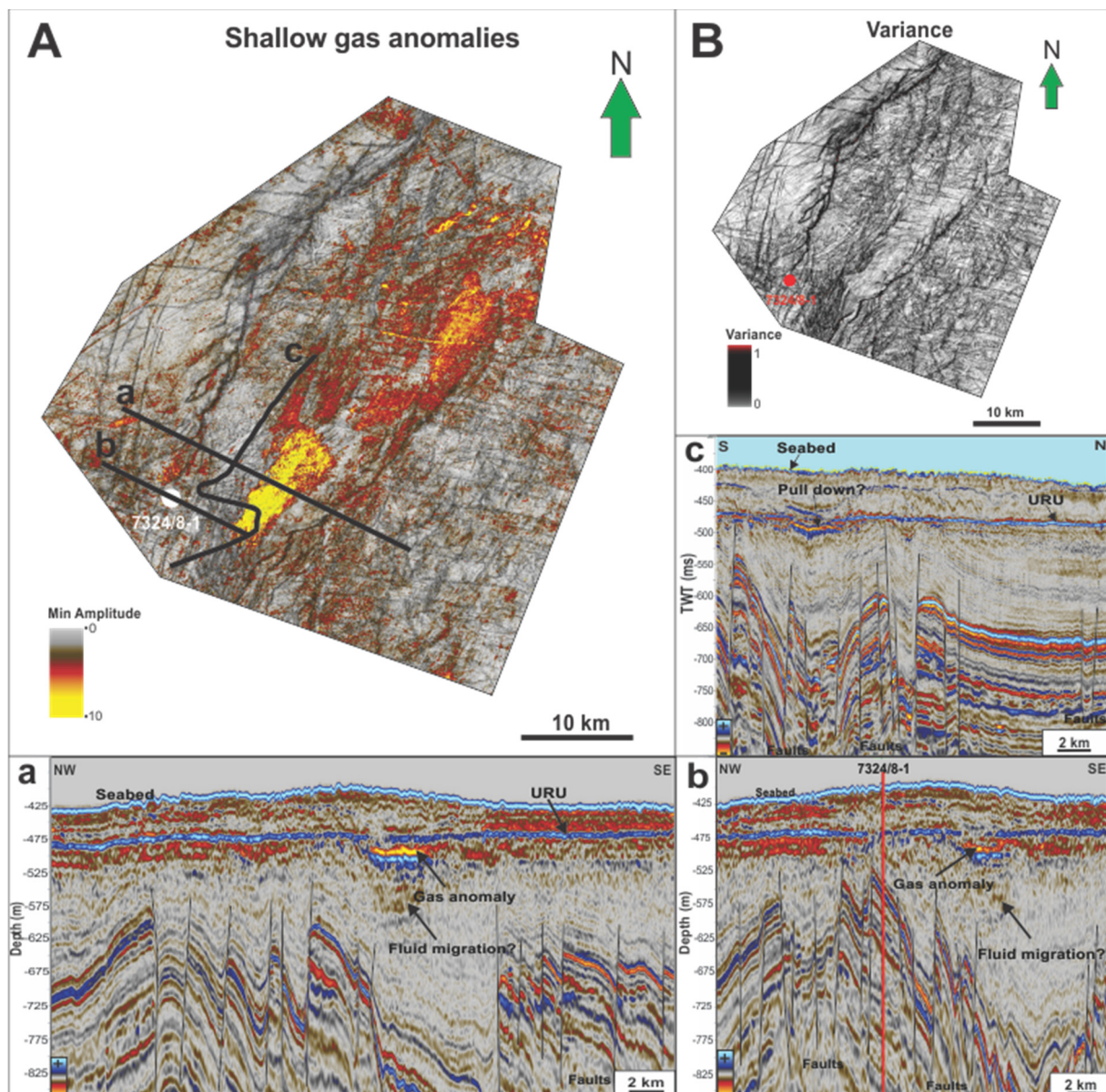


Figure 29. A) Minimum amplitude map of the shallow gas anomalies in the study area Hoop 3D. The yellow colored areas shows the distribution of shallow gas anomalies in the study area. In the gray areas it is absence of shallow gas anomalies. Black lines indicate seismic sections in a, b and c. B) Variance map from 630-730 m, with the purpose of illustrating fault systems in possible relation to the distributions of the overlying shallow gas anomalies. Seismic sections a, b and c illustrates shallow gas anomalies or gas hydrate related BSRs. Black lines in the seismic sections indicates possible faults.

The minimum amplitude map (Figure 29A) is a useful surface attribute to illustrate the distribution of shallow gas anomalies or BSRs possibly related to gas hydrates. Within the Hoop 3D study area, there is a significant shallow gas anomaly at the eastern side of well 7324/8-1, which may possibly relate to gas hydrates. However, the minimum amplitude map also suggest distribution of possible gas hydrates elsewhere within the study area. This is also evidenced by seismic sections (i.e. Figure 29a,b,c), where it has been observed high amplitude anomalies which subparallel the seafloor reflector at a depth which coincides with the large shallow gas anomaly (Figure 29A). Observation of a significantly large faulting system (Figure 29B) in the deeper sediments, supports the belief of an active fluid flow system in the region and enhance the possibility of upwards migrating fluids into shallower sediments.

5.2.3 Gas Hydrate stability model at well 7324/8-1

The numerical model for gas hydrate stability at the location of well 7324/8-1 uses the exact gas composition given in the geochemistry data report for the well (Harding, et al., 2014). The gas composition is sampled at only 198 meters sub bottom depth, which is 40 meters above top reservoir of well 7324/8-1. The gas composition used for the modelling is described in Table 3:

Gas type	C1%	C2%	C3%	iC4%	nC4%	iC5%	nC5%	C6%	CO <sub>2</sub>
Value (%)	97.1	0.9	1.4	0	0	0	0	0	1.84

Table 3. The table shows the content of gas composition used for the GHS model at the location of well 7324/8-1.

The gas composition (Table 3) is used in the model for both present day conditions, conditions during deglaciation and for conditions during Last Glacial Maximum. For each model, it has also been generated a numerical model for a gas composition of 100% methane. Table 4 provides information about other important parameters used in the gas hydrate stability model at the location of well 7324/8-1:

	<b>Present day</b>	<b>Early Deglaciation</b>	<b>Last Glacial Maxim</b>
<b>BWT/Bottom ice Temp.</b>	2.47°C	2.0°C	-1.78°C
<b>Geothermal Gradient</b>	0.048 °C/m	0.048 °C/m	0.048 °C/m
<b>Water/Ice column</b>	402 m (water)	469 m (water)	1 723 m (Ice)

*Table 4. The table provide information about the bottom water temperature (BWT), geothermal gradient water/ice column used in the GHS model at the location of well 7324/8-1.*

Well 7324/8-1 did not provide bottom water temperature, thus bottom water temperature has been estimated from CTD measurements (NODC, 2009) in the study area. The geothermal gradient is calculated by using the average of three of the shallowest bottom hole temperatures (14.03°C) at a depth of 241-245 m subbottom and an estimated bottom water temperature of 2.47 °C. This gives a calculated geothermal gradient in the shallowest sediments of 0.048 °C/m. Based on the values in Table 3 and Table 4, the models (Figure 30) indicates the numerical depths of both gas hydrates and pure methane hydrates at present day conditions, during early deglaciation, and during Last Glacial Maximum:



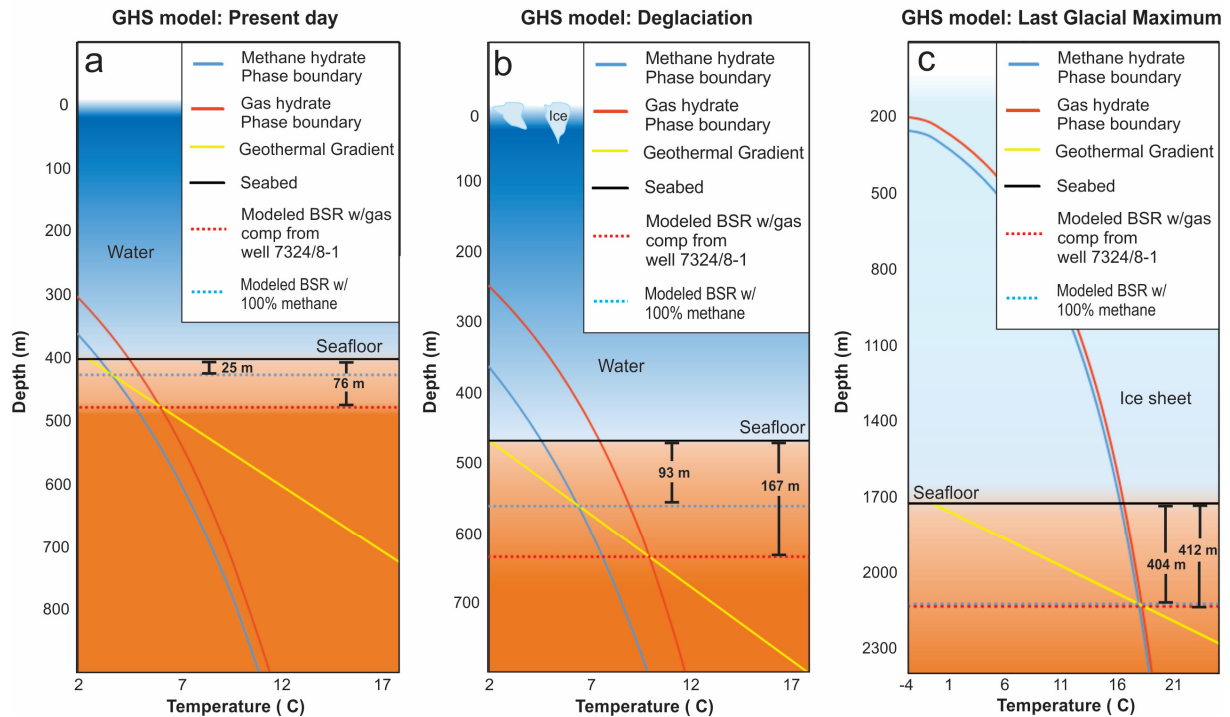


Figure 30. Gas hydrate stability model for location around well 7324/8-1. a) GHS model for present day condition: water column of 402 m, modelled gas hydrate stability down to 76 m below the seafloor. Modelled methane hydrate stability down to 25 m below the seafloor. b) GHS model for time of deglaciation (16 830 BP): water column of 469 m, modelled methane hydrate stability down to 93 m below seafloor, modelled gas hydrate stability down to 167 m below seafloor. c) GHS model for time of LGM (22 580 BP): ice sheet column of 1723 m, modelled methane hydrate stability down to 404 m below seafloor, modelled gas hydrate stability down to 412 m below seafloor.

The gas hydrate stability model for present day conditions indicates stability for both methane hydrates and gas hydrates in the area around well 7324/8-1 (Figure 30a). The methane hydrate stability is estimated to 25 m below seafloor and gas hydrate stability is estimated to 76 m. For conditions during early deglaciation (around 16 830 BP) (Figure 30b), the numerical modelling suggests presence of stable conditions for methane hydrates down to 93 m below seafloor and stable conditions for gas hydrates down to 167 m. For conditions during Last Glacial Maximum (around 22 580 BP) (Figure 30c), the numerical modelling suggests presence of stable conditions for methane hydrates down to 404 m sub bottom depth and stable conditions for gas hydrates down to 412 m sub bottom depth.



## 6 Discussion

### 6.1 Study area

Both within Ververis 3D and Hoop 3D, seismic expressions and attributes indicate that much of the study areas are covered by shallow gas anomalies interpreted as possible BSRs. Below the seismic expressions of possible BSRs, fluid flow features such as patchy reflections, pipes, chimneys and faults are observed. Here, the possible relation between these fluid flow features and formation of gas hydrates will be discussed to enlighten the conditions for formation of gas hydrates within the study areas. Furthermore, gas hydrate stability modelling is carried out for present day conditions, conditions during early deglaciation, and conditions during Last Glacial Maximum. The result from this numerical modelling will be compared and discussed as possible indirect evidence for presence of gas hydrates in the areas.

#### 6.1.1 Seismic indications of gas hydrates

Seismic evidence such as bright spots, enhanced reflectors and polarity reversals strongly suggests presence of shallow gas anomalies in the study areas. Observing that these shallow gas anomalies are paralleling or sub-paralleling the seafloor reflector gives an indication that the anomalies may be related to gas hydrates. Hence, they may be interpreted as gas hydrate-related BSRs. This is consistent with previous studies where bottom simulating reflectors have been observed in seismic sections worldwide as paralleling reflectors to the seafloor reflector (Andreassen, et al., 1996; Hornbach, et al., 2003; Lee, et al., 2005). Andreassen et al. (1996) also relates the reversed polarity of the BSR to a decrease in acoustic impedance due to a decreasing compressional velocity when going from gas hydrates into free gas sediments. This reversed polarity coincides with the polarity of the shallow gas anomalies in the study areas, indicating trapped free gas in the sediments.

In contradiction to most previous studies, the shallow gas anomalies observed in Ververis 3D are located at the base of the Pliocene/Pleistocene sediment package. This observation enforces the discussion of other possible trapping mechanisms. The upper regional

unconformity, known as URU, has a lower boundary that truncates older bedding planes and form a major unconformity (Faleide, et al., 1984). Enhanced reflectors along bedding planes truncated by the URU may possibly be observed (Figure 21). Migration along and through these upward dipping bedding planes may form a possible trapping mechanism for hydrocarbons at their top, which is the base of the Pliocene/Pleistocene sediment package. Hence, carefully considerations should be made before interpreting such shallow gas anomalies as gas hydrate-related BSRs, and more seismic evidence is necessary.

Shipley et al. (1979) have previously described amplitude blanking as a useful indication of accumulation of gas hydrates, and evidences of such amplitude blanking above the shallow gas anomalies (Figure 21) may support the belief that the shallow gas anomalies in the study area are in fact related to gas hydrates. However, Holbrook et al. (1996) suggests amplitude blanking to be a consequence of either hydrate cementation or lithological homogeneity of sediments. Within the Ververis 3D, it has been suggested that the Pliocene/Pleistocene sediment package consist predominantly of firm to stiff clay, with some appearance of coarser material up to boulder size (Kleiven & Ersdal, 2008). This infer that lithological homogeneity of the Pliocene/ Pleistocene sediment package cannot be ruled out, hence more evidence is needed to imply presence of gas hydrates.

The shallow gas anomalies in Hoop 3D are observed below the URU, implying that the URU itself cannot be the trapping mechanism. Here, enhanced reflectors with reversed polarity compared to the seafloor reflector are paralleling the seafloor at around 20-25 m below the URU. The depth of these enhanced reflectors coincides with the larger shallow gas anomaly observed a few kilometers east of well 7324/8-1 (Figure 26, Figure 27). This enhances the belief that these reflectors may be related to gas hydrates, as gas hydrates may be the possible trapping mechanism for the upward migrating hydrocarbons in the area.

### 6.1.2 Gas migration and accumulation

Previous site survey report from Ververis 3D have suggested faulted sediments and deep-rooted faults below Pleistocene deposits (Figure 20, Figure 21, Figure 22) (Kleiven & Ersdal, 2008). In the Hoop Fault Complex area it has previously been reported a fault system of

normal faulting (Figure 27), and listric faulting in younger sediments related to the development of anticlinal salt related structures in the Maud Basin (Gabrielsen, et al., 1990).

The fault systems within both study areas are thought to provide good fluid conduits for migration of deeper seated hydrocarbons. Especially deeper faults, where the sediments are more compacted, the faults are considered important fluid conduits. This is consistent with previous studies where faults have been inferred to act as migration pathways for hydrocarbons from deeper sources and reservoirs both on the mid-Norwegian margin and in the Barents Sea (Chand & Minshull, 2003; Berndt, et al., 2003; Judd & Hovland, 2007; Vadakkepuliambatta, et al., 2014). Both faults and fractures are thought to be good conduits for fluids across low permeable sedimentary layers, and they are usually associated with high amplitude acoustic anomalies along their fault plane or adjacent sedimentary strata (Løseth, et al., 2009).

Some of the shallow gas anomalies in Ververis 3D are located right above the faults (Figure 22), implying a distinct relationship between the faults and hydrocarbon leakage from deeper sediments. In addition, fluid pipes are observed deep below the faults (Figure 22), and intersect with the faults underneath Cretaceous sediment. This is another strong evidence of fluid migration, and both the fluid pipes and the observed faults are suggested to provide good fluid conduits for the shallow gas anomalies resulting in formation of gas hydrates.

Below the larger shallow gas anomaly within Hoop 3D, it appears an extensive system of faults (Figure 28). Some of these faults extend far into the Cretaceous sediment and almost up to the shallow gas anomaly, hence they appear to act as very nice fluid conduits into the shallow gas anomaly. Along some of the interpreted fault planes it may be observed high amplitude anomalies in the adjacent strata, which adds to support the belief of fluid leakage from deeper seated sediments in the area.

Fluid migration through carrier beds is another good fluid flow conduit which may be related to lateral formation and distribution of gas hydrates (Judd & Hovland, 2007; Freire, et al., 2011; Rajan, et al., 2013). Such carrier beds may be observed in the P-cable seismic section (Figure 28) at the northern side of the larger shallow gas anomaly within Hoop 3D survey. These bedding

planes are dipping upwards in the sediment in the direction of the shallow gas anomaly, and they may act as a fluid conduit for migration of hydrocarbons into shallower sediments.

It has also been observed such carrier beds in Ververis 3D (Figure 21), but here the bedding planes are truncated by the URU. The enhanced reflectors along these truncated bedding planes suggests lateral migration of hydrocarbons resulting in widespread lateral distribution of shallow gas anomalies inferred as the base of the gas hydrate stability zone (BGHSZ). Also numerous depressions have been reported from multi-beam sonar scanning within Ververis 3D. These depressions generally range from 1-3 m in depth and <20 m in diameter and is interpreted as pockmarks (Kleiven & Ersdal, 2008). Chand and Minshull (2003) suggest presence of pockmarks in regions where fluid conduits reaches the seabed. The evidence of reported pockmarks in Ververis 3D may thereby support the interpretation of the faults and pipes in the area as good fluid flow features for migration of deeper seated hydrocarbons. Chand et al (2008) have previously reported pockmarks within Nordkapp Basin and suggested a relationship to faults and leakage from hydraulic fractures caused by overpressure due to build up of gas below the gas hydrate stability zone. The strong suggested relationship between pockmarks, fluid flow and gas hydrates, and the reported presence of pockmarks in the study area may thus be regarded as another indirect evidence of presence of gas hydrates.

### 6.1.3 Gas hydrate stability modelling

When hydrocarbons migrate through the above mentioned and discussed fluid flow conduits and into the GHSZ, a drop in solubility towards the seabed may cause methane to precipitate from its fluid solution and crystallize into gas hydrates as described in Chand & Minshull (2003). Hence, the numerical model made for gas hydrate stability within the two study areas may provide additionally good evidence for presence of gas hydrates. Numerical modelling of methane hydrates in the study areas, indicate that pure methane hydrates are instable in Ververis 3D. In Hoop 3D however, numerical modelling indicate stable conditions for methane hydrates in the shallowest sediments at present day conditions. Previous studies in the SW Barents Sea (i.e. Chand, et al., 2008; Chand, et al., 2012; Vadakkepuliambatta, et al., 2014) have suggested that the distribution of methane hydrates is limited to only parts of the Bjørnøya Trough and its adjacent flanks.



Vadakkepuliambatta et al. (2014) suggests shallow depths and high bottom water temperature to be the major factors limiting the stability of methane hydrates in most parts of the SW Barents Sea.

The main factors controlling the gas hydrate stability in the SW Barents Sea are thought to be the presence of higher order hydrocarbons and their fluid conduits to migrate upwards into shallower sediments (Andreassen, et al., 1990; Chand, et al., 2008; Vadakkepuliambatta, et al., 2014).

The gas hydrate stability model for present day conditions at well 7226/2-1 (Figure 31) in Ververis 3D suggest presence of gas hydrate stability down to 87 m below the seafloor for a geothermal gradient of 0.036 °C/km.

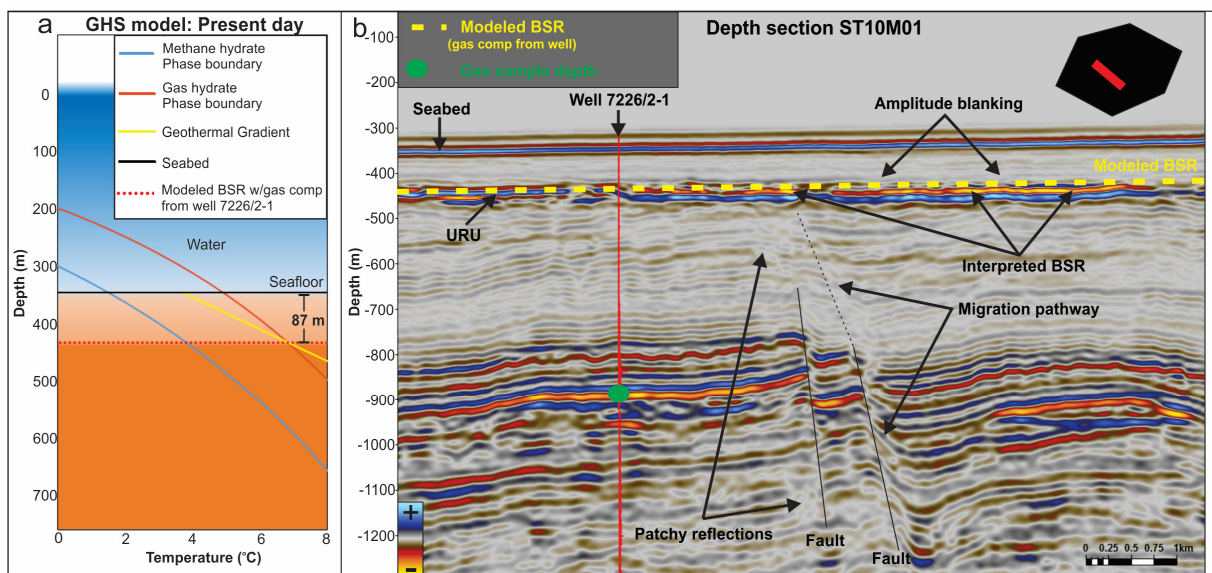


Figure 31. a) GHS model for present day conditions at the location of well 7226/2-1. Gas composition from the well: 98% $C_1$ , 1.2% $C_2$ , 0.31% $C_3$ , 0.04% $iC_4$ , 0.03% $nC_4$ , 0.01% $iC_5$ , 0.03% $C_6$  and 0.38% $CO_2$  b) Depth-converted seismic section. The modelled gas hydrate stability is estimated to be stable down to 87 m below the seafloor and indicated by the yellow dashed line. Interpreted BSR are illustrated with black arrows. The red vertical line indicates the position of well 7226/2-1. The green dot illustrates the depth at which the gas composition is sampled at (534 m sub bottom depth).

The modelled depth for gas hydrate stability coincides with the base of the Pliocene/Pleistocene sediment package and the shallow gas anomalies interpreted as gas hydrate-related BSRs (Figure 31). Such a correlation between the modelled BSR and the shallow gas anomalies, adds to strengthen the confidence of the interpretation of gas hydrate-related BSRs. Using real data gas samples from the well increases the confidence of the model, although the gas sample are sampled much deeper than the expected GHSZ. The

implication is that gas composition may change slightly as it migrates upwards due to changes in temperature and pressure, and this may affect the estimated BSR up to few tens of meters (Ostanin, et al., 2013; Vadakkepuliambatta, et al., 2014). Although the average geothermal gradient in well 7226/2-1 is suggested by Vadakkepuliambatta et al. (2014) to be around 0.036 °C/km, the geothermal gradient for the shallower sediment is likely to be higher. Using the uppermost bottom hole temperature of 28 °C at a depth of 534 m below the seafloor, and an estimated bottom water temperature of 3.7 °C (NODC, 2009), it can be suggested a geothermal gradient for the shallower sediments of 0.052 °C/km. This would imply gas hydrate stability down to 50 m below the seafloor (Figure 32), hence 37 m shallower than for a geothermal gradient of 0.036 °C/km.

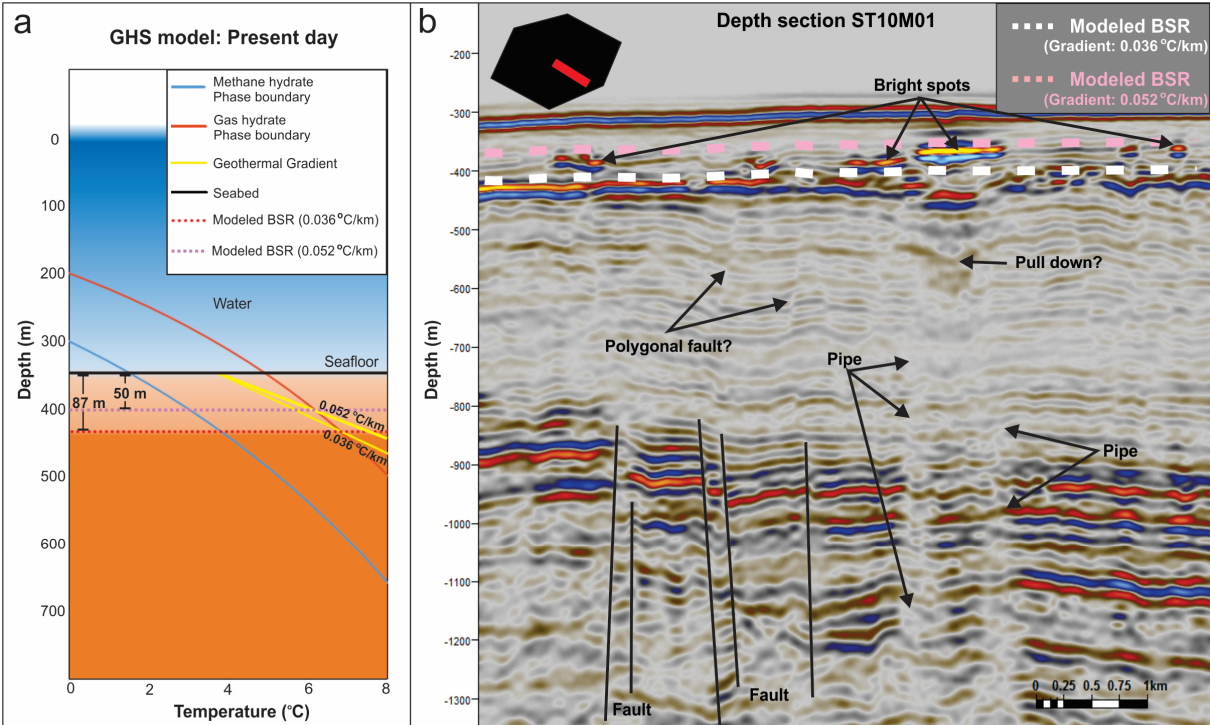


Figure 32. a) GHS model for present day conditions at the location of well 7226/2-1. b) Depth-converted seismic section. The modelled BSR for a geothermal gradient of 0.036 oC/km is calculated to appear 87 m below the seafloor and indicated by the white dashed line. The modelled BSR for the geothermal gradient 0.052 °C/km is calculated to appear 50 m below the seafloor and indicated by the pink dashed line. Illustrated possible seismic evidence that may be related to gas hydrates are: amplitude blanking, bright spots, patchy reflections, polygonal faults, pull down, pipe and chimney structures.

The modelled BSR from this higher geothermal gradient (Figure 32a; 0.052 °C/km) indicates that the bright spots above Pliocene/Pleistocene sediments (Figure 32b) may in fact be related to gas hydrates, thus gas hydrates itself may possibly be the trapping mechanism for this anomaly. Considering the underlying fluid flow conduits such as pipes, faults and polygonal faults, it is tentative to infer a working fluid flow system within Ververis 3D. Below

the larger bright spot above the Pliocene/Pleistocene sediments (Figure 32b), there is a possible pull down in the reflectors insinuating presence of shallow gas above. There is also a possible pipe structure below, which leads to suggest migration of thermogenic hydrocarbons from deeper sediments. The trapped shallow gas anomaly above this pipe structure are located above adjacent high amplitude reflectors interpreted as the base of Pliocene/Pleistocene sediments, and between the two different gas hydrate stability zones estimated from numerical modelling. This is consistent with previous studies of shallow gas anomalies related to gas hydrates in the SW Barents Sea, where large portions of observed gas hydrate-related BSRs are observed in relation to pipes or chimney structures, faults and other structural elements where migration of thermogenic gases from deeper sources or reservoirs may occur (Andreassen, et al., 1990; Chand, et al., 2008; Vadakkepuliambatta, et al., 2013; Vadakkepuliambatta, et al., 2014).

The gas hydrate stability model for present day conditions at well 7324/8-1 (Figure 33) in Hoop 3D suggests presence of gas hydrate stability down to 76 m sub bottom depth for a geothermal gradient of 0.048 °C/km.

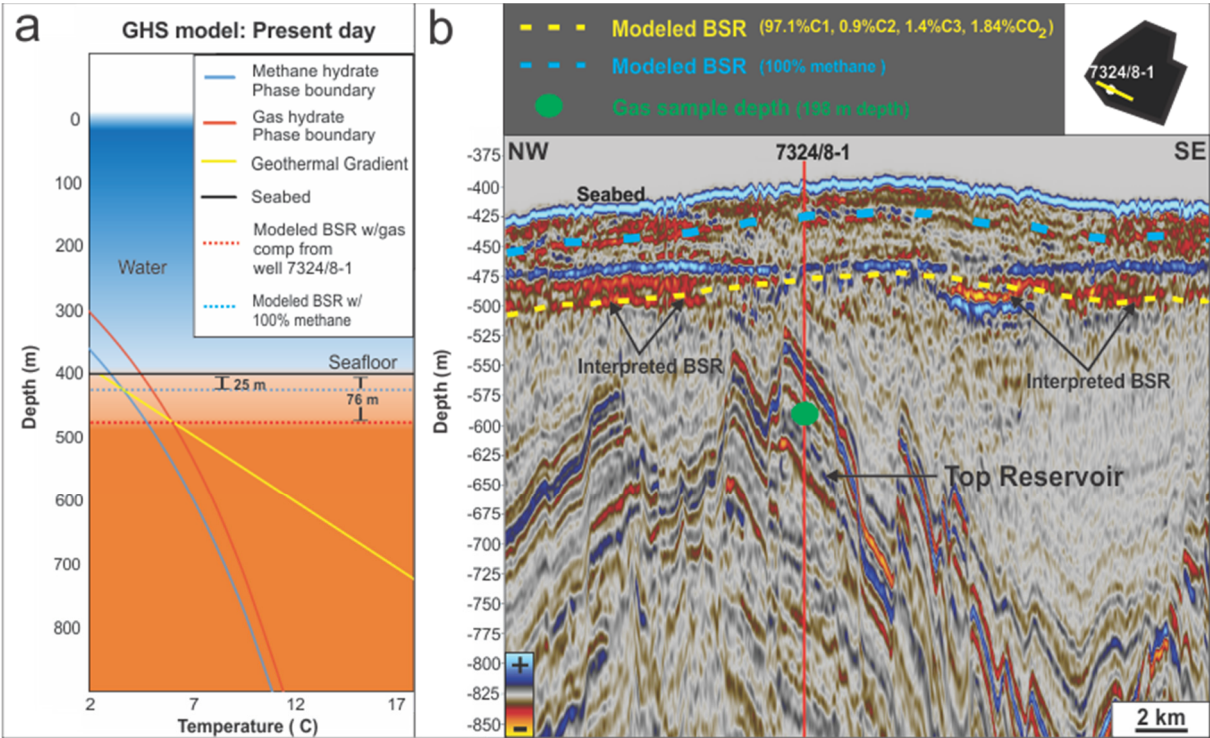


Figure 33. a) GHS model for present day conditions at the location of well 7324/8-1. b) Depth-converted seismic section. The modelled gas hydrate stability is estimated to be stable down to 76 m below the seafloor and indicated by the yellow dashed line. The modelled methane hydrate stability is estimated to be stable down to 25 m below the seafloor and indicated by the blue dashed line. Interpreted BSR are illustrated with black arrows. The green dot illustrates the depth at which the gas composition is sampled at (198 m sub bottom depth). The red vertical line indicates the position of well 7324/8-1.

The water column at present day conditions is 402 m at the location of well 7324/8-1 (Figure 33), and the bottom water temperature is estimated to 2.47 °C (NODC, 2009). Numerical modelling also suggest stability of methane hydrates in the area, where it is suggested stability down to 25 m sub bottom depth.

The result from gas hydrate stability modelling coincides with the depth of the interpreted BSRs, and thus adds to strengthen the confidence of the seismic interpretations of gas hydrates in the area. The gas sample from well 7324/8-1 is sampled at only 198 m sub bottom depth, hence it is one of the shallowest analyzed gas samples from the SW Barents Sea. As biodegradation of hydrocarbons in shallow sediments may affect the gas composition and result in CO<sub>2</sub> rich gas accumulation (Matapour, 2013), gas sample analyses of these shallow depths may provide a more detailed gas composition that perhaps would be more representative for the shallower sediments where gas hydrates normally exist, than the deeper seated gas samples elsewhere in the Barents Sea. In well 7324/8-1 biodegradation of hydrocarbons is reported (Harding, et al., 2014), and analyses of the gas composition indicates a relatively high level of CO<sub>2</sub> in the gas samples. It was reported 1.84% CO<sub>2</sub> at the sampled gas at 198 m depth, and as much as 5.52% CO<sub>2</sub> at the top reservoir gas sample at a depth of 238 m. This may affect gas hydrate stability modelling significantly depending on how the total gas composition changes. As such, the gas composition from these shallow sediments at well 7324/8-1 would strongly add to increase the confidence of the numerical modelling of gas hydrate stability in the area.

The top reservoir at the well is located at 238 m sub bottom depth, and the analyzed gas samples from the top reservoir indicate considerable changes in the gas composition from the gas sample at 198 m sub bottom depth. The gas composition from the top reservoir is 90.88% methane, 1.4% ethane, 0.98% propane, 0.28% i-butane, 0.49% n-butane, 0.24% i-pentane, 0.19% n-pentane and 5.52% CO<sub>2</sub>. Numerical modelling of this gas composition indicates a gas hydrate stability of 201 m sub bottom depth (Figure 34).



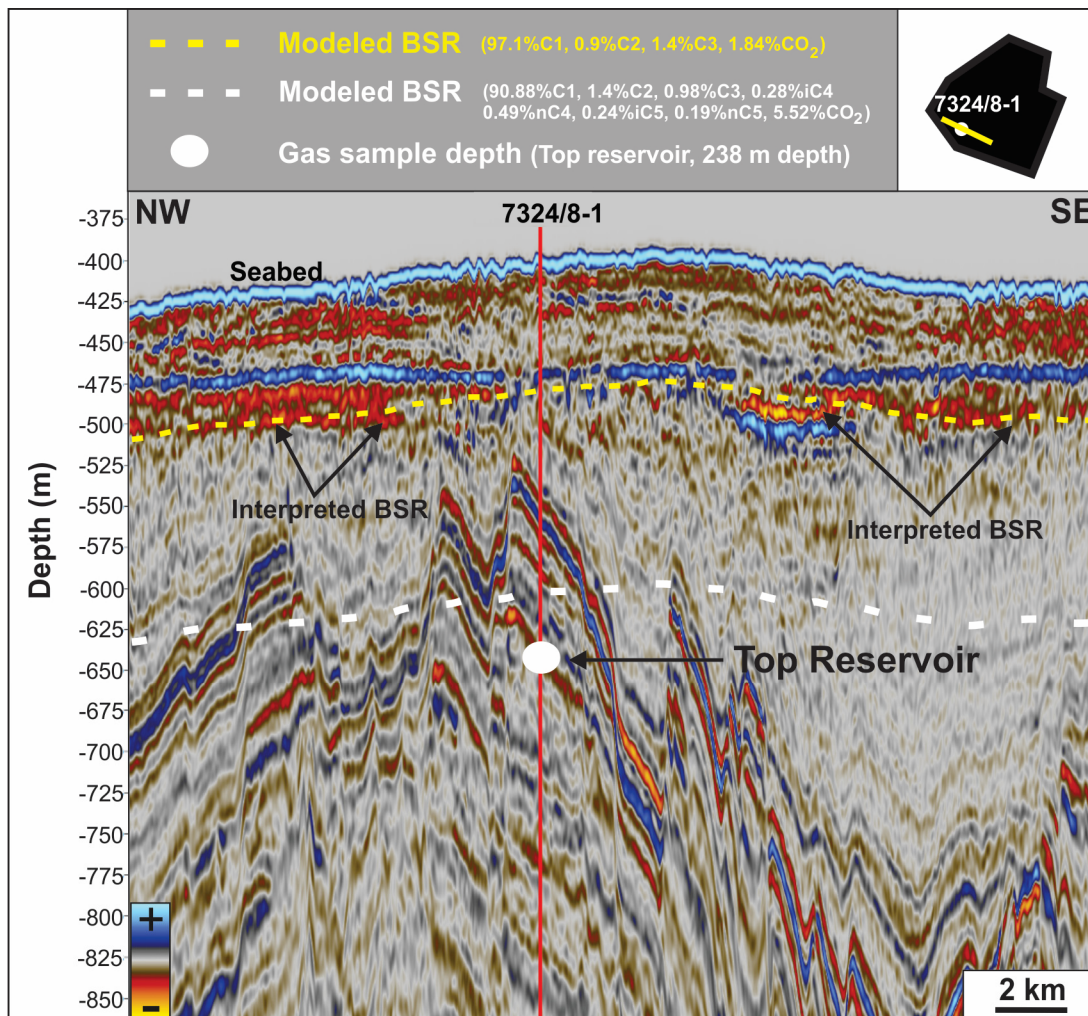


Figure 34. The yellow dashed line illustrates the modelled BSR when using the sampled gas analysis from 198 m sub bottom depth. The white dashed line illustrates the modelled BSR when using the sampled gas analysis from top reservoir (238 m sub bottom depth). The white dot illustrates the gas sample depth and top reservoir for well 7324/8-1.

The modelled gas hydrate stability increases significantly when using gas composition from the top reservoir gas sample (Figure 34). In fact, it increases by 125 m when using this gas composition compared to the gas composition from the gas sampled at 198 m sub bottom depth. Hence, local changes in gas composition may significantly alter the gas hydrate stability zone. In this case the quantity of methane molecules in the gas composition changes from 90.88% at a depth of 238 m to 97.1% at a depth of 198 m, which may possibly help explain the significantly large change in gas hydrate stability between the two numerical modellings. Methane molecules are smaller molecules compared to ethane, butane, pentane and CO<sub>2</sub>. This makes methane more mobile when it comes to upward migration in relatively low permeable sediments compared to higher order hydrocarbons, and may possibly explain the relatively higher quantity of methane in the shallower gas



composition. Contradictory to Ostanin, et al. (2013) where it is suggested that gas composition only changes slightly as it migrates upwards in the sediments, the gas composition in well 7324/8-1 changes significantly from the top reservoir to only 40 m above top reservoir. As a consequence, the gas hydrate stability increases significantly instead of few tens of meters as proposed by Ostanin et al., (2013).

#### 6.1.4 Numerical modelling and pitfalls

Although numerical modelling support the seismic interpretations of gas hydrates both in Ververis 3D and Hoop 3D, possible pitfalls needs to be elaborated and explained. The lateral resolution of the model is unknown as local changes in gas composition, geothermal gradient and water depth may affect the result of modelling. In Ververis 3D, a change in geothermal gradient from 0.036 °C/km to 0.052 °C/km, would decrease the modelled gas hydrate stability thickness by 37 m. Here, the average geothermal gradient in well 7226/2-1 has been estimated to 0.036 °C/km, whereas the geothermal gradient in the shallowest 534 m of the sediments was calculated to 0.052 °C/km. In Hoop 3D it has been established a significant change in gas composition in well 7324/8-1 in only a depth difference of 40 m. Numerical modelling from the two different gas compositions, reveals a difference in gas hydrate stability thickness of as much as 125 m. Local changes in water depth may also affect numerical modelling because it changes the pressure conditions in the shallow sediments where gas hydrates may form and exist. The seabed at Ververis 3D and Hoop 3D is relatively flat, insinuating relatively small changes in water depth. However, in other parts of the SW Barents Sea where significant local changes in water depths exist, the lateral resolution of numerical modelling of gas hydrate stability would be limited by these relative changes in water depth.

As such, gas hydrate stability modelling alone should not be used as evidence for existence of gas hydrates. However, it is a useful tool when used as supporting evidence in combination with seismic or other evidence of presence of gas hydrates.

### 6.1.5 Impacts of LGM and deglaciation on present day gas hydrate accumulations

During Last Glacial Maximum (22 780 BP) the seabed was covered by an 1870 m thick ice sheet in Ververis 3D according to modelling made by researcher Henry Patton from CAGE and described in Patton et al (2016) (In Prep). This would alter the pressure conditions significantly. The bottom ice temperature is estimated to  $-3.2^{\circ}\text{C}$ , and would also affect the gas hydrate stability conditions during Last Glacial Maximum. The gas hydrate stability modelling for LGM indicates a gas hydrate stability down to 618 m sub bottom depth in the area (Figure 35).

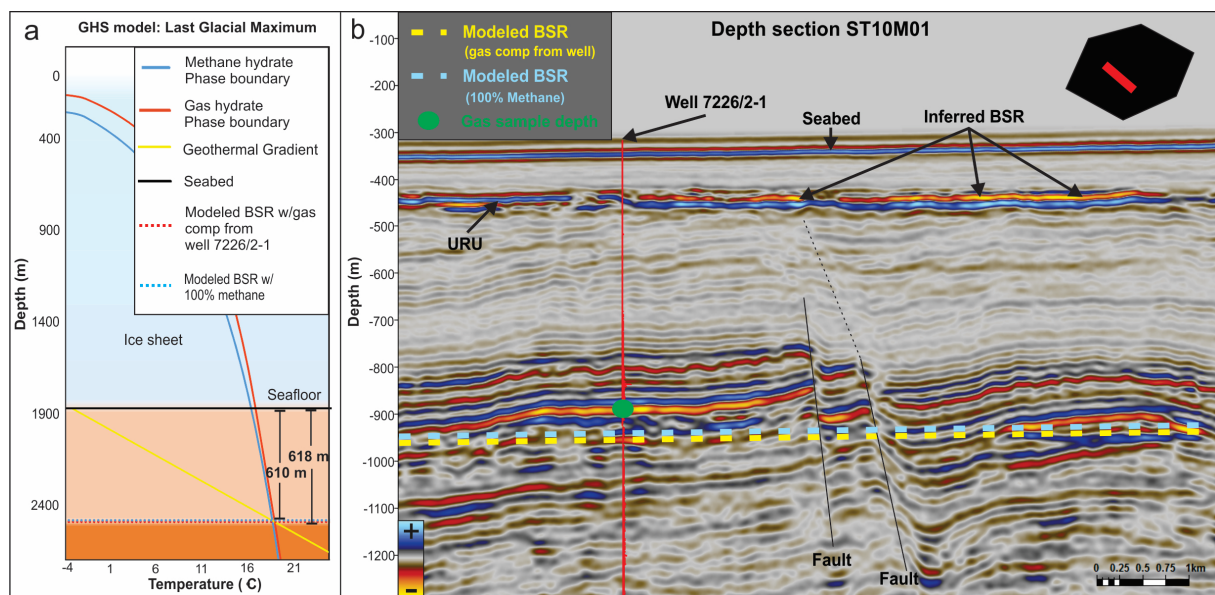


Figure 35. a) GHS model for conditions during LGM at the location of well 7226/2-1. Gas composition from the well: 98% $\text{C}_1$ , 1.2% $\text{C}_2$ , 0.31% $\text{C}_3$ , 0.04% $\text{iC}_4$ , 0.03% $\text{nC}_4$ , 0.01% $\text{iC}_5$ , 0.03% $\text{C}_6$  and 0.38% $\text{CO}_2$ . b) Depth-converted seismic section. The modelled gas hydrate stability is estimated to 618 m sub bottom depth and indicated by the yellow dashed line. The modelled methane hydrate stability is estimated to 610 m sub bottom depth, indicated by a dashed blue line. Interpreted BSR are illustrated with black arrows. The red vertical line indicates the position of well 7226/2-1. The green dot illustrates the depth at which the gas composition is sampled at (534 m sub bottom depth).

Numerical modelling of methane hydrate stability indicate stable conditions down to 610 m sub bottom depth at LGM (Figure 35). This is just slightly shallower than the estimated gas hydrate stability, and is consistent with previous gas hydrate stability modelling for the SW Barents Sea where methane hydrates have been modelled to be stable down to 600 m sub bottom depth during LGM (Chand, et al., 2012). Ostanin et al. (2013) suggests loading caused by marine ice sheets during LGM to have led to an increased pressure and a decrease in temperature, which in turn have caused favorable conditions for formation of hydrates. In turn, cementing hydrates have acted as a trapping seal for vertical fluid migration, and caused the BGHSZ to deepen as thermogenic gas migrates into the seal zone (Ostanin, et al.,

2013). This coincides with the observations from the gas hydrate stability modelling for conditions during LGM in Ververis, where the model predicts a gas hydrate stability down to 618 m, which is slightly deeper than for pure methane hydrates. Hence, migration of thermogenic gas into the seal zone may have deepened the base of the gas hydrate stability zone from 610 m (pure methane) to 618 m. However, the heavy loading from the vast ice sheet and low bottom ice temperature is considered the major controlling factor for the gas hydrate stability during LGM.

In Hoop 3D, modelling made by researcher Henry Patton from CAGE predicts that the seabed was covered by a 1723 m thick ice sheet during Last Glacial Maximum in the area (22 580 BP), which alter the pressure conditions in the area significantly. The bottom ice temperature is estimated to  $-1.78\text{ }^{\circ}\text{C}$ , and will add to increase the gas hydrate stability from present day conditions (Figure 36).

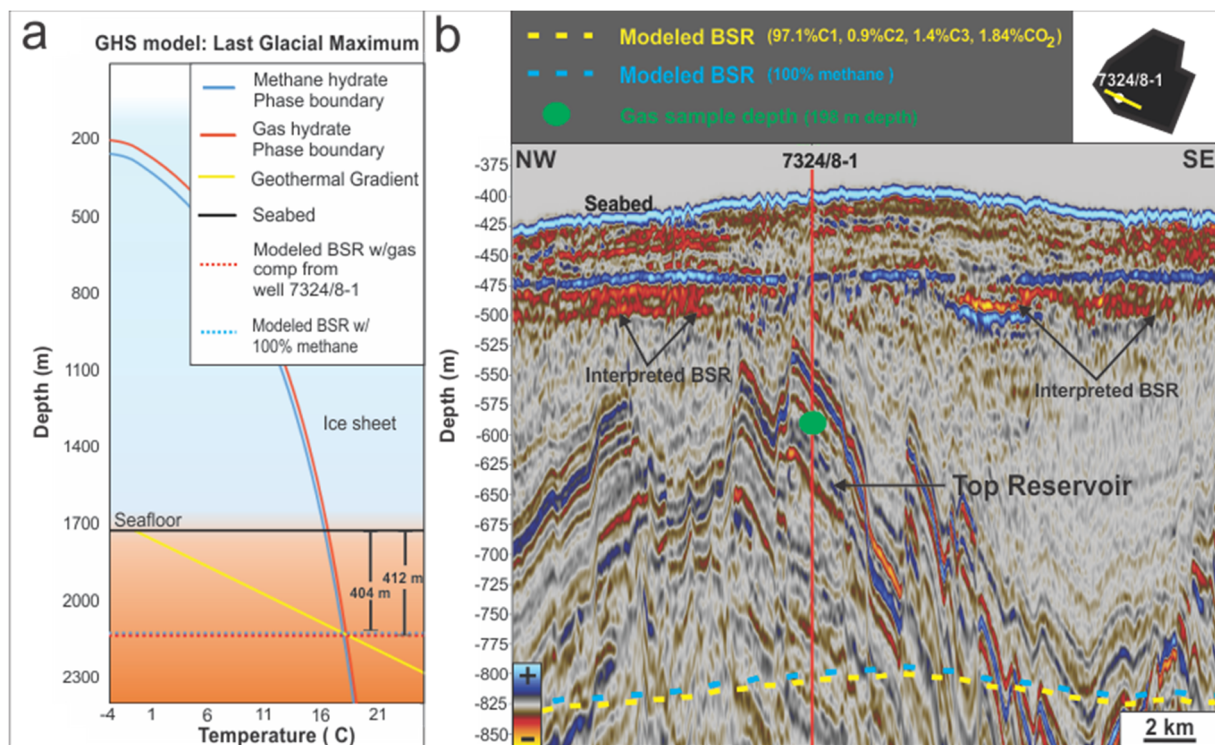


Figure 36. GHS model for conditions during Last Glacial Maximum at the location of well 7324/8-1. b) Depth-converted seismic section. The modelled gas hydrate stability is estimated to be stable down to 412 m sub bottom depth and indicated by the yellow dashed line. The modelled methane hydrate stability is estimated to be stable down to 404 m sub bottom depth and indicated by the blue dashed line. Interpreted BSR are illustrated with black arrows. The green dot illustrates the depth at which the gas composition is sampled at. The red vertical line indicates the position of well 7324/8-1.

Numerical modelling of gas hydrate stability during Last Glacial Maximum indicate stability down to 412 m sub bottom depth (Figure 36). The methane hydrate stability is estimated to appear almost as deep; 404 m sub bottom depth. Hence, the effect from migration of

thermogenic gas into the gas hydrate stability zone described by Ostanin et al. (2013), may possibly have increased the hydrate stability zone from 404 m to 412 m. Also in Hoop 3D, the heavy loading of ice sheets and the low bottom ice temperature is suggested as the major controlling factor for the gas hydrate stability during LGM.

The gas hydrate stability modelling for conditions during deglaciation (15 380 BP), predicts a methane hydrate stability of 122 m and a gas hydrate stability down to 233 m below the seafloor at the location of well 7226/2-1 in Ververis 3D (Figure 37).

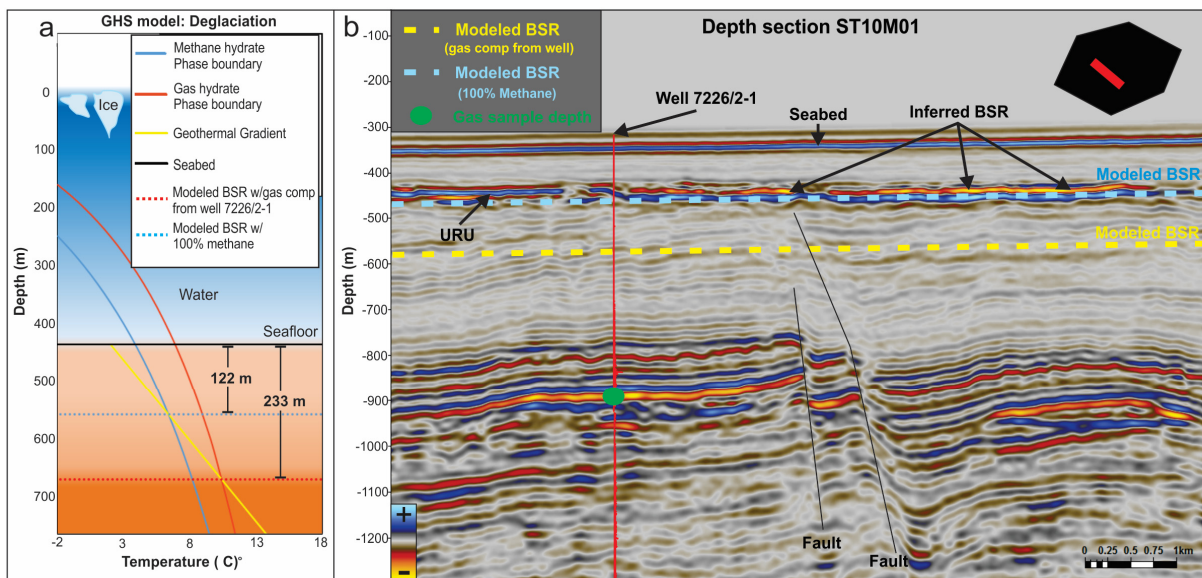


Figure 37. a) GHS model for conditions during early deglaciation at the location of well 7226/2-1. Gas composition from the well: 98% $C_1$ , 1.2% $C_2$ , 0.31% $C_3$ , 0.04% $iC_4$ , 0.03% $nC_4$ , 0.01% $iC_5$ , 0.03% $C_6$  and 0.38% $CO_2$ . b) Depth-converted seismic section. The modelled gas hydrate stability for gas hydrates is estimated to a depth of 233 m below the seafloor and indicated by the yellow dashed line. The modelled methane hydrate stability is estimated to a depth of 122 m below the seafloor, indicated by a dashed blue line. Interpreted BSR are illustrated with black arrows. The red vertical line indicates the position of well 7226/2-1. The green dot illustrates the depth at which the gas composition is sampled at (534 m sub bottom depth).

The significant decrease in the stability of hydrates from LGM may be explained by the change in pressure and temperature conditions from the LGM to the time of deglaciation. During LGM the pressure was caused by the weight of an ice sheet column of approximately 1870 m, whereas the water column during deglaciation was approximately 435 m (Figure 37a). The bottom ice temperature was approximately  $-3.2\text{ }^{\circ}\text{C}$  during LGM, compared to the bottom water temperature during deglaciation at approximately  $2\text{ }^{\circ}\text{C}$ . This is consistent with the suggested theory from Ostanin et al. (2013) from another area in the SW Barents Sea where increased bottom water temperature and reduced pressure due to unloading of ice sheets, accompanied by sediment erosion due to ice streaming, may have led to

destabilization of hydrates in the Hammerfest Basin. Furthermore, upward migration of thermogenic gas along with destabilization of hydrates are thought to cause overpressure and possibly migration of gas through pipes resulting in formation of pockmarks (Ostanin, et al., 2013). This fluid flow scenario is also supported by reports of similar fluid flow scenarios in Loppa High in the SW Barents Sea by Chand et al. (2012). There, it is suggested that gas charged fluids may have created pockmarks after glacial retreatment of ice sheets followed by quick deposition of glaciomarine sediments. The gas charged fluid is suggested to be dissociated gas from methane hydrates, migrating through stratigraphic boundaries connected to faults (Chand, et al., 2012). Site survey from the Ververis 3D study area indicate numerous pockmarks on the seafloor, ranging up to 20 m in diameter and 1-3 m in depth (Kleiven & Ersdal, 2008). It has also been interpreted and illustrated a large quantity of faults in Ververis 3D (Figure 20, Figure 21, Fig. 22) and also fluid pipes have been interpreted and illustrated (Figure 22, Figure 32). The gas hydrate stability modelling for the study area indicates a decreasing gas hydrate stability zone from LGM to times during deglaciation, thus it is likely that destabilization and dissociation of gas hydrates may have resulted in migration of gas through faults and fluid pipes, and eventually forming pockmarks on the seafloor.

Numerical modelling of gas hydrate stability conditions during times of deglaciation at the location of well 7324/8-1 within Hoop 3D, suggests methane hydrate stability down to 93 m and gas hydrate stability down to 167 m sub bottom depth (Figure 38).



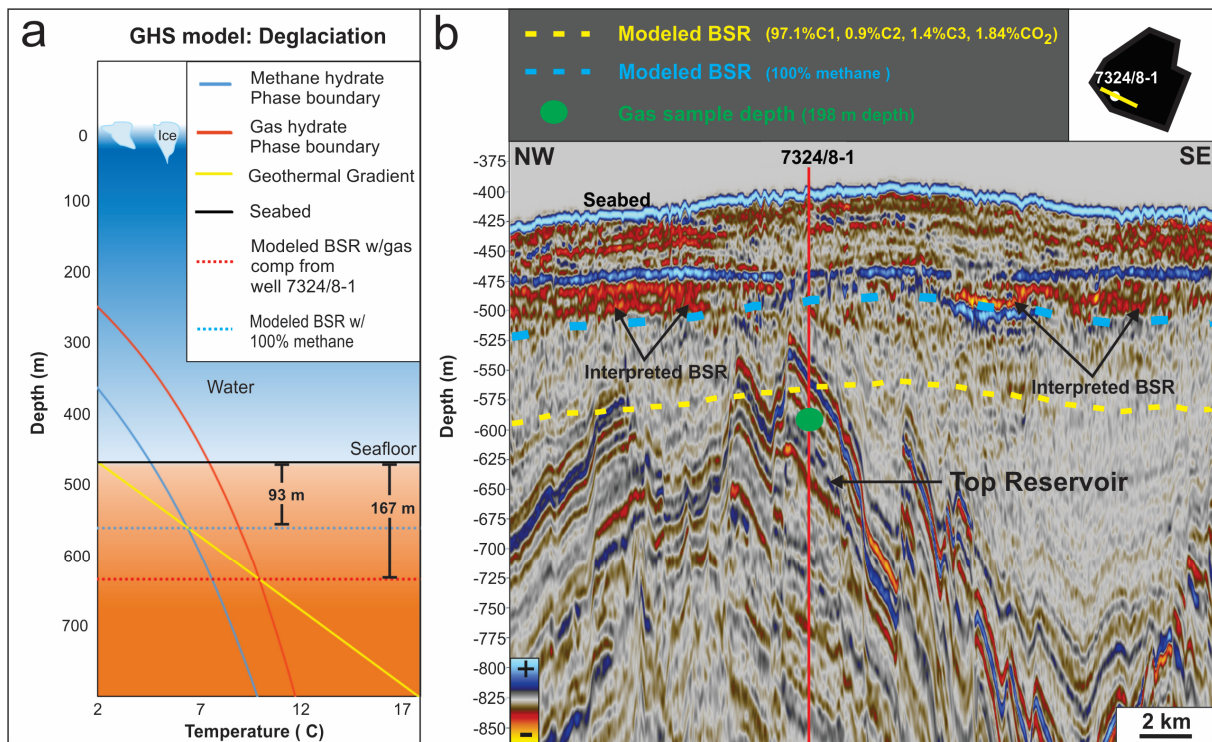


Figure 38. GHS model for conditions during deglaciation at the location of well 7324/8-1. b) Depth-converted seismic section. The modelled gas hydrate stability is estimated to be stable down to 167 m below the seafloor and indicated by the yellow dashed line. The modelled methane hydrate stability is estimated to be stable down to 93 m below the seafloor and indicated by the blue dashed line. Interpreted BSR are illustrated with black arrows. The green dot illustrates the depth at which the gas composition is sampled at. The red vertical line indicates the position of well 7324/8-1.

The numerical modelling from time of deglaciation (16 830 BP) insinuates a massive decrease in hydrate stability from LGM, and may possibly be explained by thawing of the ice sheet column of 1723 m into a seawater column of approximately 469 m (Figure 38). The significant release in pressure conditions along with the rising bottom water temperature from  $-1.78\text{ }^{\circ}\text{C}$  to approximately  $2\text{ }^{\circ}\text{C}$ , would cause a major effect on the stability conditions for both methane hydrates and gas hydrates. Both Chand et al. (2008) and Dore et al. (1996) emphasizes that much of the thinning of gas hydrate stability since LGM is thought to relate to the reduction of pressure due to glacial unloading and a significant increase in bottom water temperature. Dore et al. (1996) suggests that the pressure reduction caused by the unloading of ice sheets during deglaciation not only decreased the hydrate stability, but also caused release of soluble methane gas in formation water as free gas. A previous study of gas hydrate stability modelling in the SW Barents Sea (Chand, et al., 2008) indicates that an increase in the bottom water temperature of  $7\text{ }^{\circ}\text{C}$  (from  $-1.5\text{ }^{\circ}\text{C}$  to  $5.5\text{ }^{\circ}\text{C}$ ) alone, would possibly decrease the gas hydrate stability zone thickness by up to 400 m. Another hydrate stability modelling made by Chand et al. (2012) suggests the methane hydrate stability zone to have thinned out from 600 m to zero in most parts of the SW Barents Sea. Furthermore,

here it is suggested fluid expulsion due to glacial retreat to have caused dissociation and migration of methane hydrates into shallower sediments. Faults and fractures related to uplift after the retreating ice sheets are suggested to act as migration pathway for higher order hydrocarbons and CO<sub>2</sub>. At the locations where the faults and fractures allow migration of higher order hydrocarbons and CO<sub>2</sub>, it is suggested patchy formation of structure II gas hydrates. This would add to support the observation and interpretation of gas hydrates in Hoop 3D, where a significant system of faults are observed and described in the area (Gabrielsen, et al., 1990) and the gas analyses from well 7324/8-1 (Harding, et al., 2014) indicates presence of higher order of hydrocarbons and CO<sub>2</sub> both at the top reservoir at 238 m sub bottom depth and at the gas sample sampled at 198 m sub bottom depth. Hence, the observed and interpreted BSRs within Hoop 3D (Figure 33, Figure 36, Figure 38) may possibly be related to fluid expulsion due to pressure reduction and uplift caused by the retreat of ice sheets after LGM in the SW Barents Sea.

## 7 Conclusion

- High resolution 3D seismic data and 2D P-cable seismic data reveal geophysical evidence of prominent shallow gas anomalies possibly related to gas hydrates in both Ververis Dome structure and Hoop Fault Complex on the Bjarmeland Platform.
- Numerical modelling suggests favorable conditions for gas hydrate stability in both study areas. The gas hydrate stability within Ververis 3D is estimated to 87 m sub bottom depth, whereas within Hoop 3D the gas hydrate stability is estimated to 76 m sub bottom depth. In addition, modelling also suggests favorable conditions for methane hydrate stability within Hoop 3D down to 25 m sub bottom depth.
- The results from numerical modelling coincides with the interpretations of gas hydrate-related BSRs, thus increasing the confidence of the interpreted BSRs. Furthermore, the gas compositions used in the modelling are from detailed analysis of mud gas samples at relatively shallow depths in the study areas. The mud gas sample from well 7226/2-1 is sampled at a depth of 534 m below the seafloor, whereas the mud gas sample from well 7324/8-1 is sampled as shallow as 198 m below the seafloor.
- Numerical modelling of gas hydrate stability during glacial conditions was carried out by using the results from ongoing work at Centre for arctic gas hydrate, environment and climate (CAGE) on numerical modelling of the ice sheet and isostatic conditions during the last glaciation. Modelling of gas hydrate stability during Last Glacial Maximum suggests stable conditions as deep as 618 m sub bottom depth within Ververis 3D and 412 m sub bottom depth within Hoop 3D.
- During times of deglaciation numerical modelling suggests gas hydrate stability down to 233 m sub bottom depth within Ververis 3D and 167 m sub bottom depth within Hoop 3D. The thinning of the gas hydrate stability zone from Last Glacial Maximum is

thought to relate to unloading of vast ice sheets and increasing bottom water temperatures as the ice melts into water.

## 8 References

- Andreassen, K., Hart, P. & MacKay, M., 1996. *Amplitude versus offset modelling of the bottom simulating reflection associated with submarine gas hydrates*, Tromsø: Elsevier, Marine Geology.
- Andreassen, K., Hogstad, K. & Berteussen, K., 1990. Gas hydrate in the southern Barents Sea, indicated by a shallow seismic anomaly. *First Break*, 8(6), pp. 235-245.
- Archer, D., Buffett, B. & Brovkin, V., 2009. Ocean methane hydrates as a slow tipping point in the global carbon cycle. *Proceedings of the National Academy of Sciences of the United States of America*, pp. 20596-20601.
- Auriac, A. et al., 2016. *Glacial isostatic adjustment associated with the Barents Sea ice sheet: A modelling inter-comparison*, s.l.: Quaternary Science Reviews (In Press).
- Bangs, N. L. B., Hornback, M. J. & Berndt, C., 2011. The mechanics of intermittent methane venting at South Hydrate Ridge inferred from 4D seismic surveying. *Earth and Planetary Science Letters*, Volume 310, pp. 105-112.
- Beauchamp, B., 2004. Natural gas hydrates: myths facts and issues. *Comptes Rendus Geoscience*, 336(9), pp. 751-765.
- Berndt, C., Bünz, S. & Mienert, J., 2003. Polygonal fault systems on the mid-Norwegian margin: a longterm source of fluid flow. *Geological Society*, Volume 216, pp. 283-290.
- Bjarnadóttir, L. R., Winsborrow, M. C. M. & Andreassen, K., 2014. Deglaciation of the central Barents Sea. *Quaternary Science Reviews*, Volume 92, pp. 208-226.
- Boswell, R., 2009. Is gas hydrate energy within reach?. *Science*, Volume 325, pp. 957-958.
- Boswell, R. & Collett, T., 2006. The Gas Hydrate Resource Pyramid. *Natural Energy Technology Laboratory*, Fire in the ice(NETL).
- Bryn, P. et al., 2005. Explaining the Storegga Slide. *Marine and Petroleum Geology*, Volume 22, pp. 11-19.
- Bugge, T. et al., 2002. Shallow stratigraphic drilling applied in hydrocarbon exploration of the Nordkapp Basin, Barents Sea. *Marine and Petroleum Geology*, Volume 19, pp. 13-37.
- Butt, F. A., Elverhøi, A., Solheim, A. & Forsberg, C. F., 2000. Deciphering late cenozoic development of the western Svalbard Margin from ODP Site 986 results. *Marine Geology*, Volume 169, pp. 373-390.
- Bünz, S. & Mienert, J., 2004. Acoustic imaging of gas hydrate and free gas at the Storegga Slide. *JOURNAL OF GEOPHYSICAL RESEARCH*, Volume 109.
- Bünz, S., Mienert, J. & Berndt, C., 2003. Geological controls on the Storegga gas-hydrate system of the mid-Norwegian continental margin. *Earth and Planetary Science Letters*, 209(3-4), pp. 291-307.
- Bünz, S. et al., 2012. Active gas venting through hydrate-bearing sediments on the Vestnesa Ridge, offshore W-Svalbard. *Marine Geology*, Volume 332-334, pp. 189-197.



- Cartwright, J. A., 1994. Episodic basin-wide hydrofracturing of overpressured Early Cenozoic mudrock sequences in the North Sea Basin. *Marine and Petroleum Geology*, 11(5), pp. 587-607.
- Chand, S. et al., 2008. Gas hydrate stability zone modelling in areas of salt tectonics and pockmarks of the Barents Sea suggests an active hydrocarbon venting system.. *Marine and Petroleum Geology*, 25(7), pp. 625-636.
- Chand, S. & Minshull, T., 2003. Seismic constraints on the effects of gas hydrate on sediment physical properties and fluid flow. *Geofluids*, Volume 3, pp. 275-289.
- Chand, S., Minshull, T., Gei, D. & Carcione, J., 2003. Gas hydrate quantification through effective medium theories - a comparison.. *Geophysical Research Abstracts*, Volume 5.
- Chand, S. et al., 2012. Multiple episodes of fluid flow in the SW Barents Sea (Loppa High) evidenced by gas flares, pockmarks and gas hydrate accumulation. *Earth and Planetary Science Letters*, Volume 331-332, pp. 305-314.
- Chand, S. et al., 2012. Multiple episodes of fluid flow in the SW Barents Sea (Loppa High) evidenced by gas flares, pockmarks and gas hydrate accumulation. *Earth and Planetary Science Letters*, Volume 331-332, pp. 305-314.
- Collett, T., 2002. Energy resource potential of natural gas hydrates. *American Association of Petroleum Geologists Bulletin*, Volume 86, pp. 1971-1992.
- Dore, A. & Jensen, L., 1996. The impact in late Cenozoic uplift and erosion on hydrocarbon exploration: offshore Norway and some other uplifted basins. *Global and Planetary Change*, Volume 12, pp. 415-436.
- Downs, R. & Knox, M., 2007. *Report on Contractor's Performance: ST0715 Ververis 3D Marine Seismic Survey*, s.l.: RPS Energy.
- Elverhøi, A., Pfirman, S. L. & Larssen, B. B., 1989. Glaciomarine sedimentation in epicontinental seas exemplified by the northern Barents Sea.. *Marine Geology*, Volume 85, pp. 225-250.
- Faleide, J. I., Gudlaugsson, S. T. & Jacquart, G., 1984. Evolution of the western Barents Sea. *Marine and Petroleum Geology*, 1(2), pp. 123-150.
- Faleide, J. I. et al., 1996. Late Cenozoic evolution of the western Barents Sea-Svalbard continental margin. *Global Planet*, Volume 12, pp. 53-74.
- Fichler, C., Henriksen, S., Rueslaatten, H. & Hovland, M., 2005. North Sea Quaternary morphology from seismic and magnetic data: indications for gas hydrates during glaciation?. *Petroleum Geoscience*, Volume 11, pp. 331-337.
- Freire, A. F. M., Matsumoto, R. & Santos, L. A., 2011. Structural-stratigraphic control on the Umitaka Spur gas hydrates of Joetsu Basin in the eastern margin of Japan. *Marine and Petroleum Geology*, Volume 28, pp. 1967-1978.
- Gabrielsen, R. H. et al., 1990. *www.npd.no*. [Online]  
Available at: <http://www.npd.no/global/norsk/3-publikasjoner/npd->

[bulletin/npd\\_bulletinnr6.pdf](#)

[Accessed 16 February 2016].

Grozic, J., 2010. Interplay Between Gas Hydrates and Submarine Slope Failure. In: *Submarine Mass Movements and Their Consequences*, eds. D. Mosher, R. C. Shipp, L. Moscardelli, J. Chaytor, C. P. Baxter, H. Lee & R. Urgeles. s.l.:Springer Netherlands, pp. 11-30.

Haacke, R. R., Westbrook, G. K. & Hyndman, R. D., 2007. Gas hydrate, fluid flow and free gas: Formation of the bottom-simulating reflector. *Earth and Planetary Science Letter*, Volume 261, pp. 407-420.

Halland, E. K., Mujezinovic, J. & Riis, F., 2013. [www.npd.no](http://www.npd.no). [Online]

Available at: <http://www.npd.no/Global/Norsk/2-Tema/Lagring-og-bruk-av-CO2/CO2-ATLAS-Barents-Sea.pdf>

[Accessed 16 February 2016].

Harding, R., Hansen, G. & Johansen, I., 2014. *Geochemistry Data Report - Vitrinite Reflectance, Gas Analysis and Isotopes on Fractions Well 7324/8-1 (Central Wisting)*, s.l.: Applied Petroleum Technology AS.

Helgeland, L. R., Kinn, A. A., Kvalheim, O. F. & Wenaas, A., 2012. *Gas kick due to hydrates in the drilling for offshore natural gas and oil*, Trondheim: Department of Petroleum Engineering and Applied Geophysics.

Holbrook, W., 2000. Seismic studies of the Blake Ridge: Implications for hydrate distribution, methane expulsion, and free gas dynamics, in *Natural Gas Hydrates: Occurrence, Distribution, and Detection. Geophysical Monograph Series, 124* (edited by Paull, C.K.; Dillon, W.P.), pp. 235-256.

Holbrook, W. et al., 1996. Methane Hydrate and Free Gas on the Blake Ridge from Vertical Seismic Profiling. *Science*, 273(5283), pp. 1840-1843.

Holbrook, W. S. et al., 2002. Seismic detection of marine methane hydrate. *The Leading Edge*, Volume 21, pp. 686-689.

Hornbach, M. et al., 2003. Direct seismic detection of methane hydrate on the Blake Ridge. *Geophysics*, Volume 68, pp. 92-100.

Hovland, M., 2005. *Gas Hydrates*, Stavanger: Elsevier Ltd.

Hovland, M., Gardner, J. V. & Judd, A. G., 2002. *The significance of pockmarks to understanding fluid flow processes and geohazards*, s.l.: s.n.

Hovland, M. & Gudmestad, O. T., 2001. *Potential Influence of Gas Hydrates on Seabed Installations*, Stavanger: American Geophysical Union.

Hyndman, R. & Davis, E., 1992. A mechanism for the formation of methane hydrate and seafloor bottom simulating reflectors by vertical fluid expulsion. *Journal of Geophysical Research*, Volume 97, pp. 7025-7041.

Jacobsen, M. et al., 2012. *The International Bathymetric Chart of the Arctic Ocean (IBCAO) Version 3.0*, Stockholm: Geophysical Research Letters.

- Jakobsson, M. et al., 2014. Arctic Ocean glacial history. *Quaternary Science Reviews*, Volume 92, pp. 40-67.
- Judd, A. G. & Hovland, M., 1992. *The evidence of shallow gas in marine sediments*, Sunderland: Pergamon Press Ltd.
- Judd, A. & Hovland, M., 2007. *Seabed Fluid Flow. Impact on Geology, Biology and the Marine Environment*. s.l.:Cambridge University Press.
- Kjøllhamar, B., Serck, C. S., Pedersen, C. B. & Myklebust, R., 2015. Hoop Basin: Drilling success and playground for new exploration methods. *GEO ExPro*, 11(4).
- Kleiber, H.-P., Knies, J. & Niessen, F., 2000. The Late Weichselian glaciation of the Franz Victoria Through, northern Barents Sea: ice sheet extent and timing.. *Marine Geology*, Volume 168, pp. 25-44.
- Kleiven, A. & Ersdal, G., 2008. *Site Survey at Ververis: Planned well location 7226/2-1 ST0792, PL395*, Oslo: Fugro Survey AS.
- Kvenvolden, K., 1993. Gas hydrates as a potential energy resource-A review of their methane content. *US Geological Survey Professional Paper*, Volume 1570, pp. 555-561.
- Kvenvolden, K., 1998. A primer on geological occurrence of gas hydrate. *Geological Society of London Special Publication*, Issue 137, pp. 9-30.
- Kvenvolden, K., 2000. Natural gas hydrate: Introduction and history of discovery. In: M. MD, ed. *Natural Gas Hydrate in Oceanic and Permafrost Environments*. Max MD ed. The Netherlands: Kluwer Academics, pp. 9-16.
- Kvenvolden, K., 2006. Natural Gas Hydrate Occurrence and Issues. *Annals of the New York Academy of Sciences*, Volume 715, pp. 232-246.
- Kvenvolden, K. A., 1999. Potential effects of gas hydrate on human welfare. *Proceedings of the National Academy of Sciences*, Volume 96, pp. 3420-3426.
- Laberg, J. S. & Andreassen, K., 1996. Gas hydrate and free gas indications within the Cenozoic succession of the Bjørnøya Basin, western Barents Sea. *Marine and Petroleum Geology*, 13(8), pp. 921-940.
- Laberg, J. & Vorren, T., 1995. Late Weichselian submarine debris flow deposits on the Bear Island Trough Mouth Fan. *Elsevier Ltd*, Volume 127, pp. 45-72.
- Landvik, J. Y. et al., 1998. The last glacial maximum of Svalbard and the Barents Sea Area: ice sheet extent and configuration.. *Quaternary Science Reviews*, Volume 17, pp. 43-75.
- Lee, J. H., Baek, Y. S., Ryu, B. J. & Riedel, M. H. R. D., 2005. A seismic survey to detect natural gas hydrate in the East Sea of Korea.. *Marine Geophysical Researches*, 26(1), pp. 51-59.
- Lee, M. et al., 1993. Method of estimating the amount of situ gas hydrates in deep marine sediments. *Marine and Petroleum Geology*, Volume 10, pp. 493-506.
- Lubinski, D. et al., 1996. The last deglaciation of the Franz Victoria Through, northern Barents Sea.. *Boreas*, Volume 25, pp. 89-100.

- Lundschien, B. A., Høy, T. & Mørk, A., 2015. *www.npd.no*. [Online] Available at: [http://www.npd.no/global/norsk/3-publikasjoner/npd-bulletin/bulletin11\\_lav.pdf](http://www.npd.no/global/norsk/3-publikasjoner/npd-bulletin/bulletin11_lav.pdf) [Accessed 16 February 2016].
- Løseth, H., Gading, M. & Wensaas, L., 2009. Hydrocarbon leakage interpreted on seismic data.. *Marine and Petroleum Geology*, Volume 26, pp. 1304-1319.
- Løvø, V. et al., 1990. *Submarine permafrost and gas hydrates in the northern Barents Sea*, s.l.: Institutt Rapportserie 56, 171.
- Makogon, Y., 1997. *Hydrates of Hydrocarbons*.. Tulsa: Penn Well Publishing.
- Makogon, Y., 2010. Natural gas hydrates – A promising source of energy. *Journal of Natural Gas Science and Engineering*, Volume 2, pp. 49-59.
- Maslin, M. et al., 2010. Gas hydrates: past and future geohazard?. *Philosophical Transactions of the Royal Society A: Mathematical, Physical and Engineering Sciences*, Volume 368, pp. 2369-2393.
- Matapour, Z., 2013. *The effects of Biodegradation on Barents Sea residual oils, live oils and gases*, Oslo: University of Oslo.
- McGinnis, D. F. et al., 2006. The fate of rising methane bubbles in stratified waters: How much methane reaches the atmosphere?. *Journal of Geophysical Research*, 111(doi:10.1029/2005JC003183).
- Mienert, J. & Posewang, J., 1999. Evidence of shallow- and deep-water gas hydrate destabilizations in the North Atlantic polar continental margin sediments.. *Geo-Marine Letters*, Volume 19, pp. 143-149.
- Mienert, J. et al., 2005. Ocean warming and gas hydrate stability on the mid-Norwegian margin at the Storegga Slide. *Marine and Petroleum Geology*, 22(1-2), pp. 233-244.
- Milkov, A. V., 2004. Global estimates of hydrate-bound gas in marine sediments: how much is really out there?. *Earth-Science Reviews*, Volume Earth-Science Reviews, 66, pp. 183-197.
- Minshull, T. & Singh, S., 1994. Seismic velocity structure at a gas hydrate reflector, offshore Western Columbia, from full waveform inversion. *Journal of Geophysical Research*, Volume 99, pp. 4715-4734.
- Murphy, W., 1984. Acoustic measurements of partial gas saturation in tight sandstones.. *Journal of Geophysical Research*, Volume 89, pp. 1549-1559.
- Mørkved, P. T., Kaaby, F. M. & Johansen, P. E., 2008. *Geochemistry Data Report - Gas Analysis Well 7226/2-1*, s.l.: Applied Petroleum Technology AS.
- NETL, 2011. *Energy Resource Potential of Methane Hydrate*, US Department of Energy: Laboratory, National Energy Technology.
- NODC, 2009. *World Ocean Database*. [Online] Available at: <http://www.nodc.noaa.gov/General/temperature.html>

NPD, n.d. *Norwegian Petroleum Directorate, Factpages*. [Online]  
Available at: <http://npdmap1.npd.no/website/NPDGIS/viewer.htm>

Ostanin, I., Anka, Z., di Primio, R. & Bernal, A., 2013. Hydrocarbon plumbing systems above the Snøhvit gas field: Structural control and implications for thermogenic methane leakage in the Hammerfest Basin, SW Barents Sea. *Marine and Petroleum Geology*, Volume 43, pp. 127-146.

Patton, H. et al., 2015. *Geophysical constraints on the dynamics and retreat of the Barents Sea ice sheet as a paleobenchmark for models of marine ice sheet deglaciation*, s.l.: American Geophysical Union.

Patton, H. et al., 2016. *The build-up, configuration, and dynamical sensitivity of the Eurasian ice-sheet complex to Late Weichselian climate and ocean forcing*, Tromsø: In Prep to Quaternary Science Review.

Pau, M., Hammer, Ø. & Chand, S., 2014. *Constraints on the dynamics of pockmarks in the SW Barents Sea: Evidence from gravity coring and high-resolution, shallow seismic profiles*, Oslo: Elsevier B.V..

Phrampus, B. J. & Hornbach, M. J., 2012. *Recent changes to the Gulf Stream causing widespread gas hydrate destabilization*, Dallas: Macmillan Publishers Limited.

Polyak, L. et al., 1997. . Late Weichselian deglacial history of the Svyataya (Saint) Anna Through, northern Kara Sea, Arctic Russia.. *Marine Geology*, Volume 143, pp. 169-188.

Rajan, A., Bünz, S., Mienert, J. & Smith, A. J., 2013. Gas hydrate systems in petroleum provinces of the SW-Barents Sea. *Marine and Petroleum Geology*, Volume 48, pp. 92-106.

Rokstad, S.-O., Tofighi, A. & Eikefet, Ø., 2014. *7324/8-1 Wisting Central PL 537 (End of well report)*, Stavanger: OMV.

Ruppel, C. D., 2011. *Methane Hydrates and Contemporary Climate Change*. s.l.:Nature Education.

Ruppel, C. & Noserale, D., 2012. Gas Hydrates and Climate Warming - Why Methane Catastrophe is Unlikely. *Sound Waves, USGS*, FY 2012(140).

Shipley, T. H. et al., 1979. Seismic reflection evidence for the widespread occurrence of possible gas hydrate horizons on continental slopes and rises. *American Association of Petroleum Geologists Bulletin*, Volume 63, pp. 2201-2213.

Sloan, E., 1990. *Clathrate Hydrates Of Natural Gases*. 1st ed. New York: Marcel Dekker.

Sloan, E., 2003. Fundamental principles and applications of natural gas hydrates. *Nature*, Volume 426, pp. 353-362.

Sloan, E. D. & Koh, C., 2008. *Clathrate Hydrates of Natural Gases*. Third Edition ed. New York: CRC Press.

Sloan, E. J., 1998. Clathrate hydrates of natural gases. In: New York and Basel: Marcel Dekker Inc., p. 705.



- Solheim, A., Andersen, E. S., Elverhøi, A. & Fiedler, A., 1996. Late Cenozoic depositional history of the western Svalbard continental shelf, controlled by subsidence and climate. *Global Planet*, Volume 12, pp. 135-148.
- Solheim, A. & Elverhøi, A., 1985. *A pockmark field in the Central Barents Sea; gas from a petrogenic source.*, Oslo: Norsk Polarinstitutt.
- Suess, E. et al., 1999. Gas hydrate destabilization: enhanced dewatering, bethic material turnover and large methane plumes at the Cascadia convergent margin.. *Earth and Planetary Science Letters*, Volume 170, pp. 1-15.
- Svendsen, J. I. et al., 2004. Late Quaternary ice sheet history of northern Eurasia. *Quaternary Science Reviews*, Volume 23, pp. 1229-1271.
- Svendsen, J. I., Gataullin, V., Mangerud, J. & Polyak, L., 2003. *The glacial History of the Barents Sea and Kara Sea Region*, Bergen: s.n.
- TGS, 2014. *Seismic Processing Report HR14 P-Cable*, UK: TGS.
- Vadakkepuliambatta, S., 2014. *Sub-seabed fluid-flow systems and gas hydrates of the SW Barents Sea and North Sea margins*, Tromsø: Department of Geology, University of Tromsø.
- Vadakkepuliambatta, S., Bünz, S., Mienert, J. & Chand, S., 2013. Distribution of subsurface fluid-flow systems in the SW Barents Sea. *Marine and Petroleum Geology*, Volume 43, pp. 208-221.
- Vadakkepuliambatta, S., Chand, S. & Bünz, S., 2014. *Can ocean warming destabilize gas hydrate accumulations in the SW Barent Sea*, Tromsø: UiT The Arctic University of Norway.
- Vadakkepuliambatta, S., Hornbach, M. J., Bünz, S. & Phrampus, B. J., 2016. *Controls on gas hydrate system evolution in a region of active fluid flow in the SW Barents Sea*, Tromsø: Marine and Petroleum Geology.
- Vanneste, M., Guidard, S. & Mienert, J., 2005. Bottom-simulating reflections and geothermal gradients across the western Svalbard margin. *Terra Nova*, Volume 17, pp. 510-516.
- Vorren, T. & Laberg, J., 1996. Trough mouth fans – palaeoclimate and ice-sheet monitors.. *Quaternary Science Reviews*, Volume 16, pp. 865-881.
- Vorren, T. O., Hald, M. & Thomsen, E., 1984. Quaternary sediments and environments on the continental shelf off northern Norway. *Marine Geology*, Volume 57, pp. 229-257.
- Vorren, T. O., Kristoffersen, Y. & Andreassen, K., 1986. Geology of the inner shelf west of North Cape, Norway. *Norsk Geologisk Tidsskrift*, 66(2), pp. 99-105.
- Vorren, T. O. & Laberg, J. S., 1997. Through mouth fans - palaeoclimate and ice-sheet monitors. *Quaternary Science Reviews*, Volume 16, pp. 865-881.
- Winsborrow, M. C. M., Andreassen, K., Corner, G. D. & Laberg, J. S., 2010. Deglaciation of a marine-based ice sheet: Late Weichselian palaeo-ice dynamics and retreat in the southern Barents Sea reconstructed from onshore and offshore glacial geomorphology. *Quaternary Science Reviews*, 29(3-4), pp. 424-442.

Wood, W. et al., 2002. Decreased stability of methane hydrates in marine sediment owing to phase boundary roughness. *Nature*, Volume 420, pp. 656-660.